Spring 4-25-2013

Development of Optimization Models for the Set Behavior and Compressive Strength of Sodium Activated Geopolymer Pastes

Brian Albert Fillenwarth
Washington University in St. Louis

WASHINGTON UNIVERSITY IN ST. LOUIS

School of Engineering and Applied Science

Department of Mechanical Engineering and Materials Science

Dissertation Examination Committee:
Shankar Sastry, Chair
Richard Axelbaum
Thomas Harmon
Mark Jakiela
Kenneth Jerina
Alexander Rubin

DEVELOPMENT OF OPTIMIZATION MODELS FOR THE SET BEHAVIOR AND COMPRESSIVE STRENGTH OF SODIUM ACTIVATED GEOPOLYMER PASTES

by

Brian Albert Fillenwarth

A dissertation presented to the
Graduate School of Arts and Sciences
of Washington University in
partial fulfillment of the
requirements for the degree
of Doctor of Philosophy

May 2013
Saint Louis, Missouri

Contents

List of Figures

List of Tables

List of Abbreviations

CFA – Class C fly ash

C-S-H – Calcium silicate hydrate

GGBFS – Ground granulated blast furnace slag

MMT – Million metric tons

OH^- – Hydroxide ion

w/c – Water to cement ratio

XRF – X-ray fluorescence

Acknowledgements

I would like to thank the Consortium for Clean Coal Utilization for providing funding for this project. In addition I would like to thank the power companies who provided the fly ash needed for the completion of this project. Finally I wish to thank the Department of Mechanical Engineering and Materials Science for providing funding throughout my degree program.

A special thanks goes to the people who helped coordinate and gather the fly ash samples at the various power stations used in this research.

Brian Fillenwarth

Washington University in St. Louis
May 2013

Dedicated to my parents.

ABSTRACT

Development of Optimization Models for the Set Behavior and Compressive Strength of Sodium Activated Geopolymer Pastes

by

Brian Albert Fillenwarth

Doctor of Philosophy in Mechanical Engineering

Washington University in St. Louis, 2013

Professor Shankar Sastry, Chair

As large countries such as China begin to industrialize and concerns about global warming continue to grow, there is an increasing need for more environmentally friendly building materials. One promising material known as a geopolymer can be used as a portland cement replacement and in this capacity emits around 67% less carbon dioxide. In addition to potentially reducing carbon emissions, geopolymers can be synthesized with many industrial waste products such as fly ash.

Although the benefits of geopolymers are substantial, there are a few difficulties with designing geopolymer mixes which have hindered widespread commercialization of the material. One such difficulty is the high variability of the materials used for their synthesis. In addition to this, interrelationships between mix design variables and how these interrelationships impact the set behavior and compressive strength are not well understood. A third complicating factor with designing geopolymer mixes is that the role of calcium in these systems is not well understood.

In order to overcome these barriers, this study developed predictive optimization models through the use of genetic programming with experimentally collected set times and compressive strengths of several geopolymer paste mixes. The developed set behavior models were shown to predict the correct set behavior from the mix design over 85% of the time. The strength optimization model was shown to be capable of predicting compressive strengths of geopolymer pastes from their mix design to within about 1 ksi of their actual strength. In addition to this the optimization models give valuable insight into the key factors influencing strength development as well as the key factors responsible for flash set and long set behaviors in geopolymer pastes.

A method for designing geopolymer paste mixes was developed from the generated optimization models. This design method provides an invaluable tool for use in future geopolymer research as well as commercial development of geopolymer products.

Chapter 1

Why Study Geopolymers?

A recent push towards the development of more environmentally friendly materials has brought the relatively new material known as a geopolymer into the spotlight. Geopolymers can be synthesized from several industrial waste products that are rich in aluminum oxide (Al_2O_3) and silicon dioxide (SiO_2). One waste product that is often used for their synthesis is fly ash, which is the main waste product of coal power plants. Other industrial waste products such as ground granulated blast furnace slag (GGBFS) and silica fume are also routinely used in the synthesis of geopolymers.

Not only does the manufacture of geopolymers result in using up material that would otherwise be landfilled, it also has the potential to substantially reduce global carbon dioxide (CO_2) emissions. One of the most promising applications of geopolymers is as a portland cement replacement. For this particular application geopolymers could potentially reduce global CO_2 emissions by more than 6%. Geopolymer cements also have numerous performance benefits over portland cements which will be discussed. Several other applications of geopolymers will be outlined, and a brief overview of the cost of geopolymers will be discussed.

1.1 Potential Environmental Impact of Geopolymers

As large countries such as China and India have begun to industrialize, the demand for, and use of cheap building materials such as portland cement has grown substantially [84]. In addition to an increasing demand for portland cement globally, fly ash produced by coal power plants is becoming a major concern. A survey by the American Coal Ash Association in 2009 indicated that only 40% of the fly ash produced in the U. S. is currently being used while the remaining 60% is being landfilled [3]. This clearly illustrates the need for more applications which use the produced fly ash. One promising application to both of these problems is using the fly ash produced by coal power plants to create geopolymers.

1.1.1 CO_2 Emission Reduction of Geopolymers from Portland Cement Replacement

Portland cement is currently a major source of total global CO_2 emissions. As a result a reduction in the use of portland cement will have a notable impact on CO_2 emissions. Each ton of portland cement produced generates approximately 0.51 tons of chemical CO_2 and 0.40 tons of CO_2 from fuel combustion [16, 83]. It has been estimated that the energy required to produce the activators for geopolymers is less than half the energy required to produce portland cement, and the chemical CO_2 produced by geopolymers is less than 20% the amount produced by portland cement [19]. So, a conservative estimate shows that each ton of geopolymer produced will result in 0.3 tons of CO_2 emissions, 67% less than the amount produced by portland cement.

This finding for material emissions alone is comparable to a case study investigating the carbon emissions from geopolymer concrete in comparison to ordinary portland cement concrete in the Australian market. The case study factored in transportation emissions as well as the material emissions and found that production and placement of geopolymer concrete emits 44-64% less CO_2 than ordinary portland cement concretes [57].

The total CO_2 emissions in the U. S. as well as the emissions due to portland cement production in the U. S. are illustrated in Figure 1.1 [83, 84]. Similarly, total CO_2 emissions worldwide and the emissions due to Portland cement production worldwide are illustrated in Figure 1.2 [8, 84].

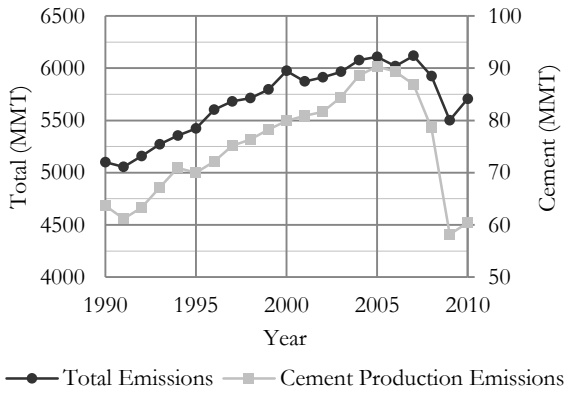

Figure 1.1 – U. S. CO_2 Emissions

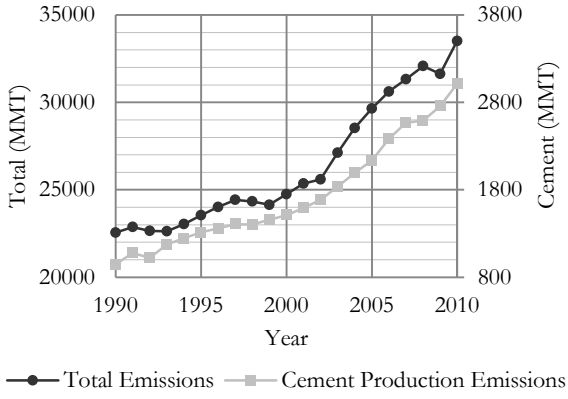

Figure 1.2 – Worldwide CO_2 Emissions

These figures indicate that the CO_2 emissions due to portland cement production in the U. S. has stayed around 1% of the total from 1990 to the present, but the CO_2 emissions due to portland cement production worldwide has steadily increased from 4% of the total in 1990 to 9% of the total in 2010. From this and knowing geopolymers will produce at least 67% less CO_2 emissions than portland cement, it can be concluded that a complete replacement of portland cement with geopolymer cement will yield at least a 6% reduction in global CO_2 emissions.

1.1.2 Industrial Waste Usage in Concrete

The largest industry that portland cement is used for is the concrete industry where cement is the main binding agent. The concrete industry accounts for over 95% of the total portland cement used [65]. One way that portland cement usage is already being reduced is through the use of supplementary cementitious materials in concrete. Common supplementary cementitious materials used are fly ash, GGBFS, and silica fume. These materials reduce the amount of portland cement in concrete and also use up industrial waste products that would be landfilled otherwise. The industries these products are generated from are as follows: fly ash is derived from coal power plant waste, GGBFS from iron and steel making, and silica fume from silicon and silicon alloy manufacturing processes [66].

Fly ash is the most common supplementary cementitious material used in ready mix concrete, being used in around 50% of all ready mix concrete in the U. S. These fly ash concrete mixes have an average portland cement replacement of 20% wt. with half of the fly ash concrete mixes using Class C fly ash (CFA) and half using Class F fly ash [66]. The portland cement used in ready mix concrete accounts for about 75% of the total portland cement market [65]. By assuming the remaining 25% of the portland cement market produces concrete in similar proportions to the ready mix industry, it can be concluded that 10% wt. of all portland cement needed for concrete production is currently replaced by fly ash. Although it is clear that some work has been done towards reducing the use of portland cement in concrete through the use of industrial waste products, geopolymers completely eliminate the need for portland cement in concrete production.

In addition to this, geopolymers use substantially more industrial waste products than are currently being used in concrete. To illustrate this, in 2010 the fly ash produced in the U. S. was about 57 million metric tons (MMT) and the usage in concrete totaled to about 8.9 MMT, or 16% wt. of the total produced [3]. The average quantity of fly ash used in a geopolymer is 70% wt. and the portland

cement consumption in 2010 in the U. S. was about 71.2 MMT [84]. From these statistics, it can be concluded that for each 1% wt. of the portland cement market captured by geopolymers, 0.87% wt. of the fly ash produced in the U. S. will be used. This shows that the usage of geopolymer concrete results in about five times the use of fly ash over portland cement based concrete. Thus, even though fly ash is currently used in portland cement based concrete, it is only a fraction of the amount that would be used in geopolymer based concrete.

1.2 Applications of Geopolymers

Geopolymers have potential uses in numerous industries in addition to the concrete industry as previously discussed. A brief description of specific examples of how geopolymer systems can be used in several industries follows.

1.2.1 In-situ Concrete Industry

A geopolymer paste is suitable as a partial or full replacement of the cement slurry in concrete products and is currently used commercially in this capacity by Iveron Materials in Florida as well as by Zeobond in Australia. For in-situ concrete applications the three critical design considerations are the set time, the strength, and how safe the material is to handle. Two common concerns about the use of geopolymer paste as a cement replacement in concrete are how it will impact steel rebar, and if alkali-aggregate reactions will result from their use [18].

The main concerns about the steel rebar are if the pH of the geopolymer system will cause corrosion, and if carbonation near the rebar will deteriorate it. With regard to the first concern about the pH, studies indicate that the pH of hardened geopolymers is between about 11.5 and 12.5 while the pH of hardened portland cement based concrete is between about 12 and 13 [18, 41, 76]. In addition to this, studies specifically investigating the stability of steel rebar in geopolymer matrices have been done and found that the rebar does not corrode in them [43, 59, 60]. As for the second concern, in portland cement based concretes, the calcium hydroxide species in the system have the potential to be involved in carbonation to form calcium carbonate [41]. Calcium carbonate has a relatively low pH of around 7-8 which provides a path for corrosion to occur. Since the quantity of calcium hydroxide species in geopolymer systems is limited, the carbonation of geopolymers results in potassium carbonate or sodium carbonate with a pH around 10-10.5 [14, 18]. This pH reduction does not provide a favorable path for corrosion as it does with portland cement based concrete.

Alkali-aggregate reaction is a condition sometimes seen in concrete where aggregates react with alkali hydroxides in concrete resulting in expansion and cracking over time. Studies have been done investigating the addition of potassium or sodium aluminosilicates and zeolites in high-alkali cements [58, 73]. These studies all conclude that the addition of aluminosilicates substantially reduces, or completely eliminates the alkali-aggregate reaction. Additionally, studies have been conducted on geopolymers which demonstrate that alkali-aggregate reactions simply do not take place in geopolymer systems [20, 50].

1.2.2 Precast Concrete Industry

The precast concrete industry can benefit even more than the in-situ concrete industry from the use of geopolymers. This industry already has the infrastructure in place to produce optimal geopolymer concrete due to the capability of curing specimens at elevated temperatures. Exposure to elevated temperature curing has been demonstrated to produce higher strength geopolymers much faster than ambient conditions [10, 11, 34, 35, 52, 75, 86]. Precast geopolymer concrete is currently being produced commercially by Antonello Precast Concrete in Australia.

1.2.3 Composites Industry

Geopolymer pastes are excellent resins for heat and fire resistant composites. Carbon fiber-reinforced geopolymer composites were found to be an ideal material for use in aircrafts due to their high specific strengths, high temperature capabilities, and non-combustibility in a study conducted by the Federal Aviation Administration [54]. A recent patent filed by Airbus indicates they will be using geopolymer composites to make conduits in areas of the plane that see high temperatures, like the power plant [64]. Another industry currently using carbon fiber-reinforced geopolymer composites is the racing industry, where the geopolymer composites have replaced titanium in the exhaust systems of several Formula One and IndyCar race cars [15].

1.2.4 Architectural Industry

Geopolymer pastes can be used in combination with a filler to create decorative stone wall tiles and pavers. Geopolymer pavers have very good wear resistance compared to some other typical pavers such as synthetic marble. In addition to this, they are stable to ultraviolet and infrared radiation [16].

1.2.5 Thermal Insulation

Foamed geopolymer pastes with mica fillers have been shown to be a very effective thermal insulator, especially when very high temperature thermal insulation is necessary [49].

1.2.6 Pharmaceutical Industry

In this industry, geopolymers have been proposed and tested as a high strength pellet to contain and allow for controlled release of highly potent opioids used to treat chronic pain [38, 39]. For this application the rate at which the drug is released is a critical parameter to control. Too high of a rate could be fatal, and too low of a rate could prove ineffective. It is also critical for the pellet to have a fairly high strength in order to prevent rapid release of the entire dose due to accidental breakage from chewing, and also to deter recreational abuse of these drugs by crushing them. Only certain base materials can be used in this application due to concerns of toxicity.

1.2.7 Toxic Waste Immobilization

For this application, an encapsulation matrix with an extremely low leach rate is imperative. A study on this particular application indicates that geopolymers are capable of immobilizing uranium waste (Ra-226) as well as several heavy metals such as mercury and lead [12].

1.3 Performance Benefits of Geopolymers

In addition to the environmental benefits geopolymer use has over portland cement use, there are several performance benefits they have. Since the majority of portland cement produced is used in concrete, the geopolymer performance benefits discussed focus on geopolymer based concrete benefits over portland cement based concrete.

1.3.1 Rate of Strength Development

A major performance benefit geopolymer products have over portland cement products is they gain strength at a much faster rate. When cured at room temperature, geopolymer based concrete has been shown to have the same strength at 4 hours as type III (high early strength) portland cement concrete does after 12 hours [17]. One application where this would be beneficial is in road repairs where a geopolymer based concrete could be driven on soon after the repair has been made. Another application this would benefit is in multistory concrete building construction by potential eliminating the need to shore lower floors during construction.

1.3.2 Drying Shrinkage & Creep Strain

It has been shown that geopolymer based concrete results in much lower drying shrinkage strain and creep strain than portland cement based concrete. Drying shrinkage has the potential to cause damaging cracks in concrete when restrained internally or externally. Geopolymer based concrete typically has drying shrinkage strains around 100 micro strains while portland cement based concrete has drying shrinkage strains of 500 micro strains on average [76, 87]. Creep deals with the amount a material deforms under constant load over time. S. Wallah and B. Rangan found that the actual creep strains of geopolymer based concrete were consistently about half the maximum values recommended for portland cement based concrete [87].

1.3.3 Sulfate Resistance

Another benefit geopolymer based concrete has over portland cement based concrete is they have better sulfate resistance. This is a critical property for concrete used in environments with high sulfur content, particularly in and around the ocean. Sodium sulfate is used to test concrete for external sulfate attack which causes concrete to expand, crack, and lose the bonding between the paste and aggregates. All of these cause a decrease in the strength of the concrete. Geopolymer based concrete was found to expand around 0.015% when immersed in a 5% sodium sulfate solution for a year [87]. In comparison, a portland cement based concrete immersed for half a year in an identical solution expanded around 0.1% which indicates geopolymer based concrete has a superior resistance to sulfate attack [88].

1.3.4 High Temperature Properties

One application geopolymer based concretes are well suited for that portland cement based concretes are not is in high temperature applications. portland cement based concretes lose their entire load bearing capabilities between 300°C and 400°C. Geopolymer based concrete however doesn't start losing strength until 600°C, and gradually decreases from that point until it loses most load bearing capabilities around 1100°C [17]. This particular property also makes geopolymers well suited for high temperature composite applications as well as fire insulation applications.

1.3.5 Material Weight

The use of a geopolymer will also result in a lighter product than if portland cement were used. For most applications, a reduced weight material with identical strength will result in a less costly final

product. This is due to the product not needing as much material to hold its own weight. One particular application where this is a very desirable trait is in any transportation application of the material. For these applications, a lower weight translates to a larger amount of cargo or passengers that can be transported for a set amount of fuel.

1.4 Cost Assessment of Geopolymers

A major driving factor behind any commercial decision is cost. In order for widespread commercialization of geopolymers to occur, they must be able to compete with the cost of portland cement based products. Although the cost of raw materials are highly variable to market conditions and location, a comparative cost analysis with current market data is outlined below for the United States. A similar study conducted in the Australian market is also briefly discussed.

1.4.1 Comparative Cost Analysis for the United States

Since a geopolymer paste is analogous to a portland cement paste, the relative costs of these must be compared for an accurate assessment. A portland cement paste consists of portland cement and water, where the weight ratio of water to cement (w/c) controls the strength. A high strength portland cement paste will have a w/c close to 0.25, and a moderate strength Portland cement paste will have a w/c close to 0.45 [41].

Geopolymer mixes unfortunately are not nearly as straightforward as portland cement mixes. Two mixes formulated for this research have been chosen for comparison. The high strength mix chosen for comparison (C3222) and the moderate strength mix chosen (C2021) have fly ash, sodium hydroxide, sodium silicate, and water in proportions as outlined in Table 1.2. These mixes have not been optimized for cost effectiveness, and were simply chosen because they represent a high strength and a moderate strength geopolymer mix. Recent market prices for the materials used in these mixes are given in Table 1.1.

Table 1.1 – Current Material Prices

Material	$/Short Ton	Source
Portland Cement	100	[56]
Fly Ash	20	[40]
Sodium Hydroxide	340	[80]
Sodium Silicate	500	[68]

Table 1.2 – Cost Comparison of Portland Cement Paste and Geopolymer Paste

Mix Description	Mix Constituents (% wt. of Mix)					$/Short Ton
	Cement	Fly Ash	NaOH	Na Silicate	Water	
High Strength Portland Cement (w/c = 0.25)	80.00	0.00	0.00	0.00	20.00	80
Moderate Strength Portland Cement (w/c = 0.45)	68.97	0.00	0.00	0.00	31.03	69
High Strength Geopolymer (9.81 ksi at 28 hours)	0.00	67.91	6.89	11.60	13.60	95
Moderate Strength Geopolymer (6.00 ksi at 28 hours)	0.00	73.09	4.83	2.28	19.81	29

As is clear from Table 1.2, the cost of geopolymer paste is highly variable depending on the desired strength and the quantity of materials used to achieve that strength. Although the high strength geopolymer paste is shown to be a higher cost than the high strength portland cement paste in Table 1.2, the density of geopolymer pastes are much less than the density of cement pastes.

To illustrate this point, the density of the high strength portland cement paste in Table 1.2 would be approximately 165 lbs./ft^3, while the density of the high strength geopolymer paste in Table 1.2 was measured to be approximately 122 lbs./ft^3. So, the yield per short ton of the Portland cement paste is 12.12 ft^3 while the yield per short ton of the geopolymer paste is 16.39 ft^3. This shows that even though the price per short ton of the geopolymer paste is higher than the portland cement paste, when the actual yield of both is considered the geopolymer paste comes out to be cheaper.

1.4.2 Comparative Cost Analysis for Australia

Cost assessments conducted with prices in the Australian market resulted in similar findings to the United States market. One cost analysis comparing geopolymer concrete and ordinary portland cement concrete found that the material cost for the geopolymer concrete is typically lower than ordinary portland cement concrete by about 10-30% [24]. A more recent and detailed case study found that the cost of geopolymer concrete, including both material and transportation costs, is between 10% lower and 40% higher than that of ordinary portland cement concrete [57]. So, it can be concluded that regardless of the particular market, geopolymer based products can be produced at comparable costs to portland cement based products making them a viable competitor.

Chapter 2

Formation of Geopolymers

Geopolymers are synthetic amorphous aluminosilicates that are formed from materials rich in Al_2O_3 and SiO_2, which are generically referred to as the base material, combined with an activating solution. The activating solutions allow the base material to be broken down and reformed into a three-dimensional aluminosilicate network. Both acidic (phosphoric acid) and basic (sodium hydroxide and potassium hydroxide) activating solutions have been successfully used for synthesis. Often additional silicon, typically in the form of sodium silicate or potassium silicate, is added to increase the quantity of Si-O-Si bonds in the final aluminosilicate network. This study focuses on basic activating solutions, and as such, only alkali activated geopolymers are discussed further.

2.1 Formation of Alkali Activated Geopolymers

The geopolymer formation process is generally understood to take place in three main stages which are ongoing. The first stage, often called the dissolution stage, begins immediately when the base material is combined with the activator solution to form a geopolymer paste. During this stage the high concentration of hydroxide ions (OH^-) breaks apart covalent Si-O-Si, Si-O-Al, and Al-O-Al bonds present in the base material. The amorphous particles in the base material are the most impacted areas since they dissolve faster than more crystalline particles. This releases silicon and aluminum ions into the solution which then form groups such as ortho-sialate ($(OH)_3$-Si-O-Al-$(OH)_3$), ortho-silicic acid ($Si(OH)_4$), and other groups high in Si-OH and Al-OH bonds [16, 30].

The second stage begins when the Si-OH and Al-OH groups in the geopolymer paste begin forming aluminosilicate oligomers consisting of sialate (-Si-O-Al-O-) repeat units throughout the solution due to polycondensation [9, 16]. These oligomers combine into three-dimensional polymer networks with free alkali cations (K^+, Na^+, Ca^{2+}) acting as charge balancers [70]. As the rate of formation of these networks increases due to more available species, the rate of dissolution is slowed. This is due to the forming networks partially covering incompletely dissolved particles from the alkaline solution as well as available OH^- needed for dissolution being used up [29]. There is a noticeable setting of the geopolymer paste when the rate of formation of the three-dimensional polymer networks exceeds the rate of dissolution of the base material. As the networks begin to develop and grow, a small

amount of strength gain occurs. These networks formed in the second stage consist mostly of Al-O-Si bonds that are concentrated around inert particles in the paste [30]. This is due to the aluminum being faster to react and polymerize than the silicon, and Al-O-Al bonds not being energetically favorable [28, 32, 58, 85, 86].

In the third stage more silicate monomers are incorporated into the three-dimensional aluminosilicate polymer networks forming large amounts of Si-O-Si bonds, often resulting in sialate-siloxo (-Si-O-Si-O-Al-O-) being the most abundant repeat unit [16, 30]. In order to maximize the quantity of free silicate monomers, the geopolymer paste is often heated at a temperature between about 50°C and 100°C (122°F and 212°F). This increases the rate of the dissolution of Si-O-Si bonds in the unreacted fly ash. Some of the Al-O-Si bonds in the formed network may also be broken and replaced by more stable Si-O-Si bonds in addition to some alkaline cations being replaced by the silicate monomers. This rearrangement of bonds results in much more stable and cross-linked polymer networks [70]. In addition to this, these smaller networks begin to combine as a result of Ostwald ripening which is the formation of larger networks at the expense of smaller ones [86]. The majority of the strength of the geopolymer develops during this stage.

The final resulting products of all the reactions taking place are large amorphous aluminosilicate three-dimensional polymer networks, and small amounts of nanocrystalline zeolite phases [4, 13, 14, 23, 30, 35, 42, 62, 63, 69, 70, 82]. The most commonly observed zeolite phases are hydroxysodalite [13, 14, 23, 30, 42, 63, 82] and chabazite-Na (herschelite) [13, 14, 30, 42, 62, 82]. Other zeolite phases such as gismondine may also form [35]. The formation of the nanocrystalline zeolite phases is inhibited by silicates, so these phases are more often discovered in geopolymer mixes with higher OH^- concentrations and lower silicate concentrations [4, 69].

2.2 Effect of Impurities in Base Material

Although some base materials used to produce geopolymers consist nearly entirely of aluminum and silicon, such as metakaolin (dehydroxylated kaolinite), most of the base materials used contain impurities. The most common impurities present in appreciable quantities are iron and calcium. A few studies have been done with iron by adding various iron oxides as impurities to the aluminosilicate as well as attempting to create purely iron based geopolymers without the aluminum. All of these studies concluded that the iron oxides present in base materials will remain essentially inert and act as a filler in the system [6, 9]. The reason the iron oxides do not take part in the

reaction is they take too long to dissolve in the alkaline environment [6]. Although the presence of iron does not directly impact the geopolymer reactions, it does inhibit the dissolution of amorphous phases in particles with higher iron contents.

Unlike the iron however, the calcium content in a base material does influence the geopolymer formation process. Several studies indicate that calcium shortens the set time of fresh geopolymer pastes [22, 45, 47, 52, 75, 85]. In addition to this, several studies indicate that some quantity of calcium in the base material is beneficial for strength development of the geopolymer due to the formation of calcium silicate hydrates (C-S-H) which are the main reaction products in the hydration of cement [7, 22, 23, 32, 34, 41, 45, 48, 52, 75, 85, 94]. Both of these points are discussed further in Chapter 3.

From a practical standpoint of the geopolymer formation process, any crystalline phases present in the base material can also be regarded as impurities. Although there is some evidence of dissolution of these phases, they dissolve at a much slower rate than amorphous phases. The most common crystalline phases found in appreciable quantities of geopolymer base materials are quartz (SiO_2), mullite ($3Al_2O_3$-$2SiO_2$), and hematite (Fe_2O_3).

2.3 An Illustrative Model

An illustrative model demonstrating the formation process of a geopolymer over time is outlined in Figure 2.1. This figure is representative of a base material with all the impurities discussed previously.

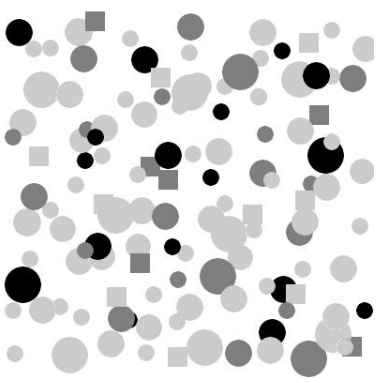

Figure 2.1.1 – Base Material

Figure 2.1.2 – Initial Set

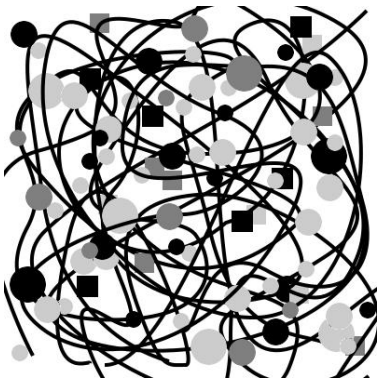

Figure 2.1.3 – Final Network

The base material as shown in Figure 2.1.1 contains a high quantity of amorphous silicon and aluminum, and a small quantity of amorphous calcium and iron based phases as indicated by the circles. It also contains a moderate quantity of quartz and mullite and a small quantity of hematite phases as indicated by the squares.

In Figure 2.1.2 the point where the geopolymer paste has set is illustrated. This point occurs within the first day of mixing the geopolymer, often within the first few hours [10, 22, 45, 74, 89]. As shown in this figure, large quantities of the amorphous silicon and aluminum phases have dissolved and smaller quantities of the amorphous calcium phases have dissolved. Additionally, small quantities of the quartz and mullite phases have dissolved. Also, as indicated by the black lines, the aluminosilicate networks have begun forming.

After a substantial amount of time has passed, the geopolymer reaches a quasi-equilibrium state where further network changes occur very slowly. This point is illustrated in Figure 2.1.3, and is reached in the first month, and often first week after the geopolymer is mixed [4, 10, 34, 35, 45, 62, 75, 82]. As indicated in this figure, minimal additional dissolution of the base amorphous and crystalline phases occurs. A substantial amount of new aluminosilicate network growth and cross-linking occurs. In addition to this, some C-S-H phases and small amounts of new crystalline zeolite phases are formed as indicated by the black squares.

Chapter 3

Impact of Design Parameters on Properties of Geopolymers

A large number of studies have been done investigating how various mix design parameters impact the initial and final properties of alkali activated geopolymers. The focus of this study is on the understanding and modeling of short term properties critical to the commercialization of geopolymer products. As a result, the conclusions presented are limited to those based on the set time and compressive strength. A third important property to the commercialization of geopolymer products, specifically geopolymer concrete, is the workability of the mix. However, the quantity and particle distribution of aggregates used in the mix is a critical consideration for this aspect and as such, is beyond the scope of this study [41, 76].

3.1 Set Time Based Conclusions

Having knowledge of the time available to cast a geopolymer into forms is critical for successful planning and execution of a project. A standard method for measuring the available time to work with cement pastes exists (ASTM C191) and has been shown to work well for determining available working time of geopolymer pastes. Since the setting of the paste in geopolymers occurs when the rate of network growth in the geopolymer begins to exceed the rate of dissolution, the set time can also be used as a relative measure of the reaction rate. The majority of the following conclusions are based on results from the standardized set time test.

3.1.1 Impact of Calcium Content on Set Time

It is well established that calcium present in the mix will result in a faster set time [22, 45, 52, 75, 85]. A small addition of calcium into the mix will result in a large reduction in set time with further additions resulting in smaller reductions [22, 45]. The main reason for this is the Ca^{2+} ions are able to act as charge balancers in addition to the Na^{+} and K^{+} ions present in the system [16, 24]. A higher quantity of available charge balancers will result in faster formation of aluminosilicate networks.

A second possible explanation for the reduced set time is that calcium silicate glasses are more reactive in water compared to glasses with higher silicate concentrations [22]. So, as the calcium content in the base material is increased, the calcium silicate glass phases present will dissolve faster than the phases with higher silicate concentrations making the species needed for network formation available sooner.

3.1.2 Impact of Particle Geometry on Set Time

Another factor that has been shown to impact the set time of geopolymers is the base material particles size and shape. Smaller particles result in faster dissolution due to having a higher specific surface area [10, 81, 89]. This makes the species needed for network formation available sooner speeding up the other stages of the formation process. It has also been demonstrated that more irregularly shaped particles result in shorter set times [81, 89]. The reason for this is the same as with the smaller particles, the irregularly shaped particles allow for more of the base material to be exposed initially speeding up the dissolution.

3.1.3 Impact of Curing Temperature on Set Time

It has been demonstrated that higher curing temperatures result in faster setting of geopolymer pastes. In a study by Sindhunata et al., the apparent set time was determined by the time it took for the paste to stop flowing [74]. Although this is an inexact measure, it is sufficient to demonstrate a trend. As was indicated in this study, a temperature of 50°C results in set times twice to three times as fast as those at ambient temperatures. Beyond this temperature, only small decreases in set time result. This conclusion can be attributed to the geopolymer network forming faster at elevated temperatures in comparison to ambient temperatures [62].

3.2 Compressive Strength Based Conclusions

In order to properly design any geopolymer products that will see loads, it is critical to know the available strength of the matrix. It has been shown that the flexure strength of geopolymer concrete closely mimics the flexure strengths of portland cement concrete in that the flexure strength is roughly 10-15% of the compressive strength [1, 41, 77]. Since use in concrete products is the largest potential market for geopolymers, knowledge of what impacts the compressive strength is essential for their commercialization. The main design factors impacting the development of compressive

strength in geopolymers will be discussed in detail. Several of these factors are interrelated which remains an area that has not yet been thoroughly investigated.

3.2.1 Impact of Alkali Content on Strength

The alkali in the mix is primarily controlled by the amount of sodium hydroxide or potassium hydroxide as well as any sodium silicate or potassium silicate added into the mix. Fly ash and other aluminosilicate sources generally only have small sodium and potassium contents, and thus do not contribute much. It is a well established conclusion that higher amounts of alkali in the mix result in higher strengths [4, 35, 42, 44, 81, 82].

A few studies indicate that after the alkali concentration in the mix becomes sufficiently high, the strength levels off suggesting there is an optimal alkali concentration for each mix [4, 82]. One study does indicate that there is an optimal concentration of alkali beyond which a notable strength decrease occurs before leveling out at the lower strength [63]. It is unclear if this anomaly would hold true for the other cases if more testing were done, however it is clear from all studies that as the amount of alkali in the mix is increased, the strength increases up to an optimal value beyond which no notable strength gain occurs.

3.2.2 Impact of Water Content on Strength

Studies on the impact of water in geopolymer mixes have been done, and conclude that the least amount of water to allow proper casting of specimens results in the highest strengths [63, 82]. This is in part due to lower amounts of water in the system resulting in fewer pores in the cured aluminosilicate matrix resulting in a denser, stronger network [49]. The water in the system is needed directly to aid in dissolution. Beyond this, the water is only needed indirectly as a medium to allow the movement of particles, and all steps in the geopolymer formation process beyond dissolution give off water as a reaction product [24]. Since the dissolution and polycondensation reactions take place simultaneously, as long as there is sufficient water in the system to provide fluidity of the system, there will be enough water for the dissolution.

3.2.3 Impact of Reactive SiO_2 Content on Strength

There appears to be universal agreement that higher amounts of reactive SiO_2 result in higher strengths [28, 30, 42, 63]. What exactly constitutes the reactive SiO_2 in geopolymer systems and how to best measure it however, has been the source of some debate [25, 55].

It is generally agreed that the quantity of amorphous SiO_2 in the mix provides a good approximation of the potential reactive SiO_2 in the system [27, 32, 51]. This is because the amorphous SiO_2 in the mix dissolves in the high alkali environment much more readily than crystalline forms of SiO_2. However not all of the amorphous SiO_2 is available for dissolution such as that which is embedded in fly ash particles with more crystalline surfaces [9, 22, 28, 51].

In addition to the amorphous SiO_2 in the base material, other sources of amorphous SiO_2 such as silica fume, cullet, rice husk ash, and more commonly, sodium or potassium silicate are often added into the mix to improve strength. It has been shown that the source of additional SiO_2 does not matter provided the quantity of amorphous SiO_2 in the system remains the same [7].

Since the geopolymer network consists of repeat units high in silicon, most commonly sialate-siloxo (-Si-O-Al-O-Si-O-), it is obvious that the quantity of silicon available to form the network is a critical factor for strength development [16]. Furthermore, the Si-O bonds formed in the geopolymer network are responsible for most of the strength of the final product [30].

3.2.4 Impact of Reactive Al_2O_3 Content on Strength

Similar to the reactive SiO_2 in geopolymer systems, there is debate over what constitutes the reactive Al_2O_3 and how to measure it. The quantity can be accurately approximated as the amorphous Al_2O_3 content in the same way as the reactive SiO_2 and for the same reasons [9, 22, 27, 28, 32, 51].

The quantity of reactive Al_2O_3 in a geopolymer system plays a role equally vital to the reactive SiO_2 since aluminum makes up the repeat units in the geopolymer network along with silicon. Since typical geopolymer base materials contain less reactive Al_2O_3 than reactive SiO_2, the quantity of available reactive Al_2O_3 can be a limiting factor in the strength development of geopolymers. It has been proposed that for optimal strength gain, the atomic ratio of available silicon to aluminum in the system should be 2 or lower, providing sufficient aluminum for the formation of solely sialate-siloxo repeat units [30].

3.2.5 Impact of Calcium Content on Strength

The calcium content commonly found in GGBFS and CFA impacts the formation of the geopolymer network in a few ways. One way that calcium impacts geopolymers is through the formation of C-S-H phases in the network [23, 32, 34, 45, 48, 52, 75, 94]. Some studies propose that

the C-S-H phases form in voids of the developed aluminosilicate network where water due to the polycondensation reactions remains [48, 94]. Thus, the presence of calcium in the system results in the conversion of a byproduct of the geopolymer formation process with no strength (water) to a high strength phase. However, since C-S-H and the aluminosilicate network both contain large quantities of silicon, the reactions may be competing. Whether an excess quantity of silicon is available would be controlled by the available silicon to aluminum ratio as previously discussed. As a result, the optimal amount of available calcium in the system is expected to be related to the available silicon to aluminum ratio of the system.

Another way the calcium impacts the geopolymer formation is the Ca^{2+} ions act as charge balancers in the aluminosilicate network in the same way that the Na^{+} and K^{+} ions do [16, 24]. A higher number of available charge balancers in the system can result in shorter polymer chains developing causing a less connected aluminosilicate network to develop. It is expected that as the geopolymer ages, and the network develops more, this is corrected. However, this does pose a potential negative impact on the strength development of the geopolymer, especially in the early stages.

3.2.6 Impact of Particle Geometry on Strength

The majority of the studies that have tested the impact of particle geometry on strength do so by mechanically milling the starting fly ash [75, 81, 89]. This reduces the median particle size and also makes the particles more irregularly shaped. One study was performed investigating just the impact of smaller particles by removing the larger particles of fly ash through sieving [10]. All of these studies indicated that both smaller and more irregularly shaped particles resulted in higher strengths. In the case of mechanically milling the fly ash, the reduced and more irregularly shaped particles likely have more of the reactive components readily exposed to the alkali environment. This is due to some of the crystalline fly ash shells being broken and the larger specific surface area exposing a larger quantity of the fly ash in general. In the case of sieving the fly ash, the reduced size particles likely have more of the reactive components available due simply to a larger specific surface area. Thus, smaller more irregular particles will in general have higher reactive Al_2O_3 and reactive SiO_2 components which can explain the higher strengths.

Some of the strength gain is, however, due solely to the smaller particle size [81]. It has been shown that the geopolymer network tends to form on particle surfaces, potentially inhibiting further dissolution of particles once the networks begin forming [46]. So, these smaller particles help reduce

the potential for incomplete dissolution of the particles. Since the vast majority of raw fly ashes have a median particle diameter in the relatively small range between 10 μm and 100 μm, particle size is a minor factor compared to others provided no mechanical processing of the raw fly ash is done [21].

3.2.7 Impact of Rest Period on Strength

The rest period is the time from when the specimen is placed into the molds to cure, to when the specimen is placed into a high temperature curing environment. Due to this, it is only relevant when elevated temperature curing is used. A few studies have shown that there is no negative impact on the strength development when prolonged rest periods are used [4, 11, 37]. This conclusion is a great benefit in practical applications of geopolymers where high temperature curing may not be possible to start immediately following casting. It is thought that the reason for the noted strength gains is the longer rest periods cause larger amounts of dissolution of the base material, resulting in more available material for the forming aluminosilicate network [11].

One study concluded that beyond a certain point, some strength decrease occurred [10]. This study found that the optimal rest period was approximately half the initial set time of the fresh geopolymer paste. The variance in strength as a function of the rest period however is minimal compared to other factors, so this is a minor consideration when developing optimal geopolymer formulations.

3.2.8 Impact of Curing Environment on Strength

Some studies have been conducted investigating the effect of the humidity of the curing environment on the strength of the geopolymers. Several of these studies concluded that covered curing (high humidity) results in higher strengths than exposed curing (low humidity) [13, 14, 42]. Exposed curing has been shown to result in carbonation of the surface which interferes with the polymerization by lowering the pH of the system significantly. By curing at higher humidity, the pores are saturated and CO_2 cannot penetrate the surface which prevents the carbonation [13]. In addition to this at higher temperatures as well as longer curing times, continued evaporation of water in the system may result in insufficient water available to allow the dissolution to proceed. For these reasons, covered curing is favorable to exposed curing.

A few studies contradict this claim, with one study showing very little difference in strength development with respect to curing technique [86], and one study claiming the exact opposite [75]. It is likely that in the case where little difference was noticed, the method used for curing the samples

was inadequate allowing water to evaporate out of the samples. In the instance where the exposed curing resulted in higher strengths than the covered curing, it is important to note that the exposed samples were cured four times longer at elevated temperatures than those cured covered. The curing time at elevated temperatures also plays a critical role in the strength development and will be discussed later. This longer curing time is the most likely cause for the discrepancy in this instance.

3.2.9 Impact of Curing Temperature on Strength

It is well accepted that elevated temperature curing results in more strength gain in geopolymers than curing at ambient temperatures [10, 11, 34, 35, 52, 75, 86]. One point that is debated however, is if the strength levels off at a certain temperature beyond which minimal strength gain occurs [4, 62, 75, 82, 86], or if the strength begins to decrease at a certain temperature with elevated temperature cured geopolymers [10, 11, 35, 78]. All studies agree that the optimal temperature is in the range of 75-85°C. Beyond this temperature, a decrease, or leveling off of the strength is seen. The reason for the higher strength at higher temperatures is attributed to the higher temperature curing resulting in a higher degree of reaction due to an accelerated reaction rate [62, 74].

In nearly all cases where a decrease in strength was seen beyond a certain temperature, the specimens were cured exposed [11, 35, 42]. As has been previously discussed, this can have a negative impact on strength development. There was one instance of samples which were cured covered that resulted in an eventual decrease in strength [10]. The authors hypothesized the likely reason for this was moisture loss in the sample, which indicates that the method used to cover the sample during curing may have been insufficient to prevent evaporation. Due to this, the samples can be effectively considered to have been cured exposed similar to the other studies that saw strength decreases beyond a certain point.

An upper limit for the curing temperature beyond which it would be expected for any method of curing to result in a strength loss is 100°C. At temperatures above 100°C chemically bonded water, which is water generated during polycondensation that gets trapped in the polymer framework, begins to evaporate out of the sample [16]. Even if the sample were covered to prevent evaporation, this water would turn to vapor and mitigate towards the surface creating a void in the polymer framework and reducing the strength. One study cured samples at temperatures as high as 120°C without showing significant strength reduction [82]. This may be because the samples were not held at this high temperature long enough for them to reach it.

3.2.10 Impact of Curing Time on Strength

It is well established that at ambient temperatures, regardless of whether the specimen was exposed to elevated temperature curing or not, older samples have higher strengths [4, 10, 11, 28, 34, 35, 45, 62, 75, 82]. This is identical to the trend seen with portland cement specimens, where as the specimen ages, it becomes stronger [41, 76]. The rate of strength increase of geopolymer specimens, however, is much faster than the rate of strength increase of portland cement specimens regardless of whether or not the geopolymer specimens are exposed to high temperature curing [17].

In addition to longer times at ambient temperatures resulting in higher strength, it is generally agreed that longer times at elevated temperatures also results in higher strengths [4, 11, 13, 14, 30, 35, 62, 82]. Identical to the ambient temperature curing, the strength gain rate is fast initially with the strength gain rate decreasing as time at the elevated temperature increases. This plateau in strength gain is typically seen once the specimens have been cured at elevated temperatures for 24-48 hour, depending on the temperature they are being cured at [11, 13, 14, 62, 82]. Higher curing temperatures reach this strength gain plateau sooner than lower curing temperatures. Similar to the higher temperatures, the strength gain due to longer curing times is attributed to the longer time resulting in a higher degree of reaction of the cured geopolymer [13, 62].

Some sources, however, indicate that there is an optimal time to cure a specimen at an elevated temperature, beyond which a decrease in strength is seen [10, 34, 78, 86]. Similar to the higher temperature specimens that saw a decrease in strength as the temperature was raised, the most likely explanation for this occurrence is due to the specimens being insufficiently, or not covered while being cured at high temperatures. This exposed curing can explain why longer curing times resulted in strength decreases in these studies.

Chapter 4

Research Overview

Although work has been done on understanding how geopolymers form and how various mix design parameters influence their properties, there are still some major barriers that must be overcome before widespread commercialization of geopolymer products is viable. This study aims to develop models that can be used to predict the set behaviors and compressive strength of geopolymer pastes. The barriers to commercialization this research will overcome are outlined, and work that has already been done towards developing predictive models is summarized. Experimental procedures used in this research are outlined in detail.

4.1 Commercialization Barriers

In order for widespread commercialization of geopolymers to occur, there are still several barriers that must be overcome. Some of these barriers, such as lack of in-service proof of long-term stability, simply cannot be overcome through laboratory testing. However, the use of geopolymer based products in non-structural applications will eventually lead to overcoming barriers such as these. Some other barriers which deal with mix design factors that can be investigated in the laboratory do still remain.

4.1.1 Variability of the Base Material

One barrier to widespread commercialization is the high amount of variability with the base material used. For example, the amorphous composition of fly ash depends on factors such as the source of coal used, the extent of pulverization of the coal, the firing temperature of the coal, and the cooling rate of the ash [2, 16, 21]. These conditions will inevitably be different for every plant, and may change over time at an individual plant due to new coal sources.

In order for geopolymers to be commercially viable, there must exist an easy way to determine the reactive components of the base material due to their high variability. It is understood that the reactive components available in the starting material play a major role in the set behavior and strength development, so it follows that there should be a way to predict these properties once the reactive components are known.

4.1.2 Mix Design Optimization for Specific Applications

As is evident from Chapter 3, there already exists some understanding of what various factors are beneficial or detrimental to the set time and strength development of geopolymer systems. Unfortunately, many of these factors are interrelated which makes it difficult to develop a clear "best" mix design. The variability in base material composition combined with different applications requiring different properties makes optimizing geopolymer mixes for cost and properties impractical without a design aid. This illustrates the need for clear relationships between mix design parameters and set behavior as well as mix design parameters and compressive strength to be known. Specific examples of how these relationships could aid in mix optimization follows.

4.1.2.1 General Concrete Applications

For applications where the fresh geopolymer may be placed by hand such as in-situ concrete applications, one necessary consideration is the potency of the activator solution. Activator solutions with a molar ratio of SiO_2/M_2O, where M represents either sodium or potassium, between about 1.25 and 1.45 are considered to be skin irritants. When the molar ratio of SiO_2/M_2O drops below 1.25, the activator solution is considered corrosive [16]. Knowledge of the relationships between mix design parameters and mechanical properties are crucial for these applications to help minimize the activator solution potency, and to know when extra precautions need to be taken during material placing.

4.1.2.2 Composite Applications

For composite applications, a mix with low workability will not fully impregnate the plies [16]. The set times, as measured by the Vicat needle, give an indication of the workability of pastes [31]. As a result, known relationships between mix design parameters and properties can aid in the design of these products by providing a maximum strength for a minimum required workability.

4.1.2.3 Architectural Applications

For many architectural applications strength is not a major concern, but a minimal setting time could be advantageous for production efficiency. Additionally, since this application lends itself well to automation, a minimal mix cost is critical. Known relationships between mix design parameters and properties could be used to provide minimum set times for a specified required minimum strength.

4.1.2.4 Thermal Insulation Applications

In order to create foamed geopolymers, it is critical to know when the paste has developed sufficient strength to hold in air formed by a foaming agent, but is not so strong as to prevent the foaming agent from being effective. Thus, it is critical to know the setting properties of the geopolymer in order to predict the proper time to add the foaming agent.

4.1.2.5 Waste Immobilization Applications

For waste immobilization, the formation of a highly cross-linked polymer networks is critical to prevent leeching of hazardous materials. More complete polymer networks result in a stronger geopolymer. So, knowledge of relationships between mix design parameters and strength can aid in the design of these systems by giving the parameters for maximum strength.

4.1.3 The Role of Calcium in Geopolymers

A third barrier to commercialization is knowledge of the role calcium plays in the reactions. More specifically, what the exact relationship between calcium and the set behavior is. It has been demonstrated that calcium has a significant impact on the set time of geopolymers [22, 45, 52, 75, 85]. In order for base materials containing large amounts of calcium in them to be practical for commercial applications, a better understanding of the relationship between set time and the relative amounts of calcium, silicon, and aluminum available in the system is needed. This is an area that remains largely unstudied due to the perception that base materials with higher calcium contents produced less desirable geopolymers [28, 93]. Recent studies clearly illustrate that this perception is unfounded and base materials with high calcium contents can be successfully used to produce high strength geopolymers [10, 52].

4.2 Existing Work

Through the review of available literature pertaining to geopolymer systems, very few instances dealing with modeling the properties were found. This is likely due to the basic factors responsible for strength development and set behavior only recently being brought to light. One model which has been developed can predict strengths as the ratio of the activating solution to base material is varied. Another model developed is capable of predicting strengths for one specific activating solution and two specific base materials as the ratio of the two base materials as well as the curing

temperature and time are varied. These models are briefly overviewed with their limitations discussed.

4.2.1 Strength from Binder-to-Fluid Ratio

Radhakrishna et al. developed a model predicting the strength of sodium hydroxide activated geopolymer mortars and concretes based on their binder-to-fluid ratio [71]. As defined in the paper, the fluid represents the weight of sodium hydroxide and additional water used in the mix (analogous to the activating solution as defined in this study). The binder represents the weight of the base material used in the mix. The predictive model is defined by Equation 4.1 below.

$$S = \left[0.79 \cdot \frac{B}{F} - 0.77\right] \cdot S_{@\frac{B}{F}=2.22} \qquad \text{Equation 4.1}$$

In this equation, B represents the weight of the binder, F represents the weight of the fluid, and $S_{@\frac{B}{F}=2.22}$ represents the strength at a binder to fluid ratio of 2.22. To use Equation 4.1, one must first know the strength of the mix at a binder-to-fluid ratio of 2.22. Once this is known the compressive strength (S) at any other binder-to-fluid ratio may be predicted.

Although this is a nice design tool, due to the simplicity of it, the model does not give much insight into why some mixes have higher strengths than others. In addition to this, the model is only useful if the base material, activators, curing conditions, and test age stay constant. Also, the applicability of this model if a mixed activator such as sodium hydroxide and sodium silicate were used is unclear. This severely limits the usefulness of the model.

4.2.2 Strength from Base Material Makeup & Curing Conditions

A more recent attempt at modeling the strength development of geopolymers from the base material composition and curing conditions was done by A. Nazari et al. [57]. The input variables used to develop this model were four base materials, the curing time, and the curing temperature. The four base material inputs were formed from two base materials, high calcium fly ash and rice husk-bark ash, which were sieved to separate the coarse particles from the fine particles of each. All tested samples had the same activating solution and the same ratio of the activating solution to the base material.

The predictive model developed was not given in the published paper, however due to the way the variables were selected for the models development it would have little practical value in industry. This is due to the high variability in the base material as has been previously discussed. The model developed in this study was able to predict strengths with a high degree of accuracy which indicates that modeling the underlying mechanisms and relationships responsible for strength development in geopolymers is practical.

4.3 Development of Mixes

In order to develop predictive models over the largest possible range of base materials, careful consideration of the mix design and what would be the best system to model was needed. Before developing mixes, some of the major conclusions from previous research were verified. After verifying key conclusions the specific system for analysis was chosen, and practical limits were put on the mixes. Once this was completed, the mixes used in this study were designed.

4.3.1 Verification of Existing Work

Through preliminary testing, some strength based conclusions that have been presented in previous research were confirmed and are as follows:

1. A higher alkali concentration in the mix tends to result in a higher strength. This was found to be true for all activators studied and is a well established conclusion as discussed in Section 3.2.1.

2. The minimum amount of water that is needed to cast the samples results in the highest strengths. This conclusion is discussed in detail in Section 3.2.2.

3. A higher amount of reactive SiO_2 in the mix results in a higher strength. In addition to this, the source of the reactive SiO_2 does not matter. This was concluded by varying the amount of sodium or potassium silicate in the mix. Both solid and liquid silicates were demonstrated to have nearly identical strength indicating the source of reactive SiO_2 is irrelevant. This conclusion is discussed further in Section 3.2.3.

4. Covered curing results in higher strengths than exposed curing does. As discussed in Section 3.2.8, this is mostly the result of carbonation of the surface halting the reaction process.

4.3.2 System for Analysis

Alkali activated geopolymer systems can be broken into several subgroups dealing with the specific activating chemicals and specific base materials used to form them. While the underlying formation mechanisms for all these systems are the same, preliminary work has demonstrated that mix designs which work for potassium activated mixes do not necessarily work for sodium activated mixes and vice versa. Due to the large quantity of variables already under investigation, it was decided that only one of these systems would be tested.

In order to decide which system to focus on, the benefits of each system were investigated. Both systems are capable of producing very high strength pastes, so this was not a factor considered. The main benefit that potassium based systems offer over sodium based systems is they have a lower viscosity and are less cohesive making them easier to work with. The main benefit of sodium based systems is they are lower in cost than potassium based systems. An additional advantage that sodium based systems have over potassium based systems is the sodium activators have a lower pH than their potassium counterparts indicating that they are safer to work with. The price difference between the two is substantial with sodium based activators being anywhere from half to a third the cost of their potassium counterparts [67, 68]. It was decided that due to the large difference in price, this would be the controlling factor in selecting an activator for a commercial application. As a result, sodium based activator systems were selected for this study. In addition to selecting a sodium based system for this study, the base material chosen for use in this study was fly ash.

4.3.3 Practical Limits on Mix Design

Over the course of designing and testing mixes, some practical limits on the mix design were determined and are as follows:

1. A water content lower than 15% wt. of the mix often results in a dry mix.

2. A fly ash content greater than 75% wt. of the mix often results in a dry mix.

3. Very little strength development occurs when mixes have water contents greater than 30% wt. of the mix.

4. Segregation of the mix becomes a problem when the quantity of fly ash is below 60% wt. of the mix.

5. The maximum possible quantity of Na_2O in the mix is around 20% wt. of the mix. The derivation for this limitation follows.

The maximum Na_2O in the mix limitation is derived from the following considerations:

1. Fly ashes rarely contain appreciable quantities of Na_2O (generally below 6%), so the majority of Na_2O comes from the NaOH and sodium silicate [2].

2. At room temperature, a saturated solution of NaOH will contain approximately 54% wt. NaOH [78]

From these considerations, it is evident that the highest Na_2O concentration possible in a mix occurs when the minimum amount of fly ash is used and the remainder of the mix is a saturated NaOH solution. Noting that 100% pure NaOH contains about 77.5% Na_2O and the minimum fly ash content is 60% wt. of the mix as explained in the fourth limiting factor, the maximum Na_2O content in a mix is calculated as follows.

$$Na_2O\ from\ ash = 60\% \cdot 6\% \quad \text{Equation 4.2}$$

$$Na_2O\ from\ NaOH = 40\% \cdot 54\% \cdot 77.5\% \quad \text{Equation 4.3}$$

$$Na_2O\ in\ mix = Na_2O\ from\ ash + Na_2O\ from\ NaOH \quad \text{Equation 4.4}$$

Solving Equation 4.2 through Equation 4.4 yields an upper limit for Na_2O in the mix of around 20% wt. of the mix.

4.3.4 Mix Design

As was detailed in Chapter 3, there are several major and minor factors that influence the strength of geopolymers. The factors dealing with the chemical composition of the mix are thought to include

the alkali, water, reactive SiO_2, reactive Al_2O_3, and calcium contents. The relationships between these parameters are unknown, and due to the number of factors a large testing matrix is needed to accurately study them.

In addition to the factors dealing with the chemical composition of the mix, factors dealing with the curing conditions of the mix have also been shown to influence the strength of geopolymers. As discussed in Section 3.2 these factors include the curing temperature, the curing time at elevated temperature, and the curing environment. It has been demonstrated that there is no relation between optimal curing temperature and mix composition. Thus it follows that there is no relation between the optimal curing time at elevated temperature and mix composition. Additionally, it is assumed that the means to cover the mix while curing exists which has been demonstrated to be the ideal curing environment and is the method used in this study, so this factor is not a consideration. For these reasons, the mix composition variables and curing environment variables are mutually exclusive.

In order to allow for the development of useful design tools, only mix composition variables are considered in the development of the compressive strength optimization model. The curing environment is not a factor for the development of the set behavior models.

4.3.4.1 Curing Parameters for Compressive Strength Model Development

One set of curing conditions were chosen and used for all compressive strength mixes. In order to develop the most useful model possible, it was decided that curing conditions which ensured the maximum possible strength development for each mix would be ideal. Since covered curing results in the highest strengths as described in Section 3.2.8, this was the curing environment used. All mixes were covered with plastic wrap and then aluminum foil immediately following casting of the specimens and remained this way until they were removed from the curing oven.

Section 3.2.9 indicated that a curing temperature of 85°C was the optimal curing temperature for strength development. Although temperatures beyond this might lead to small strength gains, as indicated in Section 3.2.10 a longer curing time could correct for this. Additionally, a temperature of 85°C as opposed to a slightly higher temperature provides a good buffer against the mix reaching the critical temperature of 100°C at some point during the curing regime due to the exothermic polycondensation reaction taking place. In order to ensure maximum reaction at this temperature, a

curing period of 24 hours was used. This is in the range for the plateau of strength gain as outlined in Section 3.2.10.

Since the curing conditions were chosen to ensure the maximum possible strength gain that could be achieved by each mix, the majority of mixes were only tested 28 hours after being cast. A 2 hour buffer was provided from the point the mix was made to the point it was put into the oven as well as from the point the mix was taken out of the oven to the point the mix was tested. The initial time buffer was provided to allow adequate time to properly cast the specimens. Additionally it was reasoned that a 2 hour buffer is a good approximation for the time it would take to cast and begin high temperature curing of geopolymers for commercial applications. Section 3.2.7 discusses the impact of the initial buffer time, or rest period, on the strength of the geopolymer and illustrates that it is a minor consideration. The 2 hour buffer at the end of curing was provided to allow the specimens to cool back to room temperature prior to being tested.

Three mixes were randomly selected to be tested at 7 days and 21 days in addition to 28 hours in order to validate that the chosen curing conditions did result in the maximum possible reaction of the mix. The results of this testing is summarized in Table 4.1

Table 4.1 – Validation of Designed Curing Regime

Mix	28 Hour Str. (ksi)	7 Day Str. (ksi)	21 Day Str. (ksi)
C1222	12.02	11.15	11.40
C2021	6.00	7.36	7.22
C3057	9.25	9.48	9.38

Table 4.1 clearly shows that little strength change occurs beyond the designed curing regime which indicates that the maximum potential strength of the geopolymer mix has been reached. Thus it is concluded that a 2 hour buffer at the beginning and end of covered curing for 24 hours at 85°C is a sufficient curing regime to ensure maximum possible strength development of each mix.

4.3.4.2 Set Behavior & Compressive Strength Model Development Mixes

Once the curing regime had been developed, the mix design proceeded by considering the practical limits given in Section 4.3.3 and the base material design results in Section 5.1. The design scheme followed to develop mixes to investigate the set behavior was first choosing three levels of H_2O and Na_2O to investigate. The three levels of H_2O chosen were 15%, 22.5%, and 30% wt. of the mix.

The three levels of Na_2O chosen were 3%, 7%, and 11% wt. of the mix. For all of these combinations, four mixes with varied reactive SiO_2 were selected. Two of these four mixes were at the extremes allowed by the base material (highest and lowest allowable reactive SiO_2 content), and the remaining two mixes were between the extremes. Similar conditions were used for several base materials having different compositions which allowed for the CaO and reactive Al_2O_3 contents in the mix to be varied as well.

Observations made from each mix dictated if each series of four reactive SiO_2 contents were tested. This was done since although the primary objective of the set time testing was to develop models for the set behavior of mixes, the secondary objective was to develop enough mix designs with reasonable set times to use for the compressive strength testing.

Once all the mixes in the primary mix design matrix were either tested or discarded, a second set of mix designs were developed to target mixes that were expected to have set times reasonable for use with the compressive strength testing. These mixes were designed to have compositions between the levels of the mixes that had been shown to work. This procedure was done for three base materials. A few mixes using other base materials were developed in addition to these three sets specifically to help investigate the set time behavior of mixes with low calcium contents. The set time testing of fly ash with very low calcium was limited due to nearly all low calcium mixes exceeding the 4 hour limit set for the set time study. A summary of all the mixes designed for use with the set time testing is provided in Table A.1 in Appendix A. The mixes presented in the table represent the as cast mixes not the as designed mixes.

All of the mixes used for the set time testing that did not exhibit flash set behavior and set within 4 hours were used for the compressive strength testing. Additional mixes that had set times exceeding 4 hours were used to bring the total number of mixes for each base material up to around 20. Due to limited quantities of some base materials, different but similar base materials were used for some of the compression testing mixes. This resulted in slight variations for some of the compressive mixes and set time mixes. A summary of all the mixes designed for use with the compressive strength testing is provided in Table A.2 in Appendix A. The mixes presented in the table represent the as cast mixes not the as designed mixes.

4.4 Experimental Methods

In order to generate enough data to develop predictive strength and set behavior models, several experiments were performed. The experimental methods which were followed to collect this data are outlined.

4.4.1 Overview of Testing Methods

For all mixes cast and tested, the chemicals listed in Table 4.2 were used. In addition to these chemicals, several fly ashes were considered for use in this study. A summary of the compositions of these fly ashes determined by x-ray fluorescence (XRF) is given in Table B.1 in Appendix B. Distilled water was used if any additional water was put in the mix in order to reduce the possibility of the pH of the water varying throughout testing.

Table 4.2 – Properties of Chemicals Used in Study

Chemical	% wt. Reactive SiO_2	% wt. Na_2O	% wt. H_2O
Na Silicate	28.70	8.90	62.40
NaOH	0.00	75.15	24.85

The procedure followed to create mixes in all cases was as follows. Any Na silicate and distilled water that was used was first mixed together. After mixing these together, any NaOH that was used was added and stirred until it was completely dissolved and cooled to room temperature. Once the activator solution had cooled to room temperature, it was combined with the fly ash and mixed until it formed a uniform paste. The paste was then cast as prescribed in the test being performed.

A flow chart detailing the complete testing program is shown in Figure 4.1. In this figure, the major test groups and starting points are denoted by the ovals, individual tests that must be performed are denoted by the boxes, results from these tests are denoted by rounded boxes and have a number designation, and major results as well as those requiring the combination of multiple tests are denoted by hexagons and a letter designation.

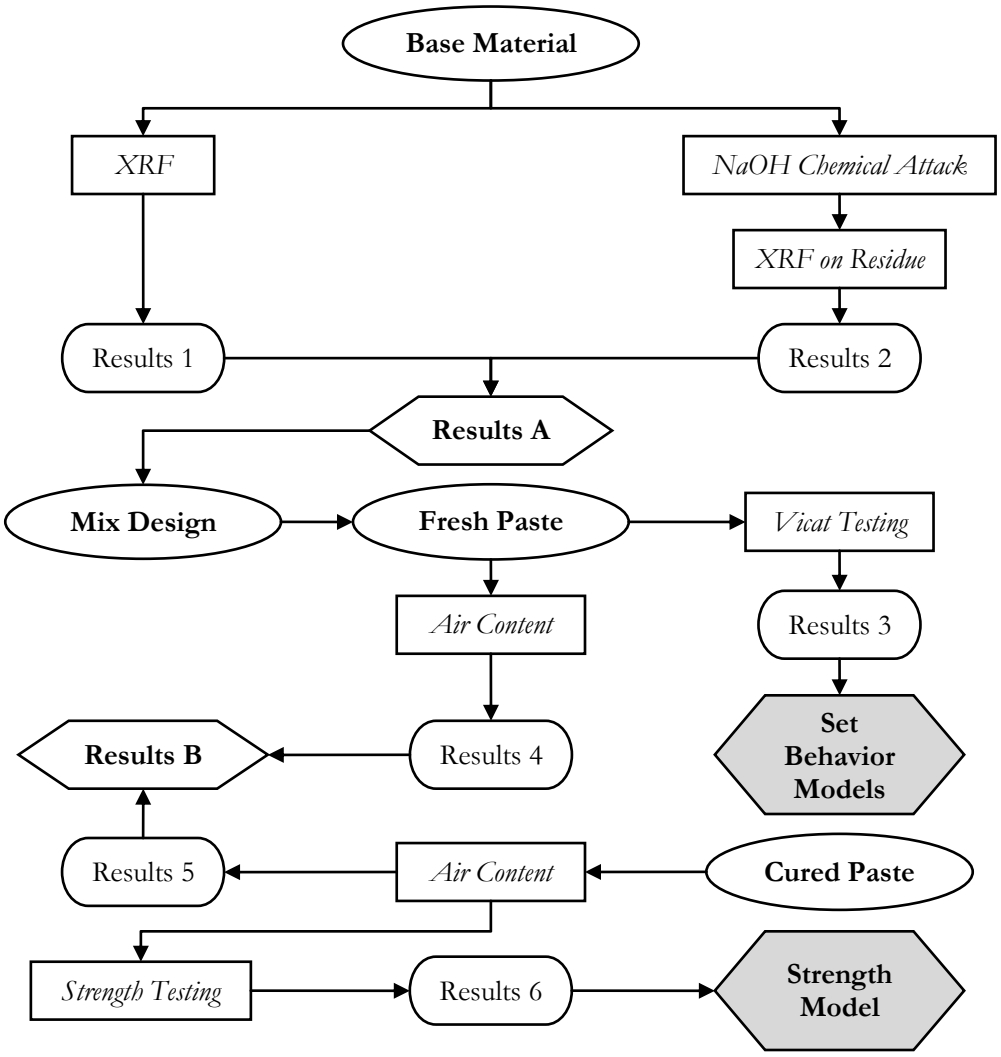

Figure 4.1 – Testing Overview

In Figure 4.1, the results that were obtained from experimental testing are as follows:

Results 1 – Compositional makeup of base material.

Results 2 – Compositional makeup of crystalline components and reactive percent of base material.

Results 3 – Initial and final set times of the geopolymer paste.

Results 4 – Density and air content of the fresh geopolymer paste.

Results 5 – Density and air content of the cured geopolymer paste.

Results 6 – Compressive strength of the geopolymer paste at 28 hours.

Results A – Reactive quantities of specific phases in the base material.

Results B – Water lost during curing and storing of geopolymer samples.

The experimental test procedures used to obtain these results are detailed in the following sections.

4.4.2 NaOH Chemical Attack

This technique was used to determine the reactive SiO_2 and reactive Al_2O_3 quantities in the base material. For this technique a NaOH solution is used to dissolve the base material as a direct measure of the total material available for dissolution. A ratio of 5 grams of the base material to 100 mL of a 30% wt. NaOH solution at a temperature of 75°C was found to be optimal [9]. Due to the large ratio of the chemical solution to the base material, the formation of aluminosilicate species is significantly inhibited.

Once combined, the base material and NaOH solution are stirred and the dissolved species are measured at various times after washing, filtering, and drying them. The parameters previously specified allowed sufficient accuracy of determining the reactive content with minimal dissolution of crystalline phases, and allowed the dissolution experiment to be performed in a reasonable time frame [9]. The time at maximum dissolution generally occurs around 60 minutes with these parameters, but the exact time the highest amount of dissolution occurs varies with different base materials.

In order to obtain the maximum dissolution with a high degree of accuracy, a 15 minute time increment was chosen. At each multiple of 15 minutes, the base material and NaOH solution were removed from the hot plate stirrer and the solution and material were washed, filtered, dried, and weighed. A new starting material needed to be used for each trial, but since the base material was the same the variance as a result of this is assumed to be minor. This assumption was tested by repeating each peak dissolution measurement as well as repeating the entire series of testing for one base material.

The eventual reduction in total weight lost occurs because when the dissolution time is too long, some aluminosilicate species will begin forming. As a result of this the point where the change in weight is highest provides the closest approximation to the weight of material available for dissolution. It is assumed that the rate of dissolution beyond the point where the change in weight is highest will be very slow. Since some additional dissolution is possible beyond this point however, the reactive quantity found using this technique will always be slightly less than the actual available reactive content.

Once the point at which the maximum weight loss occurs has been determined, the quantity of Al_2O_3 and SiO_2 dissolved can be determined. This is done by comparing XRF results of the base material prior to the dissolution experiment to XRF results of the residue left from the dissolution experiment. From these as well as the mass lost, the reactive species in the base material are determined by Equation 4.5.

$$\%wt.\,Reactive\ Oxide = \%wt.\,Oxide_{XRF} - \%wt.\,Oxide_{C} \cdot (1 - \%wt.\,Lost_{C}) \qquad \text{Equation 4.5}$$

In Equation 4.5, $Oxide$ stands for the oxide of interest (either Al_2O_3 or SiO_2), $\%wt.\,Oxide_{XRF}$ is the % wt. of the oxide determined by XRF, $\%wt.\,Oxide_{C}$ is the % wt. of the oxide determined by XRF on the chemical dissolution residue, and $\%wt.\,Lost_{C}$ is the %wt. lost from the chemical dissolution.

By using this method, a large amount of the amorphous phases on the surface of fly ash particles are dissolved in addition to a small portion of the crystalline phases. Complete dissolution of the amorphous phases does not occur with this method which is similar to what actually occurs during the geopolymer formation process as discussed in Chapter 2. Since only the amorphous and crystalline phases capable of dissolution are considered instead of assuming that all the amorphous phases dissolve and none of the crystalline phases do, the chemical dissolution technique chosen for use in this study more accurately determines the potential reactive content in a base material than other techniques do.

4.4.3 Vicat Testing

The purpose of this testing is to determine the initial and final set times of the geopolymer paste. For this testing, the procedure outlined by ASTM C191 for hydraulic cement pastes was followed.

As defined by the standard, initial set is when the needle of the apparatus penetrates 15 mm in 30 seconds and final set is when the needle does not penetrate a noticeable amount in 30 seconds. Two modifications to this standard were made due to the difference in initial behavior of geopolymer pastes and hydraulic cement pastes and the desired degree of accuracy for the testing. One modification deals with how the material is placed into the Vicat conical mold and the other modification deals with the frequency of measurements taken.

The procedure that was used to place the geopolymer paste in the mold is as follows. The mold was filled halfway with the geopolymer paste and then pressed with a ½" x 1" rectangular rod to remove air bubbles. The mold was then filled the rest of the way and pressed again. The excess material was then scraped off to form a level surface. This placing method is suitable since fresh geopolymer pastes generally start out in a more liquid state than fresh hydraulic cement pastes.

The time between needle penetration measurements was taken every 2 minutes until 1 hour had passed, and then every 5 minutes after. The standard calls for measurements to be made every 10-15 minutes, but by taking measurements more frequently, the set times was able to be determined more accurately. Since geopolymer pastes set faster than hydraulic cement pastes, this extra accuracy is necessary.

4.4.4 Air Content

The purpose of this testing is to provide a degree of quality assurance for the cast specimens. The air content as well as approximately how much water was given off during the reaction process was obtained through this testing. The procedure as outlined in ASTM C138 for this testing was followed. For geopolymer pastes, the fresh paste was weighed after it has been poured into the molds and before beginning the high temperature curing so the density of the paste could be determined. This allowed the calculation of the percent air in the paste as shown in Equation 4.6.

$$Air\ Content = \frac{\rho_i - \rho_p}{\rho_i} \qquad \text{Equation 4.6}$$

In Equation 4.6, ρ_i is the theoretical density of the mix and ρ_p is the actual density of the paste. Although some air was expected in the paste, an unusually large amount provided an early indicator of improper sample preparation. The specimens were weighed again after they were taken out of the oven. This allowed for the water given off during the reaction process to be approximated as the

change in weight of the samples. Some water loss was expected, but an unusually large amount of water loss indicated the samples were improperly covered during curing.

4.4.5 Strength Testing

The purpose of this testing is to determine the compressive strength of the geopolymer pastes. General procedures outlined by ASTM C109 for 2" cement mortar cubes were followed. Each mix was cast into 2" cube molds by filling the mold halfway and vibrating for 30 seconds, filling the mold the rest of the way and vibrating again for 30 seconds, then leveling off the top. The molds were then covered in plastic and covered again in aluminum foil to ensure a humid environment was maintained during curing. Molds were placed in the oven at 85°C 2 hours after the initial mixing. For each mix, 6 2" cubes were cast and tested at 28 hours (± 0.5 hour). All cured specimens were kept wrapped in plastic to maintain a humid environment until testing. A load rate of 200 pounds per second was used on all test specimens which is the lower recommended loading rate specified in the standard testing procedure.

4.5 Optimization Model Development Techniques

Due to the magnitude of data that was collected and the number of variable that were under consideration, specialized software was needed to aid in the analysis. The software selected to perform a regression analysis on the collected data was Eureqa II which specializes in extracting the simplest equations to model a continuous system.

4.5.1 Genetic Programming

Eureqa II is a statistical analysis program that uses genetic programming (symbolic regression) to determine the underlying relationships controlling various systems [72]. Genetic programming is a process where basic expressions are tested in the system and evolve over time. Expressions that better fit the data are kept and randomly modified and combined, while expressions that are worse are discarded.

Although this method of equation fitting is computationally intensive, the Eureqa II software allows the number of mathematical operations considered in the search to be limited to speed up the search. For example the search can be specified to consider only certain trigonometric operations, or they

can be excluded from the search entirely. Additionally, a form of an equation to find can be specified such as by forcing the expressions to always be positive for the considered data set.

The two evolutionary processes undergone in genetic programming are crossovers and mutations. Crossovers occur when blocks from different expressions are randomly traded and mutations occur when some element of one expression is modified. As an example of the genetic programming process, consider the expression given in Equation 4.7 to be the best possible expression for the data considered. Equation 4.7 is represented schematically in Figure 4.2.1. Additionally, consider Equation 4.8 and Equation 4.9 as two expressions currently in the system. These are represented schematically in Figure 4.2.2 and Figure 4.2.3 respectively.

$$y = 5 \cdot \exp\left(\frac{2 \cdot x^2}{3} - 1\right)$$ Equation 4.7

$$y = \sin(2 \cdot x^2) + \frac{x}{7}$$ Equation 4.8

$$y = 5 \cdot \exp\left(\frac{4+x}{3} + 1\right)$$ Equation 4.9

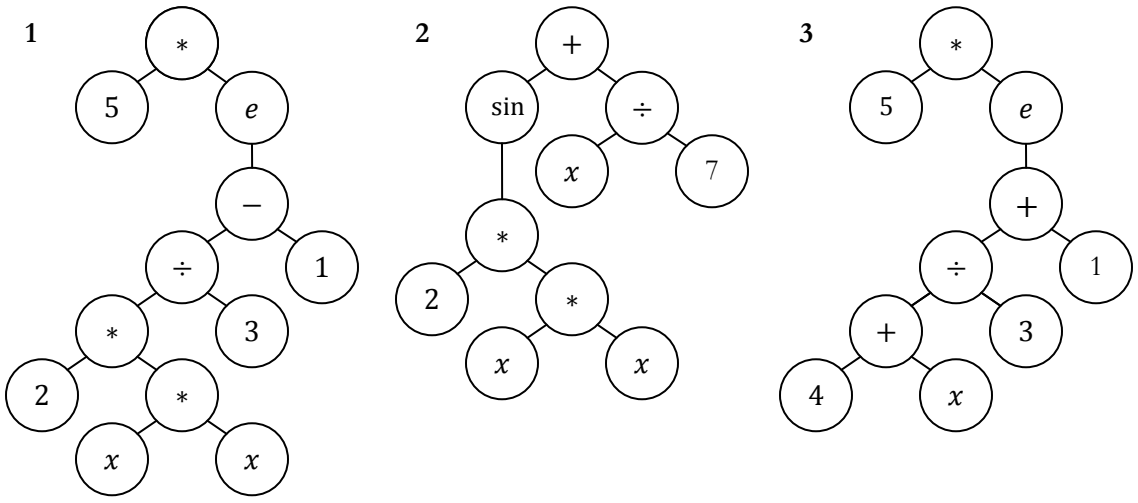

Figure 4.2 – Tree Structure Representations of Genetic Programming Expressions

An example of a possible crossover between Equation 4.8 and Equation 4.9 is shown in Figure 4.3. In this figure, the $2 \cdot x^2$ block from Equation 4.8 is exchanged with the $4 + x$ block from Equation 4.9.

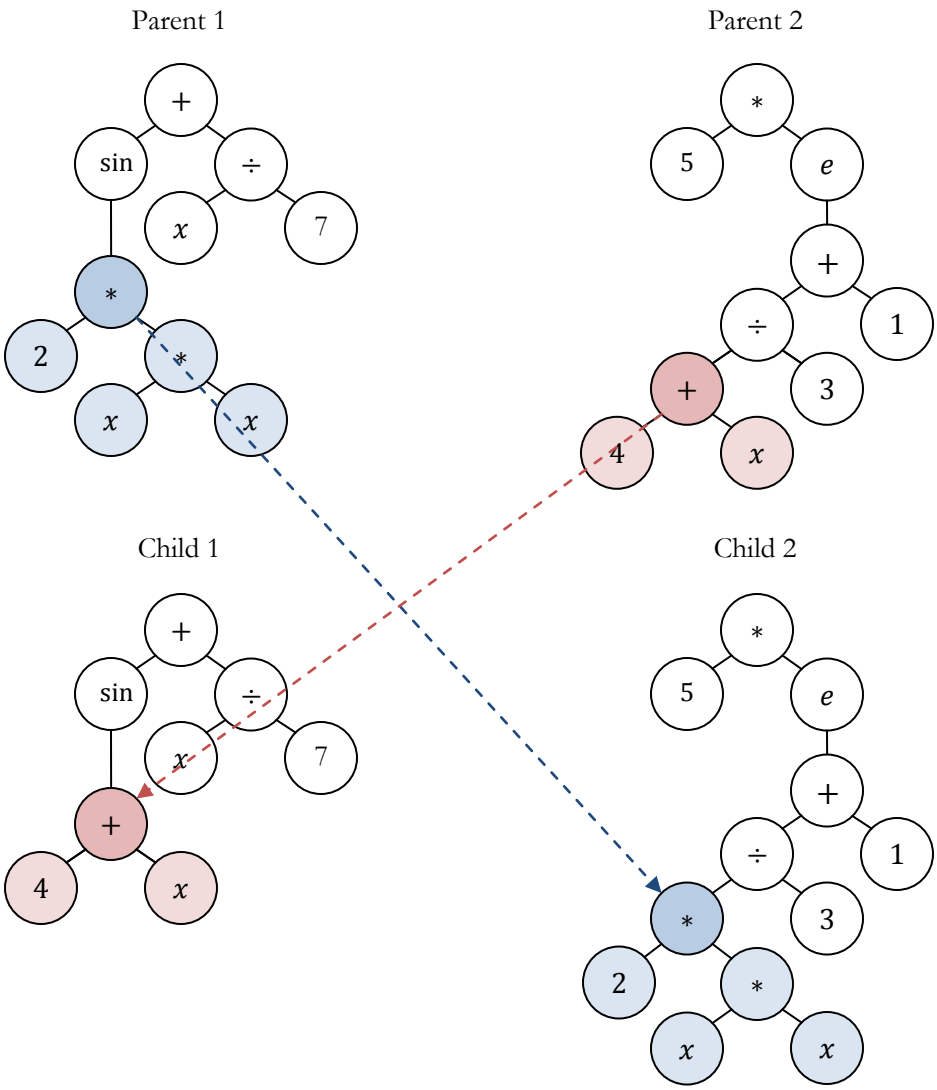

Figure 4.3 – Crossover Operation in Genetic Programming

The resulting expression for child 1 is given in Equation 4.10 and the resulting expression for child 2 is given in Equation 4.11.

$$y = \sin(4 + x) + \frac{x}{7} \qquad \text{Equation 4.10}$$

$$y = 5 \cdot \exp\left(\frac{2 \cdot x^2}{3} + 1\right) \qquad \text{Equation 4.11}$$

It is clear that child 2 as represented in Equation 4.11 models the data better than either parent or the other child generated from the crossover since it produces values much closer to those produced by the ideal expression in Equation 4.7. As a result, child 2 will be kept and the other three expressions will be discarded.

An example of a possible mutation process child 2 may undergo is the $+$ in the expression mutating into a $-$. This is shown in Figure 4.4.

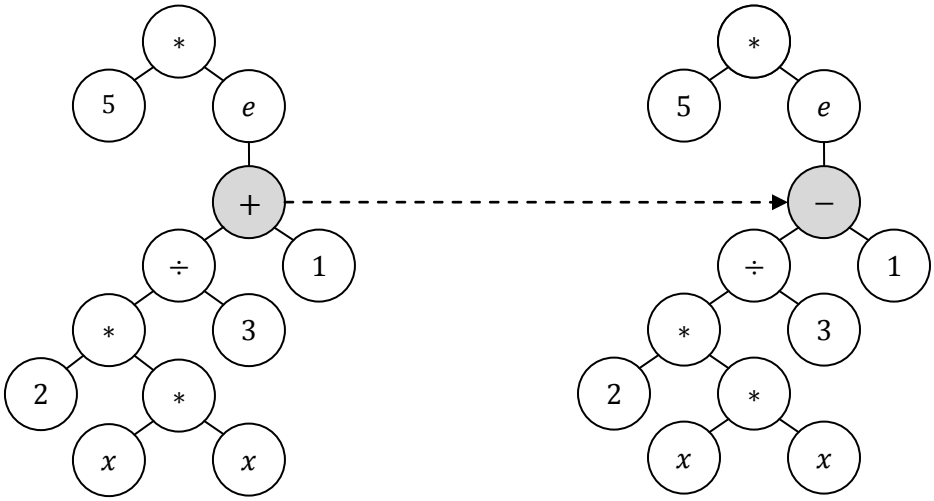

Figure 4.4 – Mutation Operation in Genetic Programming

The mutation of child 2 is now identical to the optimal expression given by Equation 4.7. From this point on, mutation and crossovers will still occur but no expression generated will be better than the shown mutation produced by child 2. As a result, this expression will be kept indefinitely and other expressions will begin to converge on this one.

4.5.2 Preliminary & Final Model Searches

For each model developed a preliminary and final model search was conducted in Eureqa II using the collected experimental data. Prior to running each model search, all variables were normalized to span the range from about 0 to 1. For each set of preliminary model searches three separate searches using different mathematical operations were run considering all chemical composition variables as outlined in Section 4.3.4.2. The mathematical operations allowed for the searches are specified in Table 4.3. In Table 4.3 c represents a constant and x represents an input variable.

Table 4.3 – Summary of Preliminary Model Search Parameters

Search Designation	Allowed Mathematical Operations	Variables Considered
Algebraic	$+, -, \div, *, c, x$	H_2O, Na_2O, R. SiO_2, R. Al_2O_3, CaO
Exponential	$+, -, \div, *, c, x$, exp, ln	
Trigonometric	$+, -, \div, *, c, x$, exp, ln, sin, cos	

As is evident from Table 4.3, the trigonometric preliminary model search allows for substantially more complicated expressions to be formed than the algebraic preliminary model search. This has the potential to lead to overfitting of the data, however the Eureqa II software penalizes more complicated mathematical operations in order to reduce the potential of this occurring. The software does this by discarding more complicated expressions if two expressions have the same fit to the data. Additionally, the software keeps consecutively less complicated expressions than the current one with the best fit in the data set. As an example if the expression $y = x^2$ is being fitted, the optimal solution set the program will find would contain $y = x^2$ and $y = x$ since these would be progressively less complicated expressions which fit the data the best.

Another technique used to reduce the potential of overfitting the experimental data, was using a portion of the collected data to train the model and a portion to test the model. Although it is ideal to keep these sets completely separate, since the experimental data sets collected were relatively small a portion of the data was allowed in both training and test sets. For all searches, 80% of the data was used for training and 50% was used for testing.

The fitting metric used in developing all models was a mean absolute error metric. This was chosen to minimize the impact of noise in the data. The preliminary model searches were allowed to run until no expressions with a better fit were generated for 12 hours. This corresponded to going through approximately 7 million generations with no better solution fit being found.

After the preliminary searches were completed, final model searches were run with more restricted parameters to reduce the computational cost of the solution and maximize the probability of the best solution being found. These searches were allowed to run until no expressions with a better fit were generated for 2 days which corresponds to no better solution fits in over 28 million generations. The function forms for the various searches as well as the restrictions imposed on the final model searches are outlined in Chapter 6.

Once the stopping criterion was met for each search, the generated solution set was analyzed. The solution with the best fit was selected as the final model provided there was not a solution of lower complexity that offered a nearly identical fit. The final models generated by the specific searches run were then compared to select the final overall model.

4.5.3 Validation of Generated Models

After the final models were developed, a final set of mixes were designed and tested as further validation that the models were not overfitting the experimental data. This series consisted of 10 mixes that were subjected to the same tests as the mixes used for development of the models. Most of the mixes in this series used fly ashes not actually used in developing the models. This was done as another measure to ensure the experimental data had not been overfit by the developed models.

Chapter 5

Results

5.1 Base Materials Design

In order to create mix designs over the widest possible range of base materials, dissolution experiments were performed on all of the fly ashes listed in Table B.1 in Appendix B to determine the reactive SiO_2 and reactive Al_2O_3 contents of the materials. Once the reactive quantities of each fly ash were determined, base materials were designed to capture the largest possible range of values with the available materials.

5.1.1 Dissolution Experiment

The NaOH dissolution technique outlined in Section 4.4.2 was followed and graphs showing the dissolution of each base material at various time increments during the experiment are given in Figure B.1 – Figure B.8 in Appendix B.

Since determining the reactive contents of the base material is critical to this research study, the repeatability of the technique used was investigated by repeating the entire dissolution study for the High Calcium 6 fly ash. Additionally, each point of maximum dissolution was tested twice to verify the accuracy of the critical point. XRF was carried out on the first trial in each case so this was the weight loss used to calculate the reactive SiO_2 and reactive Al_2O_3 quantities in the ash. As a control, each fly ash was tested mixed with water in the vacuum filtration setup used for the dissolution experiment. This was done to ensure that the filter used was fine enough so that no fly ash particles were going through prior to dissolution. From doing this, it was determined that the selected filter was adequate and the loss in the vacuum filtration system was negligible.

The test results are summarized in Table 5.1 along with the reactive quantities calculated using Equation 4.5 and the CaO content in each fly ash. A summary of the XRF results for the dissolved residue at the critical point which was used to calculate the reactive quantities from each experiment is given in Table B.2 of Appendix B.

Table 5.1 – Dissolution Experiment Results

Fly Ash	Time at max loss (min.)	Trial 1 Δ wt. (%)	Trial 2 Δ wt. (%)	R. SiO_2 (% wt.)	R. Al_2O_3 (% wt.)	CaO (% wt.)
Low Ca 1	90	25.3	24.7	13.53	4.44	1.77
Low Ca 2	60	15.9	16.2	9.52	3.76	1.89
High Ca 1	60	13.1	13.5	7.82	7.23	27.00
High Ca 2	105	19.6	18.9	11.13	8.42	23.67
High Ca 3	90	19.9	19.4	12.68	10.09	23.47
High Ca 4	75	20.6	21.0	11.47	8.73	23.51
High Ca 5	60	12.8	12.7	8.30	7.33	26.25
High Ca 6 T1	60	18.9	19.4	12.54	8.49	17.80
High Ca 6 T2	60	20.2	19.7	12.89	8.86	17.80

Table 5.1 shows that the base materials tested for this study have reactive SiO_2 contents between 7.82% wt. and 13.53% wt., reactive Al_2O_3 contents between 4.44% wt., and 10.09% wt., and CaO contents between 1.77% wt. and 27.00% wt. Comparing the High Calcium 6 trial 1 to the High Calcium 6 trial 2 shows that this method produces repeatable results. For High Calcium 6, the trial 1 results were used as the reactive quantities in the fly ash. The close change in weights between trial 1 and trial 2 for each individual fly ash also is a good indicator that this technique is repeatable and reliable.

5.1.2 Selected Base Materials

In order to capture the largest area of possible mixes for this study, several of these fly ashes were mixed to create base materials with reactive SiO_2, reactive Al_2O_3, and CaO contents between those listed in Table 5.1. The critical properties of the base materials created and used for this study are listed in Table 5.2.

Table 5.2 – Critical Properties of Selected Base Materials

Fly Ash	Fly Ash Mix	R. SiO_2 (% wt.)	R. Al_2O_3 (% wt.)	CaO (% wt.)	Na_2O (% wt.)
High Ca 1	-	7.82	12.84	27.00	2.18
High Ca 2	-	11.13	8.42	23.67	2.00
Low Ca 2	-	9.52	3.76	1.89	0.60
Mixed High Ca	75%HC2 + 25%LC1	11.73	7.43	18.20	2.34
Mixed Low Ca 1	50%HC4 + 50%LC2	10.50	6.25	12.70	1.19
Mixed Low Ca 2	33%HC2 + 67%LC2	10.05	5.30	9.08	1.06
Mixed Low Ca 3	50%HC3 + 50%LC2	11.10	6.93	12.68	1.18
Mixed Low Ca 4	25%HC2 + 75%LC2	9.92	4.93	7.34	0.95

As Table 5.2 shows, the mixed fly ashes capture the critical properties between the extremes of the individual fly ashes obtained. Due to limited quantities of some available fly ashes, different sets of fly ashes were used for the set time testing and the compressive strength testing. The base materials used for the set time testing were High Calcium 1, Low Calcium 2, Mixed High Calcium, Mixed Low Calcium 2, Mixed Low Calcium 3, and Mixed Low Calcium 4. The base materials used for the compressive strength testing were High Calcium 2, Low Calcium 2, Mixed High Calcium, Mixed Low Calcium 1, and Mixed Low Calcium 2.

5.2 Set Time Models

In total 181 mixes were designed, cast, and tested to serve as a base for developing the set time models. Of these 181 mixes, 57 exhibited normal behavior, 52 exhibited flash set behavior, and 72 exhibited long set behavior. A summary of all the mixes is given in Table B.3 in Appendix B. Note that mix T1044 was dry and did not form a paste so is not included in the results.

It was determined during the course of testing that there existed a need to predict when mixes would exhibit flash set behavior. For this study, flash set behavior was said to occur when the mix had an initial set less than 10 minutes as determined by the Vicat test described in Section 4.4.2. For the model development, flash set behavior was assigned a 0 value and normal mix behavior was assigned a 1 value. Since this models objective was to solve for a binary output, a step function equation form was specified as the solutions equation form. This is shown in Equation 5.1 Where F is the resulting binary output, f is any function containing mathematical operations outlined in Table 4.3, and a, b, c, d, g are the normalized chemical composition variables.

$$F = \text{step}\big(f(a, b, c, d, g)\big) \qquad \text{Equation 5.1}$$

By specifying a step function equation form the mixes that would flash set are predicted by any negative value of the function f, and mixes exhibiting normal behavior are predicted by any positive value of the function f.

It was also decided that a general prediction of whether the mix would take a long or short time to set was needed. The cut off for a short set time was given as mixes that would set within 4 hours at room temperature, and a long set time was any mix that would take longer than 4 hours to set at room temperature. This model was set up similar to how the flash set model was by giving a short

set time a 0 value and a long set time a 1 value. A step function as shown in Equation 5.2 where L is the resulting binary output, and the other variables are the same as used in Equation 5.1.

$$L = \text{step}\big(f(a,b,c,d,g)\big) \qquad \text{Equation 5.2}$$

Similar to Equation 5.1, any negative value of the function f gives a prediction of short set and any positive value of the function f gives a prediction of long set.

5.2.1 Flash Set Model

The flash set predictive model was developed using the results from all the set time mixes as well as results from the compressive testing mixes that were different from the set time mixes. The 12 additional mixes developed for compressive testing that were used, two of which exhibited flash set behavior, are summarized in Table B.4 in Appendix B.

5.2.1.1 Flash Set Model Development

All preliminary model searches as outlined in Section 4.5.2 indicated that the most important variables to predict flash set were the H_2O, Na_2O, and CaO contents in the mix. Additionally, all preliminary model searches were converging on algebraic solutions. In order to reduce the computational cost of finding a final model, the final model search was limited to using the H_2O, Na_2O, and CaO variables, and only algebraic solution were considered. This search was run until the stopping criterion for the search was met. Table 5.3 shows the normalized variables used in developing the flash set model.

Table 5.3 – Normalized Variables Used in Flash Set Model Development

Variable	Normalized Variable
H_2O (% wt. of mix)	$a = 6 \cdot (H_2O - 0.14)$
Na_2O (% wt. of mix)	$b = 6 \cdot Na_2O$
CaO (% wt. of mix)	$d = 5 \cdot (CaO - 0.01)$
F	F

The final flash set prediction model is given in Equation 5.3.

$$F = step(4.861 \cdot a \cdot b - 0.1215 - d^3) \qquad \text{Equation 5.3}$$

As this equation indicates, the CaO content is the main controlling factor for flash set in geopolymer pastes. This is not surprising since the CaO content has been shown to have a significant impact on the set time of a mix as discussed in Section 3.1.1, and calcium is the main factor for flash set in ordinary portland cement based products [41].

Equation 5.3 also indicates that H_2O and Na_2O in the mix inhibit flash set of geopolymers. More H_2O in the mix will impede the network formation thereby slowing it down. In addition to this, a mix with more Na_2O will have a higher initial concentration of OH^- ions in the solution which are available to break bonds in the base material as discussed in Section 2.1. The higher concentration of OH^- ions will cause the dissolution rate to be faster thus reducing the risk of the rapid network formation associated with flash set. Due to these considerations, the form of the flash set equation found agrees with the current knowledge of the geopolymer formation process.

Substituting the real variables back in to Equation 5.3 gives the prediction that flash set will occur when the condition in Equation 5.4 is met.

$$0.01 + \frac{(175 \cdot H_2O \cdot Na_2O - 24.5 \cdot Na_2O - 0.1215)^{1/3}}{5} < CaO \qquad \text{Equation 5.4}$$

The final flash set model predicts the correct behavior of the mix for 87% of the 193 mixes used to development the model.

5.2.1.2 Flash Set Model Validation

After the flash set model had been developed, ten additional validation mixes mostly using fly ashes not used for the development of the model were subjected to set time testing. This was done to ensure the model was able to predict flash set for mixes other than those used in developing the model. These mixes were tested in the same way the mixes used to develop the model were. A summary of the validation mix properties is given in Table A.3 in Appendix A with the critical properties for flash set reproduced in Table 5.4 along with the testing results.

Table 5.4 – Summary of Flash Set Model Validation Results

Mix	Fly Ash	Critical Properties (% wt. of Mix)			Mix Behavior Prediction	Actual Mix Behavior
		H_2O	Na_2O	CaO		
V0301	Low Ca 2	24.98	8.00	1.26	Normal	Normal
V0402	High Ca 5	22.95	10.00	17.23	Normal	Normal
V0660	Low Ca 1	22.00	10.99	1.18	Normal	Normal
V0708	Mixed Low Ca 2	23.56	6.37	6.18	Normal	Normal
V0962	High Ca 6	16.85	4.36	13.80	Flash Set	Flash Set
V1119	High Ca 6	16.43	10.21	12.79	Normal	Normal
V1164	High Ca 6	16.52	8.88	13.08	Normal	Normal
V1190	High Ca 6	16.77	5.80	13.35	Flash Set	Flash Set
V1194	High Ca 6	16.60	7.49	13.39	Flash Set	Normal
V1289	High Ca 6	16.69	7.15	12.94	Normal	Normal

As indicated in Table 5.4, the set behaviors for 9 of the 10 validation mixes were correctly predicted. It is noteworthy that mix V1194 which was predicted incorrectly had an initial set of only 18 minutes. Thus, although the model predicted the behavior incorrectly, the mix was not far from the 10 minute threshold that was set. These results are further proof that in addition to agreeing with the current knowledge of set behavior in geopolymers, the model is also able to accurately predict experimental results.

5.2.2 Long Set Prediction Model

The long set behavior predictive model was developed using results from all the set time testing given in Table B.3 in Appendix B.

5.2.2.1 Long Set Model Development

The preliminary model searches as outlined in Section 4.5.2 indicated that the most important variables to predict long set were the H_2O, Na_2O, reactive SiO_2, and CaO contents in the mix. Additionally, all preliminary model searches were converging on algebraic solutions. In order to reduce the computational cost of finding a final model, the final model search was limited to using the H_2O, Na_2O, reactive SiO_2, and CaO variables, and only algebraic solution were considered. This search was run until the stopping criterion for the search was met. Table 5.5 shows the normalized variables used in developing the long set model.

Table 5.5 – Normalized Variables Used in Long Set Model Development

Variable	Normalized Variable
H_2O (% wt. of mix)	$a = 6 \cdot (H_2O - 0.14)$
Na_2O (% wt. of mix)	$b = 6 \cdot Na_2O$
Reactive SiO_2 (% wt. of mix)	$c = 6 \cdot R.SiO_2$
CaO (% wt. of mix)	$d = 5 \cdot CaO$
L	L

The final long set prediction model is given in Equation 5.5.

$$L = step(1.412 + a^2 - 2.208 \cdot c - d) \quad \text{Equation 5.5}$$

As this equation indicates, the final long set model search converged on a solution that did not need the Na_2O content in the mix to make a good prediction. Additionally, from Equation 5.5 it is seen that the factor responsible for long set times is the H_2O content in the mix. This is because excess H_2O in the system impedes network formation thereby increasing the set time.

These results also indicate the CaO content is a contributing factor for the set time of geopolymer pastes which is in agreement with published works as discussed in Section 3.1.1. As indicated in Equation 5.5 as well as the literature, higher CaO contents generally result in shorter set times. In addition to higher CaO contents resulting in shorter set times, Equation 5.5 shows that higher reactive SiO_2 contents also result in shorter set times. This indicates that the network formation proceeds at a faster rate when there is a higher amount of reactive SiO_2 in the system. It is interesting to note that the reactive SiO_2 content plays a larger role in determining if a mix will have a short set time than the CaO content in the mix does.

Substituting the real variables back in to Equation 5.5 gives the prediction that long set will occur when the condition in Equation 5.6 is met.

$$0.14 + \frac{\sqrt{13.25 \cdot R.SiO_2 + 5 \cdot CaO - 1.412}}{6} < H_2O \quad \text{Equation 5.6}$$

In Equation 5.6 it is important to note that when the square root term is negative, the model prediction is that long set occurs. The final long set model predicts the correct behavior of the mix for 85% of the 181 mixes used to development the model.

5.2.2.2 Long Set Model Validation

After the long set model had been developed, ten additional validation mixes mostly using fly ashes not used for the development of the model were subjected to set time testing. This was done to ensure the model was able to predict long set for mixes other than those used in developing the model. These mixes were tested in the same way the mixes used to develop the model were. A summary of the validation mix properties is given in Table A.3 in Appendix A with the critical properties for long set reproduced in Table 5.6 along with the testing results.

Table 5.6 – Summary of Long Set Model Validation Results

Mix	Fly Ash	Critical Properties (% wt. of Mix)			Mix Behavior Prediction	Actual Mix Behavior
		H_2O	R. SiO_2	CaO		
V0301	Low Ca 2	24.98	7.27	1.26	Long Set	Long Set
V0402	High Ca 5	22.95	8.17	17.23	Short Set	Short Set
V0660	Low Ca 1	22.00	11.68	1.18	Long Set	Long Set
V0708	Mixed Low Ca 2	23.56	9.59	6.18	Long Set	Long Set
V0962	High Ca 6	16.85	12.12	13.80	Short Set	Short Set
V1119	High Ca 6	16.43	11.52	12.79	Short Set	Short Set
V1164	High Ca 6	16.52	11.37	13.08	Short Set	Short Set
V1190	High Ca 6	16.77	12.90	13.35	Short Set	Short Set
V1194	High Ca 6	16.60	11.19	13.39	Short Set	Short Set
V1289	High Ca 6	16.69	13.62	12.94	Short Set	Short Set

As indicated in Table 5.6, the behaviors for all of the validation mixes were correctly predicted. These results are further proof that the model is also able to accurately predict experimental results.

5.3 Compressive Strength Model

In total 90 mixes were designed, cast, cured, and tested to serve as a base for developing the compressive strength models. The air content testing used as quality assurance for the compressive strength testing showed that all mixes had around 10% to 15% air when cast, and generally lost about 1%-3% H_2O during the curing regime. No mixes were significantly outside of this range, so all mixes were considered to be properly cast. The results from this testing as well as the cured material densities of each mix can be found in Table B.5 in Appendix B. Mixes that did not gain strength as well as mixes which flash set or were dry are not included in this table.

For the compressive strength model development, the equation form for the model was specified so that only positive compressive strength outputs were possible in the data range considered. The equation form used is shown by Equation 5.7.

$$NS = f(a,b,c,d,g) + 0 \cdot \log\big(f(a,b,c,d,g)\big) \qquad \text{Equation 5.7}$$

In Equation 5.7, NS represents the normalized strength, f is any function containing mathematical operations specified in Table 4.3, and a,b,c,d,g are the normalized chemical composition variables. The purpose of the $0 \cdot log\big(f(a,b,c,d,g)\big)$ term in Equation 5.7 is to force solutions containing only positive values. The Eureqa software assigns not a number (NaN) results as having infinite error. Since the logarithm of a negative number is NaN, any function found containing one negative solution will be assigned infinite error and thus will be discarded from the base expression set. For functions that remain positive, the logarithm of the function will not be in the evaluated expression since it is multiplied by 0.

5.3.1 Compressive Strength Testing Results

A summary of the results from the compressive testing is given in Table B.6 in Appendix B. Note that mixes C6902 and C6909 exhibited flash set behavior, and mixes C6903 and C6907 were dry and did not form a paste so these are not included in the results. The mixes are listed in order from the lowest compressive strength to the highest, and the co.

As indicated in Table B.6 in Appendix B, the highest strength achieved was 15 ksi. In general, the mixes with lower strengths tend to have higher H_2O contents, and the mixes with higher strengths tend to have lower H_2O contents. It was also found that mixes with high and low calcium contents can be used to obtain any strength, so there is no obvious relationship between calcium content and strength. In order to determine the critical parameters for strength development in geopolymers as well as the basic format of the relationship, the parameters under consideration were normalized and subjected to genetic programming as outlined in Section 4.5.2.

5.3.2 Model Selection

The three preliminary model searches all indicated that the variables which influence the strength the most are the amounts of H_2O, Na_2O, and reactive SiO_2 in the mix. In addition to this, the trigonometric model search was converging on the same solution as the exponential model search.

For these reasons, the final model search was limited to the algebraic and exponential models. In order to reduce the computational cost of finding the final models, the variables for these searches were limited to the amounts of H_2O, Na_2O, and reactive SiO_2 in the mix. These searches were run until the stopping criterion was met. Table 5.7 shows the normalized variables used in developing the strength models. These variables can be substituted back into Equation 5.8 and Equation 5.9 to use the models for actual mix design values.

Table 5.7 – Normalized Variables Used in Strength Model Development

Variable	Normalized Variable
H_2O (% wt. of mix)	$a = 6 \cdot (H_2O - 0.14)$
Na_2O (% wt. of mix)	$b = 6 \cdot Na_2O$
Reactive SiO_2 (% wt. of mix)	$c = 10 \cdot (R.SiO_2 - 0.07)$
Strength (ksi)	$NS = \frac{7}{100} \cdot S$

The final normalized algebraic model found is expressed by Equation 5.8 which had a mean absolute error of 0.0762 (corresponds to 1.09 ksi).

$$NS = \frac{0.08256 \cdot b^3 + b^3 \cdot c}{0.07596 \cdot c^2 + 0.08256 \cdot b^3 + a \cdot b^3 + 5.926 \cdot b^7 \cdot c} \quad \text{Equation 5.8}$$

The final normalized exponential model found is expressed by Equation 5.9 which had a mean absolute error of 0.0617 (corresponds to 0.88 ksi).

$$NS = 0.7893 \cdot \exp\left(0.3866 \cdot c - \frac{0.2379 \cdot a}{b^2} + \frac{2.19 \cdot a \cdot b \cdot c}{c^2 + 1.267 \cdot b^2 - 0.3452 \cdot c} - 4.726 \cdot a \cdot b^2\right) \quad \text{Equation 5.9}$$

The properties of both of these models in their non-normalized representations are explored in detail in the following sections.

5.3.2.1 Model Predictions & Limits

In order to investigate how well the algebraic and exponential models predict the compressive strengths for the various mix designs, the model predictions were plotted against the experimentally observed strengths. These plots are shown in Figure 5.1.1 for the algebraic model and 5.1.2 for the exponential model. Both models predictions for individual mixes and the critical variables in those mixes are given in Table B.6 in Appendix B.

1.

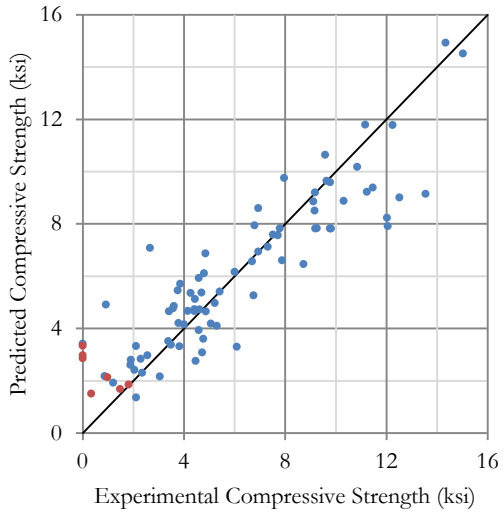

2.

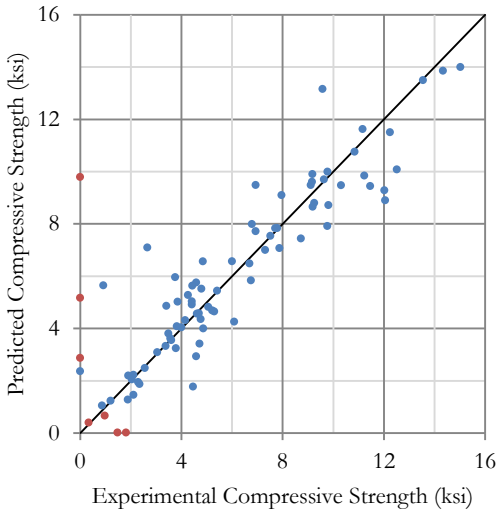

Figure 5.1 – Predicted vs. Experimental Comp. Strengths of (1) Alg. Model (2) Exp. Model

Upon inspection of the mixes that did not gain strength, it was found that they all had very low Na_2O contents. This is most likely the result of there not being sufficient Na_2O in the mix to dissolve the reactive SiO_2 and make it available to form the aluminosilicate network. As a result, a lower limit of 3% wt. Na_2O in the mix was placed on the models. The mixes with below this content of Na_2O are shown in red in Figure 5.1.1 and Figure 5.1.2. It is evident that neither model was able to capture this behavior which is likely because only mixes that gained strength were considered for the model development. In addition to this it is very unusual to have a Na_2O content in any practical mix greater than about 15% wt. of the mix as discussed in Section 4.3.3. Due to this, an upper limit for a Na_2O content of 15% wt. of the mix exists for these models.

Looking at Table B.6 in Appendix B shows the range of reactive SiO_2 used to develop these models was between about 7% wt. and 18% wt. of the mix. It is possible that different fly ashes could contain smaller or larger amounts of reactive SiO_2 in them allowing for lower or higher quantities of reactive SiO_2 in the mix. However, due to the large number of base materials tested for use in this study, reactive SiO_2 quantities substantially exceeding the limits found in this study using procedures outlined in Section 4.4.2 are unlikely. Due to this, the model limits for the reactive SiO_2 content in the mix are between 7% wt. and 18% wt. of the mix.

In developing these models, the water content of the mix designs was limited to between about 14% wt. and 30% wt. total H_2O in the mix. Experimental observations showed that the majority of mixes below 14% wt. H_2O were excessively dry and could not combine to form a paste. Additionally, mixes containing above about 30% wt. H_2O rarely showed notable strength development. This conclusion is verified from inspecting Table B.6 in Appendix B and noting that only two mixes with around 30% wt. H_2O contain strengths greater than about 2 ksi (C1052 with a strength of 4.41 ksi and C3041 with a strength of 4.86 ksi). Thus, although these models use is restricted to H_2O contents between 14% wt. and 30% wt., this range covers all practical mixes.

From Figure 5.1.1 and Figure 5.1.2 it is clear that the majority of the mixes created had strengths between 2 ksi and 13 ksi. Very few mixes had strengths outside of this range, and the majority of design applications will call for strengths within this range. Furthermore, it was observed that sodium based geopolymer mixes exceeding 13 ksi were extremely cohesive and would likely present substantial difficulties in any general casting or commercial fabrication processes using them. Due to practical considerations and the uncertainty of the models behavior outside of this range, a lower limit of 2 ksi and upper limit of 13 ksi is recommended for either models use.

5.3.2.2 Model Strength Predictions for Constant H_2O Contents in the Mix

Strength maps for low, medium, and high H_2O contents as a function of the Na_2O and reactive SiO_2 contents are shown in Figure 5.2 for the algebraic model and Figure 5.3 for the exponential model.

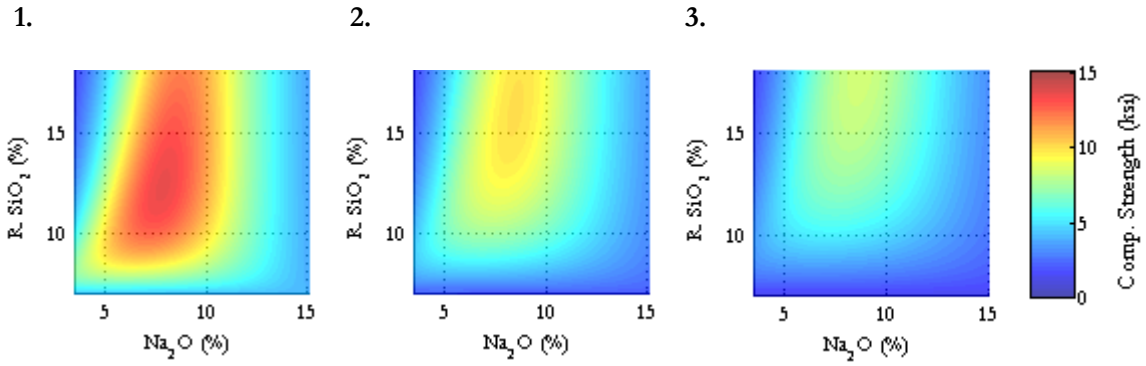

Figure 5.2 – Strength Map of Alg. Model for (1) 17.5% H_2O (2) 22.5% H_2O (3) 27.5% H_2O

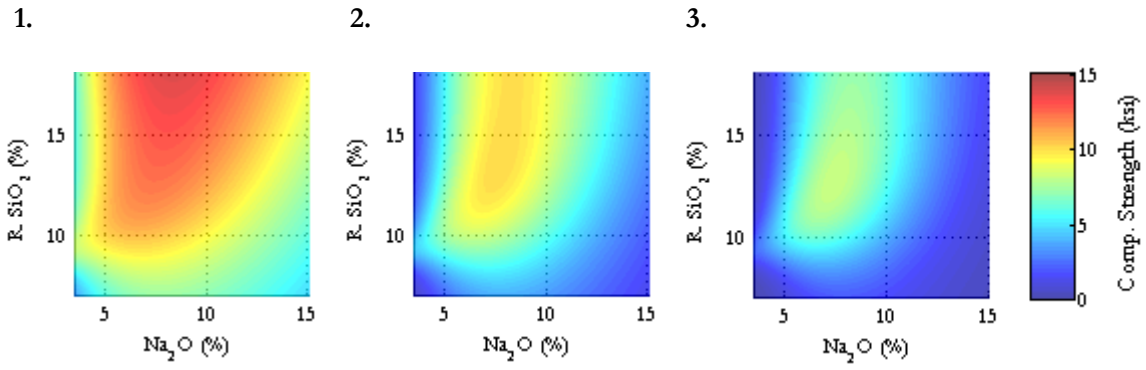

Figure 5.3 – Strength Map of Exp. Model for (1) 17.5% H_2O (2) 22.5% H_2O (3) 27.5% H_2O

Both Figure 5.2 and Figure 5.3 indicate that there exists a minimal amount of Na_2O needed to dissolve the optimal quantity of reactive SiO_2 in the mix. This is evident from the gradual increase to a maximum strength as the Na_2O content in the mix increases. Beyond this optimal point, the excess Na_2O in the mix will inhibit strength development. This is likely due to the excess Na_2O in the system reducing the average chain length in the aluminosilicate network.

As the quantity of reactive SiO_2 in the mix increases, a proportionally larger quantity of Na_2O would be required to shorten the chain length an equal amount. This is shown very well in Figure 5.3 as indicated by the contours beyond the optimal point being at an angle. From looking at Figure 5.2, it is seen that the algebraic model does not pick up this behavior since the contours after the optimal point are vertical. Thus the exponential model is able to pick up on the expected behavior of the system better than the algebraic model is.

5.3.2.3 Model Strength Predictions for Constant Na_2O Contents in the Mix

Strength maps for low, medium, and high Na_2O contents as a function of the H_2O and reactive SiO_2 contents are shown in Figure 5.4 for the algebraic model and Figure 5.5 for the exponential model.

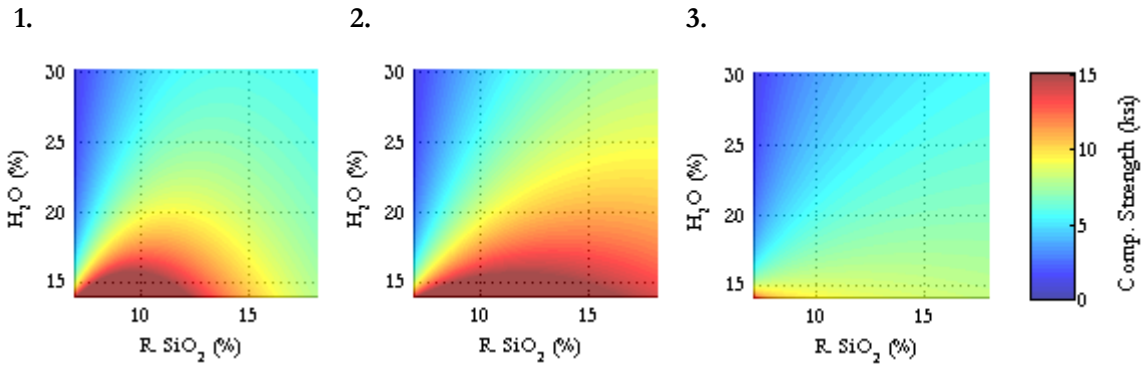

Figure 5.4 – Strength Map of Alg. Model for (1) 6% Na_2O (2) 9% Na_2O (3) 12% Na_2O

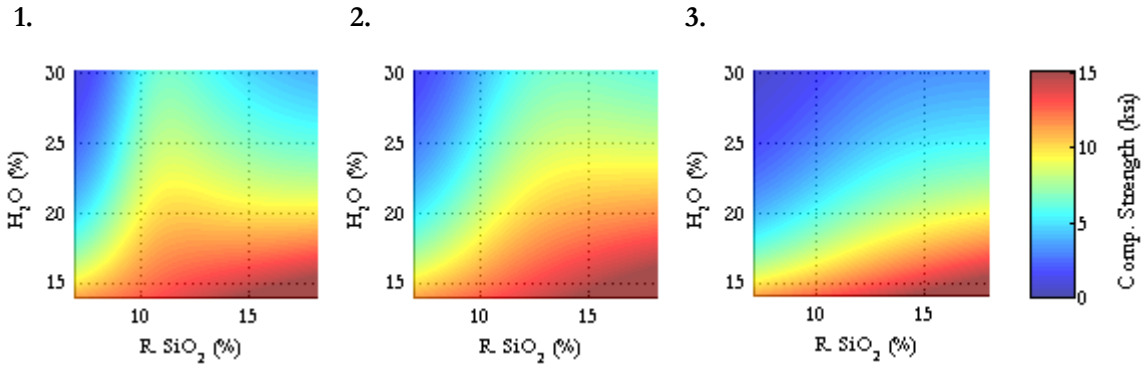

Figure 5.5 – Strength Map of Exp. Model for (1) 6% Na_2O (2) 9% Na_2O (3) 12% Na_2O

Both Figure 5.4 and Figure 5.5 Clearly show that with all other factors held constant, as the H_2O content in the mix increases, the strength decreases. This is a well established fact as discussed in Section 3.2.2. The peak around 11% wt. reactive SiO_2 shown in Figure 5.5.1 that moves to higher reactive SiO_2 concentrations at higher Na_2O concentrations is further illustration of the expected behavior beyond the optimum as previously discussed.

Another important difference between these two models that is clearly illustrated by comparing Figure 5.4 with Figure 5.5 is that the optimal reactive SiO_2 content is predicted to be at between about 8% wt. and 12% wt. depending on the Na_2O concentration for the algebraic model and at the highest possible amount of reactive SiO_2 for all Na_2O concentrations with the exponential model. As discussed in Section 3.2.3, there is near universal agreement that higher reactive SiO_2 contents produce mixes with higher strengths, thus the behavior of the exponential model is in better agreement with the expected behavior.

5.3.2.4 Model Behaviors at Low Strengths

The predicted mix designs of the algebraic model for a 3 ksi mix are shown in Figure 5.6.1 and Figure 5.6.2, and the predicted mix designs of the exponential model for a 3 ksi mix are shown in Figure 5.7.1 and Figure 5.7.2.

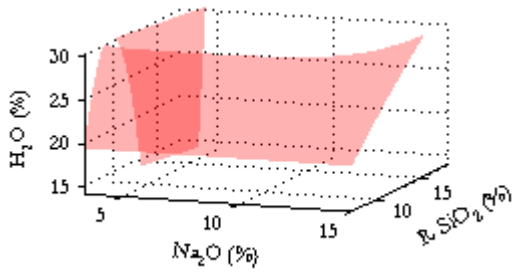

Figure 5.6.1 – 3 ksi Alg. Behavior

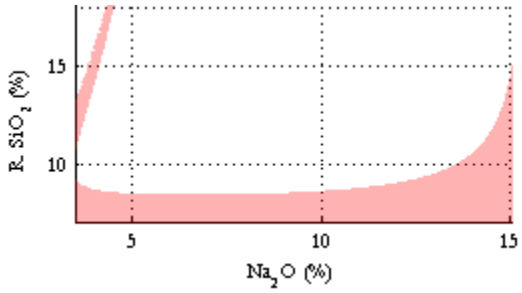

Figure 5.6.2 – 3 ksi Alg. R. SiO_2 vs. Na_2O

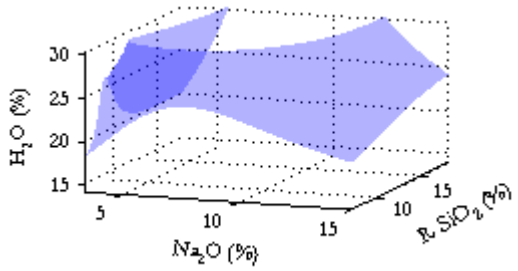

Figure 5.7.1 – 3 ksi Exp. Behavior

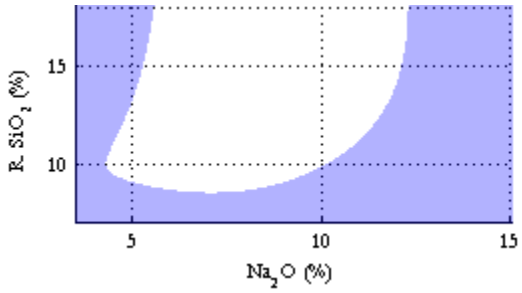

Figure 5.7.2 – 3 ksi Exp. R. SiO_2 vs. Na_2O

The algebraic model behavior in Figure 5.6.1 indicates that a 3 ksi compressive strength can be obtained for any water content in the practical mix range while the exponential model behavior in Figure 5.7.1 indicates that the water content must be greater than about 19%. Mixes C3231 and C2041 which both have strengths around 3 ksi and contain 22.41% H_2O and 29.89% H_2O respectively verify that this strength can be obtained for a wide range of water contents. Inspection of Table B.6 in Appendix B shows that the first mix to have a water content notably lower than 19% is C6131 with 15.10% H_2O which had a strength of 9.16 ksi. Thus the exponential models behavior with respect to water content in the mix at low strengths matches more closely with experimental observations than the algebraic models behavior.

When the possible range for the reactive SiO_2 and Na_2O contents in the mix as shown in Figure 5.6.2 and Figure 5.7.2 are compared, it is evident that the range of possible mixes at low strengths predicted by the algebraic model is much more restrictive. This indicates that although it is possible to develop mixes with low strengths in the practical mix range with the algebraic model, it is very difficult. Although there are some mixes such as C3032 with 4.96% Na_2O and 14.65% reactive SiO_2 that fall outside of the algebraic prediction range but within the exponential prediction range, no absolute conclusions can be made regarding which model is better at lower strengths based on the reactive SiO_2 and Na_2O contents in the mix.

5.3.2.5 Model Behaviors at Moderate Strengths

The range of mixes predicted by the algebraic model at a moderate strength of 7 ksi is shown in Figure 5.8.1 and Figure 5.8.2, and the range of mixes predicted by the exponential model at a moderate strength of 7 ksi is shown in Figure 5.9.1 and 5.9.2.

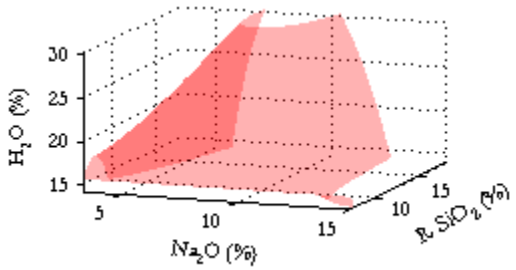

Figure 5.8.1 – 7 ksi Alg. Behavior

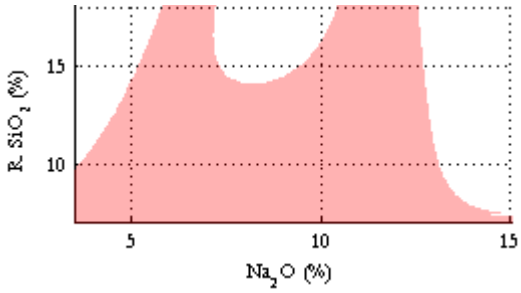

Figure 5.8.2 – 7 ksi Alg. R. SiO_2 vs. Na_2O

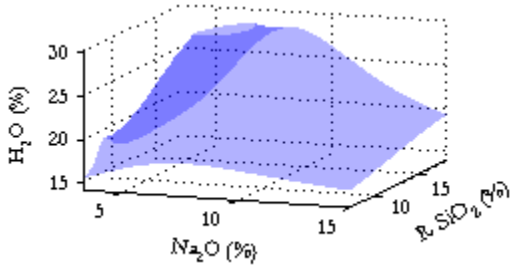

Figure 5.9.1 – 7 ksi Exp. Behavior

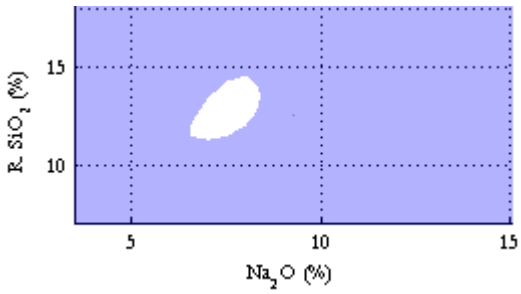

Figure 5.9.2 – 7 ksi Exp. R. SiO_2 vs. Na_2O

Both Figure 5.8.1 and Figure 5.9.1 indicate that for any water content in the practical range a 7 ksi mix can be developed, but there is a smaller range of possible mixes for a higher water content.

Mixes C2014 and C3031 with 18.84% H_2O and 26.24% H_2O respectively validate that a 7 ksi mix can be developed for any practical water content..

Similar to the low strength behavior, at moderate strengths the exponential model predicts a larger range of possible mix designs with respect to Na_2O and reactive SiO_2 contents than the algebraic model. No experimental mixes fell outside of the more restrictive algebraic models range, so both of these behaviors are reasonable.

5.3.2.6 Model Behavior at High Strengths

The behavior at a high strength of 11 ksi for the algebraic model is shown in Figure 5.10.1 and Figure 5.10.2, and for the exponential model is shown in Figure 5.11.1 and Figure 5.11.2.

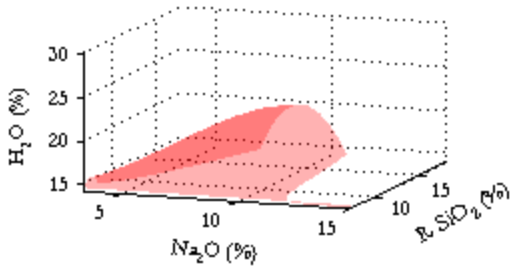

Figure 5.10.1 – 11 ksi Alg. Behavior

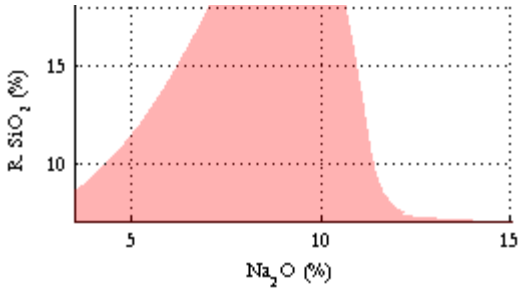

Figure 5.10.2 – 11 ksi Alg. R. SiO_2 vs. Na_2O

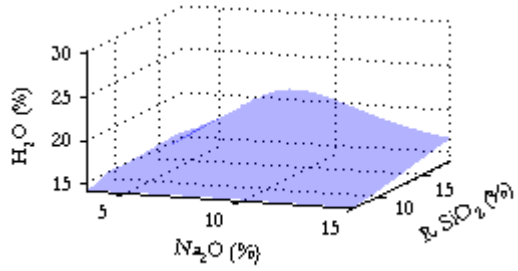

Figure 5.11.1 – 11 ksi Exp. Behavior

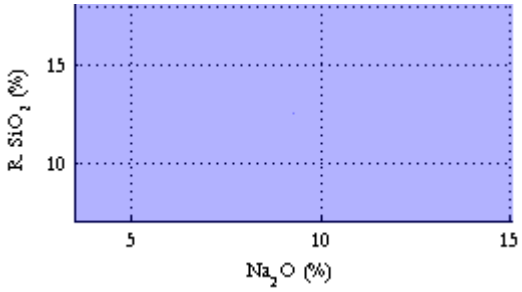

Figure 5.11.2 – 11 ksi Exp. R. SiO_2 vs. Na_2O

Both Figure 5.10.1 and Figure 5.11.1 show that in order to achieve higher strengths, a lower water content is required. The algebraic model predicts that no more than about 20% H_2O can be used for a mix with a compressive strength of 11 ksi, while the exponential model predicts that no more than about 21% H_2O can be used for a mix with a compressive strength of 11 ksi. Mixes C2051, C2024,

C1222, and C6911 all have around 22.5% H_2O with strengths just greater than 11 ksi which indicates that both of the models predict water limits a little low. Both of the models do however have reasonable limits that correlate well with the experimental observations.

Similar to the low and moderate strength behaviors, the exponential model allows for a wider range of Na_2O and reactive SiO_2 combinations than the algebraic model does. Not enough high strength mixes were created to conclusively eliminate one model based on this factor alone. However, both models do predict that as the strength increases, the possible range of Na_2O and reactive SiO_2 becomes more restricted.

5.3.2.7 Final Model Selection

Based on the analysis of both the algebraic and exponential models previously outlined, the model which was selected as the one that picks up the best on the experimental as well as expected behavior is the exponential model. The reasons for selecting this model over the algebraic model were:

1. The exponential model captures the behavior of the mix beyond the optimal Na_2O point. This model indicates that a larger reactive SiO_2 content requires a proportionally larger Na_2O content to reduce the chain length and thereby reduce the strength. (Section 5.2.2.2)

2. The exponential model indicates that the maximum strength for any base material will be obtained at some point where the reactive SiO_2 content is maximized. This is in agreement with several published studies. (Section 5.2.2.3 & Section 3.2.3)

3. The exponential model indicates that mixes with water contents lower than about 19% wt. will not produce mixes with strengths in the range of 3 ksi. This matches experimental results more closely than the algebraic model which allows for mixes with very low water contents to have strengths in the range of 3 ksi. (Section 5.2.2.4)

5.3.3 Exponential Model Validation

Once the exponential model was selected, validation mixes were created which were designed to obtain a variety of strengths using some of the fly ashes which were not used for the development of the model. These mixes were cast, cured, and tested in the same way the mixes used to develop the model were. A summary of the validation mix properties is given in Table A.3 in Appendix A with the critical properties for strength reproduced in Table 5.8 along with the testing results. A chart

showing the strength prediction of the exponential model compared to the experimental strength for all mixes in the range chosen as outlined in Section 5.2.2.1 is shown in Figure 5.12.

Table 5.8 – Summary of Exponential Model Validation Results

Mix	Fly Ash	Critical Properties (% wt. of Mix)			Design Str. (ksi)	Actual Str. (ksi)	Coefficient of Variation for 6 Cubes (%)
		H_2O	Na_2O	R. SiO_2			
V0301	Low Ca 2	24.98	8.00	7.27	3.01	2.10	10.16
V0402	High Ca 5	22.95	10.00	8.17	4.02	3.58	11.73
V0660	Low Ca 1	22.00	10.99	11.68	6.60	6.02	7.35
V0708	Mixed Low Ca 2	23.56	6.37	9.59	7.08	8.62	9.86
V1119	High Ca 6	16.43	10.21	11.52	11.19	9.60	8.43
V1164	High Ca 6	16.52	8.88	11.37	11.64	9.56	9.04
V1194	High Ca 6	16.60	7.49	11.19	11.94	12.29	14.13
V1289	High Ca 6	16.69	7.15	13.62	12.89	12.41	11.21

As indicated in Table 5.8, the exponential model was successful in predicting low and high strength validation mixes even when the fly ash used in the mix was not used to create the model.

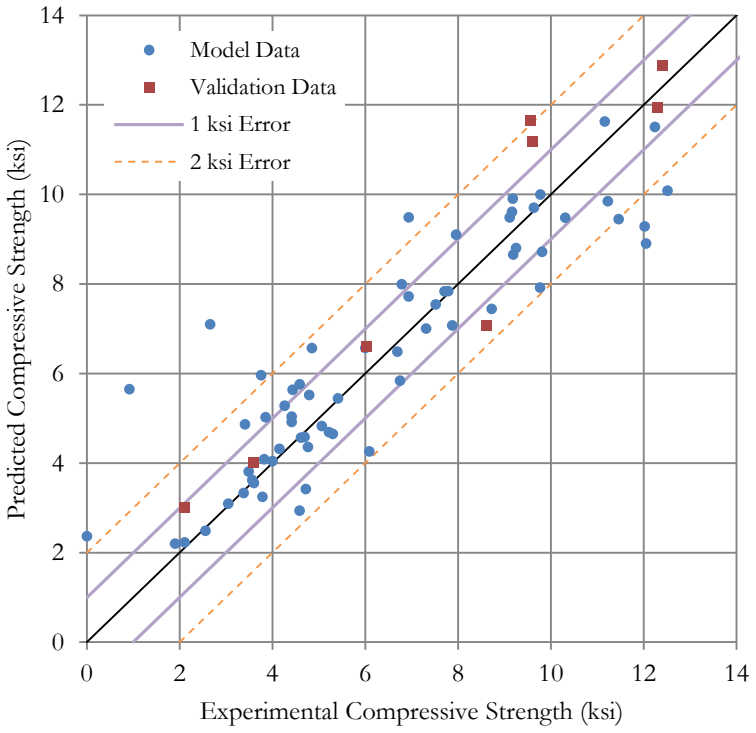

Figure 5.12 – Predicted vs. Experimental Compressive Strengths for Final Exp. Model

It is clear from Figure 5.12 that very few mixes have errors exceeding 2 ksi, and the majority of tested mixes fell within 1 ksi of the predicted value. Of the 73 mixes presented in Figure 5.12, 14% exceeded a 2 ksi difference from their predicted value with only 3 mixes exceeding it substantially. About 63% of the mixes were within 1 ksi of their predicted strength. The mean absolute error for the mixes in the recommended range of the model is 0.97 ksi. It is also important to note that the validation mixes were predicted with accuracy as good as the model development mixes. As a result, it is concluded that this model captures the behavior of any fly ash provided the mixes developed fall within the limits outlined in Section 5.2.2.1.

It has been shown that the exponential model presented can be used to provide a good starting point for the optimization of geopolymer mixes. To simplify the design of geopolymers using the exponential model, mix design tables were created and are given in Appendix C. The development of these tables as well as how they can be used in conjunction with the set time results is outlined in Chapter 6.

Chapter 6

Mix Design Using Final Models

6.1 Assumptions of Optimization Models Use

When using the generated models for mix design it is important to keep the assumptions the models makes and the limitations of the models in mind. The assumptions that the generated models make and limitations they have are as follows:

1. All generated models assume that the mix will not be dry or segregate. As long as the mix contains above 14% wt. H_2O and below 75% wt. fly ash, dry mixes will mostly be avoided. Additionally, as long as the recommended minimum fly ash content of 60% wt. is used, mixes that segregate will mostly be avoided.

2. The compressive strength model gives no indication of the workability of a mix. It is important to keep this in mind when trying to use the model in extremes such as when trying to obtain the highest possible strength. As discussed in Section 5.3.2.1, when strengths get near the maximum potential, the mix becomes very cohesive which may present difficulties in casting.

3. The performance of the set behavior and compressive strength models for mixes substantially outside the following range is unknown:

    a. 3% wt. < Na_2O < 15% wt.

    b. 7% wt. < Reactive SiO_2 < 18% wt.

    c. 14% wt. < H_2O < 30% wt.

    d. 2 ksi < Strength < 13 ksi

4. The compressive strength model assumes the mix has gained its maximum potential strength by the time it is tested. A suggested method for using the model when this is not the case is provided in Section 6.3.

5. One additional assumption that is made when using these models to design for products other than geopolymer pastes exists. This is that any materials such as fillers or reinforcement which will be incorporated into the cast product will be totally inert. If the materials incorporated into the matrix interact with the alkali activator, the strength and set behavior of the paste will not necessarily scale directly with those factors in the composite matrix. As long as these additional interactions are minor, composite strengths can be predicted from the model and use of the rule of mixtures.

6.2 Mix Design Tables

Due to the complexity of the generated models, tables have been developed to simplify the design of geopolymer mixes using the models. Strength design tables are provided in Table C.1 – Table C.12 in Appendix C. Additionally, a flash set prediction table is given in Table C.13 and a long set prediction table is given in Table C.14 in Appendix C.

The strength tables were developed using the design range the model is known to work within. The tables are provided in increments of 1 ksi strength and provide combinations of H_2O, Na_2O, and reactive SiO_2 that the model predicts will have the design table strength. Some variance from the mix design table strength and actual strength is expected due to variability of the material as well as some inherent error in the model. Due to this, these tables are intended to be used as a way to target the mix design of geopolymer pastes for optimization rather than as an absolute guarantee of a mixes average strength.

The flash set prediction table gives the maximum CaO content a mix can have without exhibiting flash set behavior for various H_2O and Na_2O combinations. The long set prediction table gives the minimum CaO content a mix needs to avoid long set for various H_2O and reactive SiO_2 combinations. An example of how the design tables can be used to target the testing area for an optimal mix is given in Section 6.4.

6.3 Mix Design Using Strength Model with Different Curing Conditions

Since the chemical mix design variables were determined to be mutually exclusive from the curing condition mix design variables as discussed in Section 4.3.5, it is expected that the compressive strength model can be scaled for use with any set of curing conditions. Thus, the recommended design procedure to use for curing conditions other than those used in this study is:

1. Follow the design process outlined in Section 6.4 to design a mix as if the curing conditions were the same as used in this study.

2. Cast, place, cure, and test the mix using the desired parameters.

3. If the tested mix has a strength outside of the mean absolute error of the model (about 1 ksi), determine the ratio of the predicted strength to the actual strength.

4. Multiply this ratio by the desired design strength to obtain a scaled design strength corresponding to the desired strength to use.

5. Follow the design process outlined in Section 6.4 to design a mix for the scaled design strength.

6.4 Design Example

To illustrate how to use the design tables provided in Appendix C, consider the following case. A company has materials to produce geopolymers with the properties given in Table 6.1. The design objective is to develop a geopolymer paste that has a strength of 6 ksi and a set time less than 4 hours.

Table 6.1 – Design Example Material Properties

Material	Critical Properties (% wt. of Mix)				Normalized Cost
	H_2O	Na_2O	R. SiO_2	CaO	
Fly Ash	0.00	1.77	11.47	23.51	4
Na Silicate	62.90	10.60	26.50	0.00	100
NaOH	24.85	75.15	0.00	0.00	68

From considering the practical fly ash range of 60% to 75% wt. of the mix the possible CaO range in the mix can be calculated:

$$CaO < 75\% \cdot 23.51\% \rightarrow CaO < 17.6\% \qquad \text{Equation 6.1}$$

$$CaO > 60\% \cdot 23.51\% \rightarrow CaO > 14.1\% \qquad \text{Equation 6.2}$$

Using the maximum CaO content in the mix determined in Equation 6.1, check the flash set table and note the H_2O-Na_2O combinations that will not work with the fly ash being used. The flash set table is reproduced in Table 6.2 with the H_2O-Na_2O combinations that are likely to result in flash set for the fly ash under consideration blocked out in dark red.

Table 6.2 –H_2O-Na_2O Mix Design Combinations to Avoid Flash Set in Design Example

		% wt. H_2O in Mix															
		15	**16**	**17**	**18**	**19**	**20**	**21**	**22**	**23**	**24**	**25**	**26**	**27**	**28**	**29**	**30**
% wt. Na_2O in Mix	**4**		6.29	9.91	11.82	13.23	14.37	15.34	16.19	16.96	17.66	18.31	18.91	19.48	20.01	20.51	20.99
	5		8.54	11.41	13.23	14.62	15.78	16.78	17.66	18.47	19.20	19.88	20.51	21.11	21.67	22.20	22.71
	6		9.91	12.57	14.37	15.78	16.96	17.99	18.91	19.75	20.51	21.22	21.88	22.51	23.10	23.66	24.19
	7	3.00	10.96	13.53	15.34	16.78	17.99	19.06	20.01	20.87	21.67	22.41	23.10	23.75	24.36	24.94	25.50
	8	6.29	11.82	14.37	16.19	17.66	18.91	20.01	20.99	21.88	22.71	23.47	24.19	24.86	25.50	26.11	26.69
	9	7.60	12.57	15.11	16.96	18.47	19.75	20.87	21.88	22.81	23.66	24.45	25.19	25.88	26.54	27.17	27.77
	10	8.54	13.23	15.78	17.66	19.20	20.51	21.67	22.71	23.66	24.53	25.34	26.11	26.83	27.51	28.16	28.78
	11	9.28	13.82	16.39	18.31	19.88	21.22	22.41	23.47	24.45	25.34	26.18	26.97	27.71	28.41	29.07	29.71
	12	9.91	14.37	16.96	18.91	20.51	21.88	23.10	24.19	25.19	26.11	26.97	27.77	28.53	29.25	29.94	30.59
	13	10.47	14.87	17.49	19.48	21.11	22.51	23.75	24.86	25.88	26.83	27.71	28.53	29.31	30.05	30.75	31.42
	14	10.96	15.34	17.99	20.01	21.67	23.10	24.36	25.50	26.54	27.51	28.41	29.25	30.05	30.80	31.52	32.21
	15	11.41	15.78	18.47	20.51	22.20	23.66	24.94	26.11	27.17	28.16	29.07	29.94	30.75	31.52	32.25	32.95

Using the minimum CaO content in the mix determined in Equation 6.2, check the long set table and note the H_2O-R. SiO_2 combinations that will not work with the fly ash being used. The long set table is reproduced in Table 6.3 with the H_2O-R. SiO_2 combinations that are likely to result in long set for the fly ash under consideration blocked out in dark blue.

Table 6.3 – H_2O-R. SiO_2 Design Combinations to Avoid Long Set in Design Example

% wt. R. SiO_2 in Mix	% wt. H_2O in Mix															
	15	16	17	18	19	20	21	22	23	24	25	26	27	28	29	30
7	9.76	9.98	10.34	10.84	11.49	12.28	13.22	14.30	15.52	16.89	18.40	20.06	21.86	23.80	25.89	28.12
8	7.11	7.33	7.69	8.19	8.84	9.63	10.57	11.65	12.87	14.24	15.75	17.41	19.21	21.15	23.24	25.47
9	4.46	4.68	5.04	5.54	6.19	6.98	7.92	9.00	10.22	11.59	13.10	14.76	16.56	18.50	20.59	22.82
10	1.81	2.03	2.39	2.89	3.54	4.33	5.27	6.35	7.57	8.94	10.45	12.11	13.91	15.85	17.94	20.17
11				0.24	0.89	1.68	2.62	3.70	4.92	6.29	7.80	9.46	11.26	13.20	15.29	17.52
12								1.05	2.27	3.64	5.15	6.81	8.61	10.55	12.64	14.87
13										0.99	2.50	4.16	5.96	7.90	9.99	12.22
14												1.51	3.31	5.25	7.34	9.57
15													0.66	2.60	4.69	6.92
16															2.04	4.27
17																1.62

These restrictions are now placed on the 6 ksi design table which is reproduced in Table 6.4 with the mixes likely to result in flash set blocked out in dark red and the mixes likely to result in long set blocked out in dark blue.

Table 6.4 – % wt. Reactive SiO_2 in Mix to Achieve 6 ksi for Fly Ash in Design Example

% wt. Na_2O in Mix	% wt. H_2O in Mix															
	15	16	17	18	19	20	21	22	23	24	25	26	27	28	29	30
4			7.74	8.33	8.71	9.04	9.49									
5				7.53	8.10	8.49	8.80	9.06	9.32	9.58	9.90					
6					7.52	8.03	8.40	8.70	8.95	9.17	9.38	9.58	9.77	9.96	10.18	10.42
7					7.14	7.77	8.21	8.56	8.86	9.11	9.34	9.55	9.75	9.94	10.12	10.31
8					7.04	7.75	8.26	8.68	9.02	9.33	9.60	9.86	10.10	10.33	10.57	10.81
9					7.20	7.98	8.57	9.06	9.48	9.86	10.21	10.56	10.90	11.26	11.65	12.11
10					7.61	8.47	9.16	9.75	10.29	10.81	11.34	11.91	12.59	13.62		
11					8.24	9.23	10.07	10.85	11.64	12.52	13.68	16.46				
12				7.69	9.12	10.31	11.44	12.64	14.20	17.35						
13				8.63	10.31	11.87	13.63	16.22								
14			7.39	9.81	11.91	14.25	17.78									
15			8.50	11.31	14.18											

In order to minimize the cost, the actual material quantities need to be calculated for the possible design combinations outlined in Table 6.4. Equation 6.3 – Equation 6.6 are now considered in order to calculate these quantities from the possible design combinations.

$$a_T = H \cdot a_H + S \cdot a_S + W \qquad \text{Equation 6.3}$$

$$b_T = F \cdot b_F + H \cdot b_H + S \cdot b_S \qquad \text{Equation 6.4}$$

$$c_T = F \cdot c_F + S \cdot c_S$$ Equation 6.5

$$100\% = F + H + S + W$$ Equation 6.6

Equation 6.3 calculates the total H_2O in the mix from the mix constituents. Equation 6.4 calculates the total Na_2O in the mix from the mix constituents. Equation 6.5 calculates the total reactive SiO_2 in the mix from the mix constituents. Equation 6.6 is simply a condition that all components in the mix must add up to 100% of the mix. The variables in these equations are summarized in Table 6.5.

Table 6.5 – Summary of Variables in Equation 6.3 – Equation 6.6

Variable	Description	Value
a_T	total H_2O in mix	from Table 6.4
b_T	total Na_2O in mix	from Table 6.4
c_T	total R. SiO_2 in mix	from Table 6.4
F	total fly ash in mix	unknown
H	total NaOH in mix	unknown
S	total Na silicate in mix	unknown
W	total additional H_2O in mix	unknown
a_H	H_2O in NaOH	24.85% (Table 6.1)
a_S	H_2O in Na silicate	62.90% (Table 6.1)
b_F	Na_2O in fly ash	1.77% (Table 6.1)
b_H	Na_2O in NaOH	75.15% (Table 6.1)
b_S	Na_2O in Na silicate	10.60% (Table 6.1)
c_F	R. SiO_2 in fly ash	11.47% (Table 6.1)
c_S	R. SiO_2 in Na silicate	26.50% (Table 6.1)

Solving Equation 6.3 – Equation 6.6 for S gives Equation 6.7.

$$S = \frac{c_T \cdot b_H + b_T \cdot c_F - c_T \cdot b_F + a_T \cdot b_H \cdot c_F - b_T \cdot a_H \cdot c_F + c_T \cdot a_H \cdot b_F - b_H \cdot c_F}{b_H \cdot c_S - b_H \cdot c_F + b_S \cdot c_F - b_F \cdot c_S - a_H \cdot b_S \cdot c_F + a_H \cdot b_F \cdot c_S + a_S \cdot b_H \cdot c_F}$$ Equation 6.7

Once S has been determined F, H, and W can be determined from substituting back into Equation 6.4 – Equation 6.6 and solving for the other unknowns. This gives Equation 6.8 – Equation 6.10.

$$F = \frac{c_T - S \cdot c_S}{c_F}$$ Equation 6.8

$$H = \frac{b_T - S \cdot b_S - F \cdot b_F}{b_H}$$ Equation 6.9

$$W = 100\% - (F + H + S)$$ Equation 6.10

With the quantities of mix constituents determined, the relative cost of each mix can be determined considering the normalized cost for each material given in Table 6.1. Calculations determining the mix constituents for all possible mixes outlined in Table 6.4 along with each mixes relative cost is given in Table 6.6. Mixes that are impossible as well as mixes with greater than 75% fly ash or less than 60% fly ash are blocked out in dark grey. The five mixes with the lowest relative cost are highlighted in light green.

Table 6.6 – Summary of Possible Mixes in Design Example

Critical Properties (% wt. of Mix)			Mix Constituents (% wt. of Mix)				Relative Cost of Mix
Na_2O	H_2O	R. SiO_2	Na Silicate	Fly Ash	NaOH	Water	
5	22	9.06	2.29	73.70	4.59	19.42	8.36
5	23	9.32	3.90	72.25	4.40	19.45	9.78
5	24	9.58	5.51	70.79	4.21	19.49	11.20
5	25	9.90	7.38	69.27	3.98	19.37	12.85
6	21	8.40	-0.53	74.46	6.31	19.77	6.74
6	22	8.70	1.25	72.96	6.09	19.70	8.31
6	23	8.95	2.82	71.52	5.90	19.76	9.69
6	24	9.17	4.26	70.11	5.73	19.90	10.96
6	25	9.38	5.65	68.72	5.57	20.06	12.19
7	20	7.77	-3.22	75.18	8.00	20.04	5.22
7	21	8.21	-0.84	73.52	7.70	19.62	7.34
7	22	8.56	1.15	71.97	7.46	19.42	9.10
7	23	8.86	2.93	70.47	7.24	19.36	10.68
7	24	9.11	4.50	69.03	7.05	19.42	12.06
7	25	9.34	5.98	67.61	6.88	19.53	13.36
8	19	7.04	-6.34	76.03	9.75	20.57	3.33
8	20	7.75	-2.81	74.05	9.30	19.46	6.48
8	21	8.26	-0.13	72.31	8.96	18.86	8.86
8	22	8.68	2.16	70.68	8.68	18.48	10.89
8	23	9.02	4.11	69.13	8.44	18.32	12.62
8	24	9.33	5.94	67.62	8.22	18.22	14.23
8	25	9.60	7.59	66.16	8.02	18.23	15.69
8	27	10.10	10.72	63.28	7.64	18.36	18.45
9	19	7.20	-5.16	74.69	10.94	19.52	5.27
9	20	7.98	-1.33	72.64	10.45	18.24	8.69
9	21	8.57	1.69	70.80	10.07	17.43	11.37
9	22	9.06	4.29	69.09	9.74	16.88	13.68
9	23	9.48	6.58	67.45	9.46	16.51	15.71
9	24	9.86	8.70	65.86	9.20	16.24	17.59
9	25	10.21	10.70	64.30	8.95	16.05	19.36

Critical Properties (% wt. of Mix)			Mix Constituents (% wt. of Mix)				Relative Cost of Mix
Na_2O	H_2O	R. SiO_2	Na Silicate	Fly Ash	NaOH	Water	
9	26	10.56	12.69	62.75	8.71	15.85	21.12
9	27	10.90	14.64	61.20	8.47	15.69	22.85
9	28	11.26	16.68	59.64	8.22	15.47	24.65
10	19	7.61	-2.91	73.06	12.00	17.85	8.17
10	20	8.47	1.27	70.92	11.46	16.36	11.89
10	21	9.16	4.71	68.97	11.02	15.30	14.96
10	22	9.75	7.73	67.14	10.63	14.49	17.65
10	23	10.29	10.54	65.36	10.28	13.82	20.14
10	24	10.81	13.26	63.61	9.94	13.19	22.56
10	25	11.34	16.02	61.85	9.59	12.54	25.02
10	26	11.91	18.96	60.04	9.22	11.79	27.63
10	27	12.59	22.36	58.10	8.78	10.75	30.66
10	28	13.62	27.26	55.76	8.15	8.83	35.03
11	19	8.24	0.28	71.18	12.92	15.61	11.92
11	20	9.23	5.01	68.89	12.31	13.79	16.14
11	21	10.07	9.10	66.77	11.78	12.35	19.78
11	22	10.85	12.93	64.72	11.29	11.06	23.20
11	23	11.64	16.81	62.66	10.79	9.75	26.65
11	24	12.52	21.06	60.49	10.24	8.21	30.45
11	25	13.68	26.52	58.00	9.53	5.95	35.32
11	26	16.46	38.90	53.64	7.89	-0.43	46.40
12	18	7.69	-2.07	71.82	14.57	15.68	10.71
12	19	9.12	4.54	69.02	13.70	12.74	16.62
12	20	10.31	10.13	66.49	12.97	10.41	21.61
12	21	11.44	15.45	64.04	12.28	8.23	26.36
12	22	12.64	21.08	61.50	11.55	5.87	31.39
12	23	14.20	28.24	58.55	10.61	2.60	37.80
12	24	17.35	42.20	53.77	8.75	-4.72	50.30
13	18	8.63	2.45	69.58	15.31	12.65	15.65
13	19	10.31	10.13	66.49	14.30	9.08	22.51
13	20	11.87	17.29	63.54	13.36	5.80	28.92
13	21	13.63	25.31	60.36	12.31	2.02	36.09
13	22	16.22	36.87	56.22	10.77	-3.87	46.45
14	17	7.39	-2.85	71.01	17.36	14.48	11.80
14	18	9.81	7.99	67.07	15.92	9.02	21.50
14	19	11.91	17.46	63.50	14.67	4.37	29.98
14	20	14.25	27.96	59.65	13.28	-0.88	39.37
14	21	17.78	43.54	54.43	11.21	-9.17	53.33
15	17	8.50	2.39	68.58	18.01	11.02	17.38
15	18	11.31	14.90	64.19	16.35	4.57	28.58
15	19	14.18	27.66	59.73	14.65	-2.04	40.01

When the 6 ksi design table is considered once more, there is a clear area where this company should target their mix design for this application. In Table 6.7 the five lowest cost mixes are highlighted in light green, mixes that are likely to flash set are blocked out in dark red, mixes that are likely to have long set are blocked out in dark blue, and mixes that are impossible or have fly ash quantities outside the design range are blocked out in dark grey.

Table 6.7 – % wt. Reactive SiO_2 in Mix for Optimal 6 ksi Mixes in Design Example

		% wt. H_2O in Mix															
		15	16	17	18	19	20	21	22	23	24	25	26	27	28	29	30
% wt. Na_2O in Mix	4			7.74	8.33	8.71	9.04	9.49									
	5				7.53	8.10	8.49	8.80	9.06	9.32	9.58	9.90					
	6					7.52	8.03	8.40	8.70	8.95	9.17	9.38	9.58	9.77	9.96	10.18	10.42
	7					7.14	7.77	8.21	8.56	8.86	9.11	9.34	9.55	9.75	9.94	10.12	10.31
	8					7.04	7.75	8.26	8.68	9.02	9.33	9.60	9.86	10.10	10.33	10.57	10.81
	9					7.20	7.98	8.57	9.06	9.48	9.86	10.21	10.56	10.90	11.26	11.65	12.11
	10					7.61	8.47	9.16	9.75	10.29	10.81	11.34	11.91	12.59	13.62		
	11					8.24	9.23	10.07	10.85	11.64	12.52	13.68	16.46				
	12				7.69	9.12	10.31	11.44	12.64	14.20	17.35						
	13				8.63	10.31	11.87	13.63	16.22								
	14			7.39	9.81	11.91	14.25	17.78									
	15			8.50	11.31	14.18											

Thus it has been shown that a targeted approach to mix design as outlined can be used to optimize mixes for specific applications using the models generated in this study.

Chapter 7

Conclusions & Future Work

7.1 Curing Time & Temperature Conclusions

This study determined that an appropriate curing regime can allow for the maximum potential of a mix to be realized in a day. More specifically, geopolymers cured at a temperature of 85°C for 24 hours will develop their full potential provided they are properly covered during curing. The majority of studies focusing on mechanical properties of geopolymers use their 7 day and 28 day strengths as measures. Waiting until 7 days or 28 days to determine the strength of a properly cured geopolymer is unnecessary. This finding has great benefit for future research done on mechanical properties of geopolymer products.

7.2 Flash Set Behavior Conclusions

The factors which determine if a mix will exhibit flash set behavior or not are the H_2O, Na_2O, and CaO contents in the mix. The CaO in the mix is responsible for the flash set while the H_2O and Na_2O contents in the mix both inhibit flash set. Through this study, a relationship between these factors was found which is that when the condition given by Equation 7.1 is met, flash set behavior is very likely to occur.

$$0.01 + \frac{(175 \cdot H_2O \cdot Na_2O - 24.5 \cdot Na_2O - 0.1215)^{1/3}}{5} < CaO \qquad \text{Equation 7.1}$$

This relationship is a key finding that makes the design of high calcium fly ash geopolymers much simpler.

7.3 Long Set Behavior Conclusions

The factors which determine if a mix will exhibit long set behavior (set times greater than 4 hours) are the H_2O, reactive SiO_2, and CaO contents in the mix. An excessive quantity of H_2O in a mix is what causes the set time to be very long. Conversely, excessive quantities of CaO and reactive SiO_2 in a mix cause the set time to be very short. The relationship found between these parameters is that when the condition given by Equation 7.2 is met, long set behavior is very likely to occur.

Additionally, if the square root term in Equation 7.2 is negative, long set behavior is very likely to occur.

$$0.14 + \frac{\sqrt{13.25 \cdot R.SiO_2 + 5 \cdot CaO - 1.412}}{6} < H_2O \qquad \text{Equation 7.2}$$

This relationship also serves as a key finding which can be used to target mix designs if long or short set times are desired. It was also determined that the reactive SiO_2 content plays a larger role in short set than the CaO content. The reactive SiO_2 content playing any role in the set time of geopolymers is a novel finding not studied in any of the literature reviewed.

7.4 Compressive Strength from Mix Design

The chemical property factors responsible for strength gain in geopolymers are the H_2O, Na_2O, and reactive SiO_2 contents in the mix. This study determined that the CaO content in the mix does not have a substantial impact on the strength development. Thus it can be reasonably concluded that the formation of the aluminosilicate networks in geopolymers is more favorable than the formations of C-S-H phases. The predictive model for determining the maximum potential strength a geopolymer mix can have is given by Equation 7.3.

$$NS = 0.7893 \cdot \exp\left(0.3866 \cdot c - \frac{0.2379 \cdot a}{b^2} + \frac{2.19 \cdot a \cdot b \cdot c}{c^2 + 1.267 \cdot b^2 - 0.3452 \cdot c} - 4.726 \cdot a \cdot b^2\right) \qquad \text{Equation 7.3}$$

Where $a = 6 \cdot (H_2O - 0.14)$, $b = 6 \cdot Na_2O$, $c = 10 \cdot (R.SiO_2 - 0.07)$, and $NS = \frac{7}{100} \cdot S\ (ksi)$. This predictive model can be used for any mix with a H_2O content between 14% and 30% wt., a Na_2O content between 3% and 15% wt., a reactive SiO_2 content between 7% and 18% wt., and a strength between 2 and 13 ksi. Mix design tables were developed with Equation 7.3 to simplify the design of mixes using it in conjunction with the set behavior models. This is the first strength model to be developed which is general enough to be used for any fly ash base material. It is likely that this model will also work for other similar base materials such as GGBFS.

7.5 Suggestions for Future Work

Although this study succeeded in developing a vital design tool for developing geopolymer mixes, there is potential to increase the usefulness of the developed models. Targeted studies of how the model can be modified to work when specific fillers such as course and fine aggregates are added

into the mix would provide even more useful tools for industry. Additionally, it would be useful to know how the model can be modified to work with curing conditions other than those used in this study. It is expected that both the addition of fillers and different curing regimes would simply scale the model by a factor, but determining these factors for common design situations would prove very useful.

In addition to the potential improvements that can be made to the compressive strength model, there is more work that can be done with the set time. This study successfully determined the conditions which cause flash set behavior to occur as well as determined the conditions for mixes to have either short or long set times. While these both provide valuable design tools, it would be more useful if the exact set time could be predicted from the mix design properties. The set behavior models found in this study provide the framework needed to develop this, but there is still work that needs to be done in the area of determining the set time of geopolymer mixes.

Appendix A

As Cast Mix Designs

Table A.1 – Set Time Mix Designs

Mix	Fly Ash Type	Mix Constituents (% wt. of Mix)			
		NaOH	Na Silicate	Distilled H_2O	Fly Ash
T1011	High Ca 1	6.09	0.00	13.45	80.46
T1012	High Ca 1	9.83	0.00	12.55	77.62
T1013	High Ca 1	9.28	7.25	8.33	75.14
T1021	High Ca 1	5.85	0.00	17.28	76.88
T1022	High Ca 1	10.03	0.00	16.28	73.70
T1023	High Ca 1	8.55	12.20	9.01	70.24
T1024	High Ca 1	11.63	9.01	10.22	69.14
T1031	High Ca 1	5.49	0.00	21.20	73.32
T1032	High Ca 1	3.98	12.26	13.87	69.90
T1033	High Ca 1	9.84	0.00	20.02	70.15
T1034	High Ca 1	8.46	13.38	12.10	66.06
T1041	High Ca 1	4.57	0.00	25.08	70.35
T1042	High Ca 1	2.71	17.13	14.96	65.19
T1043	High Ca 1	7.98	6.63	20.14	65.24
T1044	High Ca 1	7.01	17.91	13.31	61.77
T1045	High Ca 1	12.58	2.00	21.94	63.48
T1046	High Ca 1	11.64	13.13	15.14	60.09
T1051	High Ca 1	4.40	3.05	27.01	65.54
T1052	High Ca 1	3.31	14.34	20.20	62.16
T1053	High Ca 1	9.63	4.33	24.90	61.15
T1054	High Ca 1	8.51	15.58	18.10	57.81
T1111	High Ca 1	1.56	0.00	14.61	83.83
T1112	High Ca 1	1.04	4.78	11.78	82.39
T1113	High Ca 1	0.54	9.27	9.07	81.12
T1121	High Ca 1	6.98	0.00	13.30	79.72
T1122	High Ca 1	6.17	7.83	8.59	77.41
T1123	High Ca 1	5.36	15.00	4.31	75.32
T1131	High Ca 1	12.43	0.00	11.90	75.67
T1132	High Ca 1	11.86	5.35	8.70	74.08
T1133	High Ca 1	10.87	14.21	3.42	71.50
T1134	High Ca 1	10.32	19.22	0.42	70.03
T1211	High Ca 1	1.80	0.00	22.04	76.16
T1212	High Ca 1	1.20	5.47	18.80	74.53
T1213	High Ca 1	0.59	10.78	15.63	73.01
T1221	High Ca 1	7.27	0.00	20.68	72.05
T1222	High Ca 1	5.92	11.65	13.77	68.65
T1223	High Ca 1	4.72	22.97	7.01	65.31

Mix	Fly Ash Type	Mix Constituents (% wt. of Mix)			
		NaOH	Na Silicate	Distilled H_2O	Fly Ash
T1231	High Ca 1	12.64	0.00	19.36	68.00
T1232	High Ca 1	11.47	10.64	13.02	64.88
T1233	High Ca 1	10.36	21.19	6.72	61.73
T1311	High Ca 1	2.02	0.00	29.49	68.49
T1312	High Ca 1	1.35	6.14	25.84	66.68
T1313	High Ca 1	0.84	12.07	22.26	64.83
T1314	High Ca 1	0.00	17.96	18.82	63.22
T1321	High Ca 1	7.43	0.00	28.15	64.42
T1322	High Ca 1	5.66	15.75	18.74	59.85
T1323	High Ca 1	4.00	31.30	9.45	55.24
T1331	High Ca 1	12.86	0.00	26.77	60.38
T1332	High Ca 1	11.25	14.88	17.94	55.93
T1333	High Ca 1	10.21	29.36	9.11	51.31
T2011	Mixed High Ca	3.81	8.36	12.57	75.26
T2012	Mixed High Ca	9.37	6.49	12.39	71.75
T2013	Mixed High Ca	8.04	18.43	5.37	68.16
T2014	Mixed High Ca	12.27	11.40	8.63	67.70
T2021	Mixed High Ca	4.59	2.29	19.90	73.22
T2022	Mixed High Ca	2.36	22.27	7.98	67.39
T2023	Mixed High Ca	9.65	4.49	17.36	68.50
T2024	Mixed High Ca	7.59	24.30	5.33	62.78
T2025	Mixed High Ca	14.94	6.30	14.80	63.96
T2026	Mixed High Ca	13.18	22.52	5.19	59.10
T2031	Mixed High Ca	4.43	4.28	22.44	68.85
T2032	Mixed High Ca	2.21	24.28	10.56	62.95
T2033	Mixed High Ca	9.61	6.60	19.81	63.98
T2034	Mixed High Ca	7.83	22.39	10.35	59.44
T2041	Mixed High Ca	4.81	2.19	27.42	65.58
T2042	Mixed High Ca	2.96	18.30	17.86	60.88
T2043	Mixed High Ca	9.90	4.33	24.81	60.96
T2044	Mixed High Ca	13.00	1.38	25.90	59.72
T2051	Mixed High Ca	6.45	15.63	11.15	66.76
T2052	Mixed High Ca	9.82	11.75	11.44	66.99
T2053	Mixed High Ca	4.24	7.11	21.51	67.14
T2054	Mixed High Ca	8.99	15.85	8.16	67.01
T2055	Mixed High Ca	3.23	26.48	3.41	66.87
T2056	Mixed High Ca	8.21	9.97	14.84	66.98
T2111	Mixed High Ca	1.87	0.00	14.44	83.69
T2114	Mixed High Ca	0.00	16.99	4.39	78.62
T2121	Mixed High Ca	7.31	0.00	13.07	79.62
T2123	Mixed High Ca	5.65	14.72	4.45	75.17
T2124	Mixed High Ca	4.82	21.86	0.00	73.32
T2131	Mixed High Ca	12.77	0.00	11.67	75.56
T2132	Mixed High Ca	11.86	6.76	7.45	73.93
T2133	Mixed High Ca	11.34	13.17	3.94	71.55

Mix	Fly Ash Type	Mix Constituents (% wt. of Mix)			
		NaOH	Na Silicate	Distilled H_2O	Fly Ash
T2134	Mixed High Ca	10.62	19.56	0.00	69.83
T2211	Mixed High Ca	2.07	0.00	21.93	76.00
T2212	Mixed High Ca	1.41	6.05	18.34	74.20
T2213	Mixed High Ca	0.00	12.20	14.87	72.93
T2214	Mixed High Ca	0.00	18.47	10.96	70.57
T2221	Mixed High Ca	7.59	0.00	20.52	71.88
T2222	Mixed High Ca	6.25	11.38	13.84	68.53
T2223	Mixed High Ca	4.98	22.47	7.27	65.29
T2224	Mixed High Ca	3.69	34.59	0.00	61.72
T2231	Mixed High Ca	12.96	0.00	19.28	67.76
T2232	Mixed High Ca	11.87	8.68	14.13	65.33
T2233	Mixed High Ca	11.24	16.99	9.13	62.64
T2234	Mixed High Ca	10.09	26.31	3.64	59.96
T2311	Mixed High Ca	2.18	0.00	29.37	68.45
T2312	Mixed High Ca	1.53	6.79	25.37	66.31
T2313	Mixed High Ca	0.00	13.30	21.76	64.94
T2314	Mixed High Ca	0.00	20.37	17.37	62.27
T2321	Mixed High Ca	7.68	0.00	28.06	64.27
T2322	Mixed High Ca	7.23	4.89	25.25	62.63
T2323	Mixed High Ca	6.62	9.66	22.28	61.44
T2324	Mixed High Ca	6.19	14.46	19.42	59.93
T2331	Mixed High Ca	13.16	0.00	26.73	60.11
T3011	Mixed Low Ca 3	3.88	13.47	9.38	73.27
T3012	Mixed Low Ca 3	9.45	11.30	9.31	69.94
T3013	Mixed Low Ca 3	8.13	22.93	2.50	66.44
T3014	Mixed Low Ca 3	11.73	16.11	5.82	66.33
T3021	Mixed Low Ca 3	4.40	11.20	14.51	69.90
T3022	Mixed Low Ca 3	2.51	26.83	5.07	65.58
T3023	Mixed Low Ca 3	9.91	9.00	14.30	66.78
T3024	Mixed Low Ca 3	7.60	28.62	2.71	61.07
T3025	Mixed Low Ca 3	15.04	10.74	12.03	62.18
T3026	Mixed Low Ca 3	19.66	24.54	2.52	53.28
T3031	Mixed Low Ca 3	4.13	12.77	17.22	65.88
T3032	Mixed Low Ca 3	2.29	28.57	7.86	61.29
T3033	Mixed Low Ca 3	9.65	10.74	17.20	62.40
T3034	Mixed Low Ca 3	7.85	26.95	7.71	57.48
T3041	Mixed Low Ca 3	3.55	18.50	17.68	60.27
T3042	Mixed Low Ca 3	9.59	12.37	19.95	58.09
T3051	Mixed Low Ca 3	3.29	19.85	9.91	66.95
T3052	Mixed Low Ca 3	3.34	3.25	26.42	66.99
T3053	Mixed Low Ca 3	5.95	3.27	23.38	67.40
T3054	Mixed Low Ca 3	9.94	3.29	19.84	66.93
T3055	Mixed Low Ca 3	13.27	3.26	16.48	66.99
T3056	Mixed Low Ca 3	6.57	6.59	19.94	66.90
T3057	Mixed Low Ca 3	7.08	13.16	13.15	66.61

Mix	Fly Ash Type	Mix Constituents (% wt. of Mix)			
		NaOH	Na Silicate	Distilled H_2O	Fly Ash
T3058	Mixed Low Ca 3	9.81	7.08	16.46	66.64
T3059	Mixed Low Ca 3	9.82	9.89	13.23	67.06
T3111	Mixed Low Ca 3	2.40	0.30	14.26	83.04
T3114	Mixed Low Ca 3	0.00	21.47	1.89	76.64
T3121	Mixed Low Ca 3	8.52	0.00	12.93	78.55
T3124	Mixed Low Ca 3	5.62	21.69	0.00	72.69
T3131	Mixed Low Ca 3	13.33	0.37	11.49	74.80
T3132	Mixed Low Ca 3	12.87	6.67	7.61	72.86
T3133	Mixed Low Ca 3	11.86	12.95	3.89	71.31
T3134	Mixed Low Ca 3	10.90	19.26	0.26	69.59
T3211	Mixed Low Ca 3	2.64	0.00	21.83	75.53
T3212	Mixed Low Ca 3	2.08	7.65	17.25	73.03
T3213	Mixed Low Ca 3	1.09	15.17	12.76	70.97
T3214	Mixed Low Ca 3	0.00	22.93	8.18	68.90
T3221	Mixed Low Ca 3	8.03	0.37	20.28	71.31
T3222	Mixed Low Ca 3	6.80	11.66	13.63	67.91
T3223	Mixed Low Ca 3	5.60	22.81	6.78	64.81
T3224	Mixed Low Ca 3	4.37	34.09	0.00	61.54
T3231	Mixed Low Ca 3	13.51	0.00	19.13	67.36
T3232	Mixed Low Ca 3	12.38	10.85	12.62	64.15
T3233	Mixed Low Ca 3	11.13	21.46	6.36	61.05
T3234	Mixed Low Ca 3	10.08	32.07	0.00	57.85
T3311	Mixed Low Ca 3	2.73	0.29	29.11	67.87
T3312	Mixed Low Ca 3	1.97	8.41	24.27	65.34
T3313	Mixed Low Ca 3	1.07	16.05	19.59	63.29
T3314	Mixed Low Ca 3	0.00	23.96	15.20	60.84
T3321	Mixed Low Ca 3	8.40	0.00	27.88	63.72
T3324	Mixed Low Ca 3	6.83	12.52	20.40	60.24
T3331	Mixed Low Ca 3	13.54	0.00	26.63	59.83
T4111	Low Ca 2	1.44	15.96	4.72	77.88
T4114	Low Ca 2	0.65	23.63	0.16	75.56
T4121	Low Ca 2	8.59	2.13	11.51	77.77
T4124	Low Ca 2	6.25	21.26	0.20	72.29
T4131	Low Ca 2	14.04	0.06	11.60	74.30
T4134	Low Ca 2	11.85	19.35	0.00	68.80
T4211	Low Ca 2	3.46	0.25	21.44	74.86
T4214	Low Ca 2	0.00	29.10	4.30	66.59
T4221	Low Ca 2	9.41	0.19	20.03	70.37
T4224	Low Ca 2	4.72	34.14	0.00	61.14
T4231	Low Ca 2	14.03	0.13	18.99	66.85
T4234	Low Ca 2	11.46	23.58	5.00	59.97
T4311	Low Ca 2	3.58	0.31	28.96	67.15
T4314	Low Ca 2	0.66	25.52	13.96	59.86
T4321	Low Ca 2	8.81	0.37	27.70	63.13
T4324	Low Ca 2	7.42	11.91	20.83	59.85

Mix	Fly Ash Type	Mix Constituents (% wt. of Mix)			
		NaOH	Na Silicate	Distilled H_2O	Fly Ash
T4331	Low Ca 2	14.09	0.20	26.42	59.29
T5131	Mixed Low Ca 4	13.37	0.30	11.44	74.89
T5134	Mixed Low Ca 4	11.48	19.24	0.11	69.17
T6124	Mixed Low Ca 2	5.81	21.77	0.14	72.28
T6131	Mixed Low Ca 2	13.59	0.31	11.37	74.73
T6134	Mixed Low Ca 2	11.45	18.70	0.00	69.85
T6211	Mixed Low Ca 2	2.91	0.00	21.30	75.79
T6214	Mixed Low Ca 2	0.00	24.84	7.18	67.97
T6221	Mixed Low Ca 2	8.62	0.10	20.28	71.00

Table A.2 – Compressive Strength Mix Designs

Mix	Fly Ash Type	Mix Constituents (% wt. of Mix)			
		NaOH	Na Silicate	Distilled H_2O	Fly Ash
C1022	High Ca 2	10.10	0.00	16.25	73.65
C1024	High Ca 2	11.60	8.96	10.23	69.21
C1033	High Ca 2	9.81	0.00	20.20	69.99
C1034	High Ca 2	8.74	13.44	12.06	65.76
C1041	High Ca 2	4.71	0.00	25.15	70.14
C1043	High Ca 2	7.96	6.57	20.14	65.33
C1045	High Ca 2	12.80	2.00	21.90	63.30
C1046	High Ca 2	11.65	13.06	15.24	60.06
C1051	High Ca 2	4.30	3.01	27.06	65.63
C1052	High Ca 2	3.63	14.29	20.14	61.94
C1053	High Ca 2	9.59	4.29	25.00	61.12
C1112	High Ca 2	1.00	4.80	11.66	82.53
C1212	High Ca 2	1.17	5.39	18.94	74.50
C1221	High Ca 2	7.26	0.00	20.78	71.96
C1222	High Ca 2	5.89	11.62	13.79	68.70
C1231	High Ca 2	12.62	0.00	19.29	68.09
C1232	High Ca 2	11.36	10.64	12.98	65.01
C1311	High Ca 2	2.17	0.00	29.56	68.27
C1314	High Ca 2	0.00	17.91	18.86	63.23
C1321	High Ca 2	7.39	0.00	28.17	64.44
C2011	Mixed High Ca	3.80	8.38	12.55	75.28
C2012	Mixed High Ca	9.33	6.48	12.39	71.80
C2014	Mixed High Ca	12.24	11.34	8.72	67.70
C2021	Mixed High Ca	4.83	2.28	19.81	73.09
C2023	Mixed High Ca	9.78	4.45	17.34	68.43
C2024	Mixed High Ca	7.54	24.40	5.27	62.78
C2025	Mixed High Ca	14.83	6.33	14.83	64.00
C2026	Mixed High Ca	13.14	22.63	5.16	59.07
C2031	Mixed High Ca	4.34	4.28	22.51	68.87
C2033	Mixed High Ca	9.40	6.74	20.01	63.85

Mix	Fly Ash Type	Mix Constituents (% wt. of Mix)			
		NaOH	Na Silicate	Distilled H_2O	Fly Ash
C2034	Mixed High Ca	7.80	22.38	10.36	59.47
C2041	Mixed High Ca	4.77	2.18	27.34	65.70
C2043	Mixed High Ca	9.89	4.30	24.84	60.98
C2051	Mixed High Ca	6.39	15.67	11.11	66.83
C2053	Mixed High Ca	4.10	7.32	21.62	66.96
C2056	Mixed High Ca	8.11	9.89	14.89	67.11
C2131	Mixed High Ca	12.66	0.00	11.76	75.58
C2134	Mixed High Ca	11.00	19.43	0.00	69.57
C2211	Mixed High Ca	2.05	0.00	21.92	76.03
C2212	Mixed High Ca	1.33	6.11	18.44	74.11
C2214	Mixed High Ca	0.00	18.46	10.96	70.58
C2221	Mixed High Ca	7.51	0.00	20.47	72.02
C2222	Mixed High Ca	6.18	11.30	13.86	68.67
C2224	Mixed High Ca	3.61	34.72	0.00	61.67
C2231	Mixed High Ca	12.90	0.00	19.40	67.70
C2232	Mixed High Ca	11.86	8.63	14.09	65.42
C3013	Mixed Low Ca 1	8.00	22.89	2.50	66.61
C3021	Mixed Low Ca 1	4.32	11.12	14.72	69.84
C3022	Mixed Low Ca 1	2.50	26.75	4.99	65.76
C3023	Mixed Low Ca 1	9.87	8.93	14.25	66.94
C3024	Mixed Low Ca 1	7.60	28.63	2.66	61.10
C3025	Mixed Low Ca 1	15.00	10.78	12.00	62.22
C3026	Mixed Low Ca 1	19.68	24.57	2.50	53.25
C3031	Mixed Low Ca 1	4.11	12.72	17.28	65.89
C3032	Mixed Low Ca 1	2.24	28.60	7.78	61.38
C3033	Mixed Low Ca 1	9.86	10.75	17.12	62.27
C3034	Mixed Low Ca 1	7.75	27.17	7.63	57.45
C3041	Mixed Low Ca 1	3.53	18.35	17.76	60.35
C3053	Mixed Low Ca 1	6.01	3.29	23.33	67.37
C3054	Mixed Low Ca 1	9.81	3.21	20.00	66.98
C3057	Mixed Low Ca 1	7.00	13.05	13.16	66.80
C3058	Mixed Low Ca 1	9.84	7.12	16.40	66.65
C3059	Mixed Low Ca 1	9.83	9.94	13.22	67.00
C3124	Mixed Low Ca 1	5.57	21.87	0.00	72.56
C3131	Mixed Low Ca 1	13.66	0.37	11.46	74.51
C3134	Mixed Low Ca 1	11.37	19.22	0.00	69.41
C3213	Mixed Low Ca 1	1.00	15.23	12.66	71.11
C3221	Mixed Low Ca 1	7.96	0.33	20.37	71.34
C3222	Mixed Low Ca 1	6.89	11.60	13.60	67.91
C3223	Mixed Low Ca 1	5.57	22.84	6.69	64.90
C3224	Mixed Low Ca 1	4.34	34.11	0.00	61.55
C3231	Mixed Low Ca 1	13.50	0.00	19.06	67.44
C3232	Mixed Low Ca 1	12.44	11.01	13.04	63.51
C4901	Low Ca 2	12.75	9.58	9.58	68.10
C6124	Mixed Low Ca 2	5.68	21.79	0.00	72.53

Mix	Fly Ash Type	Mix Constituents (% wt. of Mix)			
		NaOH	Na Silicate	Distilled H_2O	Fly Ash
C6131	Mixed Low Ca 2	14.57	0.21	11.35	73.87
C6214	Mixed Low Ca 2	0.00	24.85	7.21	67.94
C6901	Mixed Low Ca 2	2.06	7.45	17.41	73.08
C6902	Mixed Low Ca 2	9.91	10.01	8.01	72.08
C6903	Mixed Low Ca 2	12.92	7.14	8.09	71.85
C6904	Mixed Low Ca 2	9.64	3.12	19.06	68.17
C6905	Mixed Low Ca 2	16.25	3.15	12.77	67.83
C6907	Mixed Low Ca 2	12.74	9.57	9.52	68.17
C6908	Mixed Low Ca 2	3.22	16.14	12.81	67.83
C6909	Mixed Low Ca 2	9.61	16.10	6.50	67.80
C6910	Mixed Low Ca 2	6.43	22.35	3.44	67.78
C6911	Mixed Low Ca 2	6.44	12.82	12.76	67.98
C6912	Mixed Low Ca 2	12.74	13.00	6.35	67.91
C6914	Mixed Low Ca 2	15.24	7.71	15.19	61.86
C6915	Mixed Low Ca 2	11.38	19.26	7.44	61.93

Table A.3 – Validation Mix Designs

Mix	Fly Ash Type	Mix Constituents (% wt. of Mix)			
		NaOH	Na Silicate	Distilled H_2O	Fly Ash
V0301	Low Ca 2	9.73	3.28	20.52	66.47
V0402	High Ca 5	10.42	9.48	14.45	65.65
V0660	Low Ca 1	10.55	9.30	13.58	66.57
V0708	Mixed Low Ca 2	6.38	9.60	15.98	68.04
V0962	High Ca 6	3.35	8.37	10.79	77.5
V1119	High Ca 6	11.19	8.74	8.20	71.87
V1164	High Ca 6	9.54	7.49	9.48	73.51
V1190	High Ca 6	4.86	12.18	7.96	75.00
V1194	High Ca 6	7.82	6.12	10.84	75.22
V1289	High Ca 6	6.28	15.70	5.33	72.69

Appendix B

Testing Results & Model Predictions

Table B.1 – Base Fly Ash Compositions Determined by XRF

Fly Ash	Oxide Quantity (% wt.)								
	SiO_2	Al_2O_3	CaO	Na_2O	K_2O	Fe_2O_3	MgO	P_2O_5	TiO_2
Low Ca 1	49.24	18.79	1.77	3.36	2.29	17.92	0.82	0.08	0.94
Low Ca 2	46.90	21.89	1.89	0.60	2.37	21.71	0.85	0.19	1.04
High Ca 1	33.61	20.04	27.00	2.18	0.44	5.68	6.06	1.44	1.46
High Ca 2	36.75	19.49	23.67	2.00	0.54	5.55	5.53	1.45	1.42
High Ca 3	36.55	22.06	23.47	1.76	0.63	6.15	5.02	1.15	1.47
High Ca 4	36.31	19.79	23.51	1.77	0.54	5.67	5.44	1.40	1.38
High Ca 5	34.63	19.84	26.25	2.02	0.45	6.43	5.85	1.38	1.40
High Ca 6	41.41	20.95	17.80	1.42	0.75	8.75	4.60	1.00	1.31

Table B.2 – Chemical Dissolution Residue Compositions Determined by XRF

Fly Ash	Oxide Quantity (% wt.)								
	SiO_2	Al_2O_3	CaO	Na_2O	K_2O	Fe_2O_3	MgO	P_2O_5	TiO_2
Low Ca 1	47.77	19.20	2.38	0.69	1.86	22.50	1.17	0.04	1.21
Low Ca 2	44.47	21.57	2.21	0.59	2.07	24.11	1.19	0.10	1.20
High Ca 1	29.66	14.73	30.53	1.60	0.30	6.11	6.93	0.96	1.63
High Ca 2	31.88	13.78	31.88	1.80	0.31	7.06	7.60	1.07	1.86
High Ca 3	29.81	14.95	29.25	1.06	0.34	6.97	6.37	0.79	1.79
High Ca 4	31.30	13.94	31.75	1.53	0.32	7.18	7.55	1.03	1.83
High Ca 5	30.21	14.35	29.73	1.24	0.27	6.43	6.82	0.86	1.61
High Ca 6 T1	35.61	15.37	21.81	0.98	0.45	10.42	5.71	0.54	1.63
High Ca 6 T2	35.74	15.15	21.76	0.92	0.56	10.40	5.78	0.55	1.43

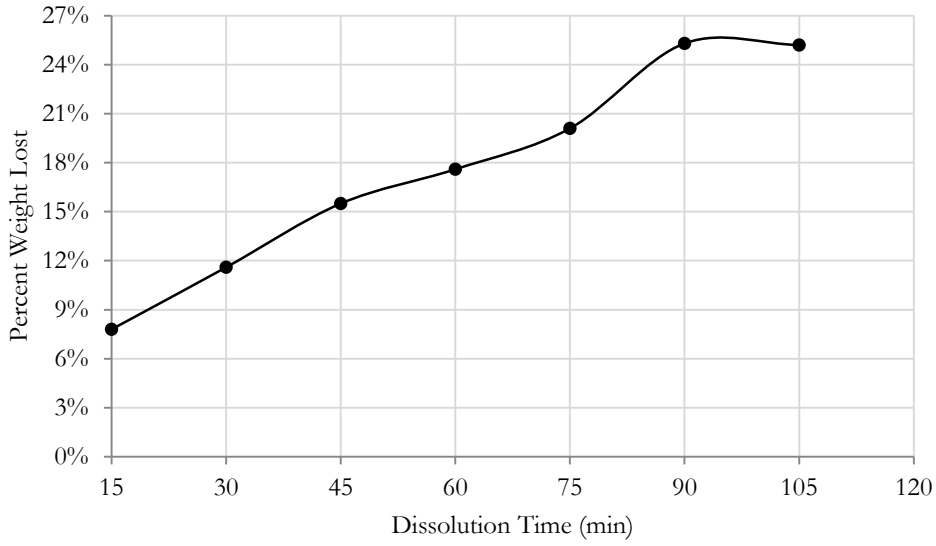

Figure B.1 – Weight Lost vs. Dissolution Time for Low Calcium 1

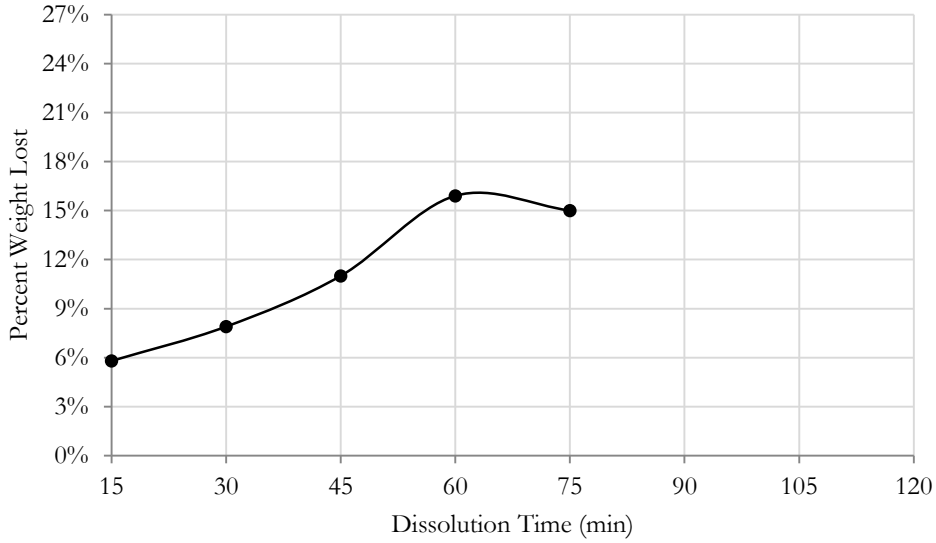

Figure B.2 – Weight Lost vs. Dissolution Time for Low Calcium 2

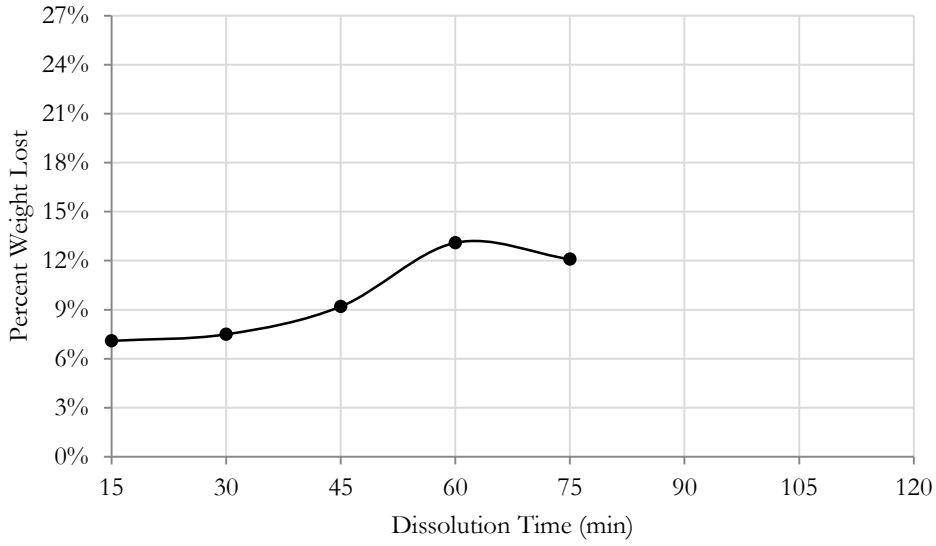

Figure B.3 – Weight Lost vs. Dissolution Time for High Calcium 1

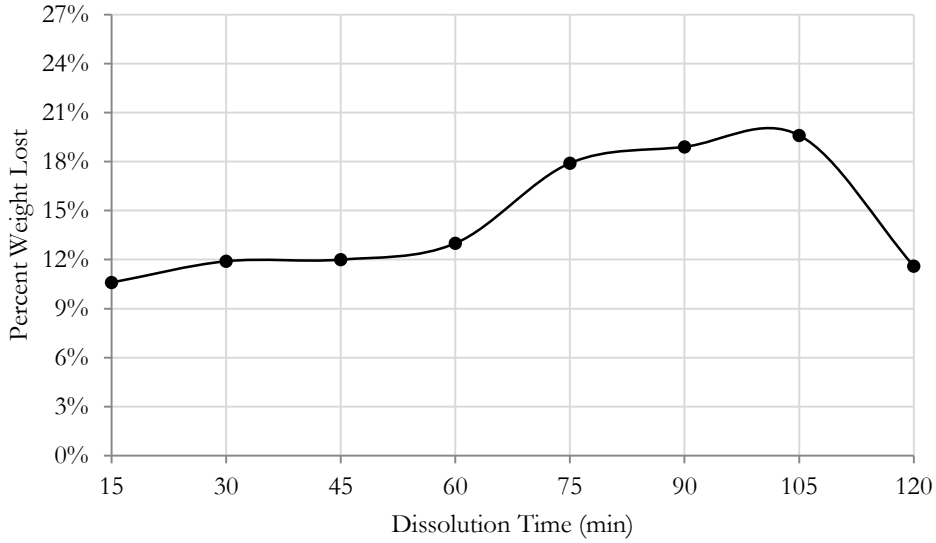

Figure B.4 – Weight Lost vs. Dissolution Time for High Calcium 2

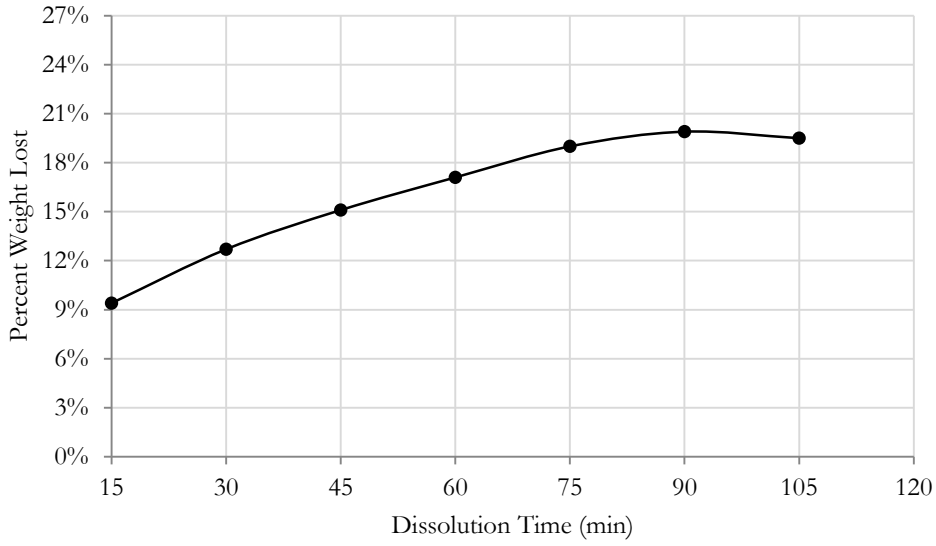

Figure B.5 – Weight Lost vs. Dissolution Time for High Calcium 3

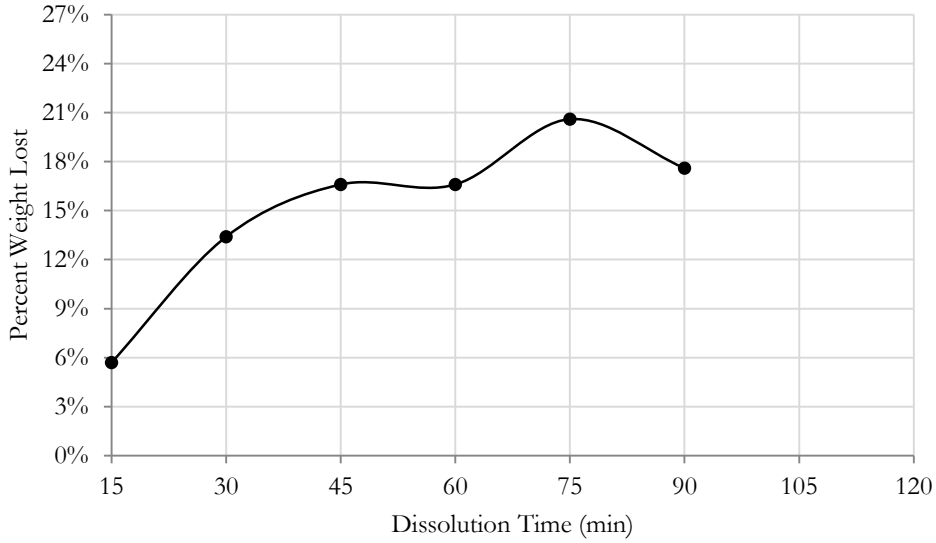

Figure B.6 – Weight Lost vs. Dissolution Time for High Calcium 4

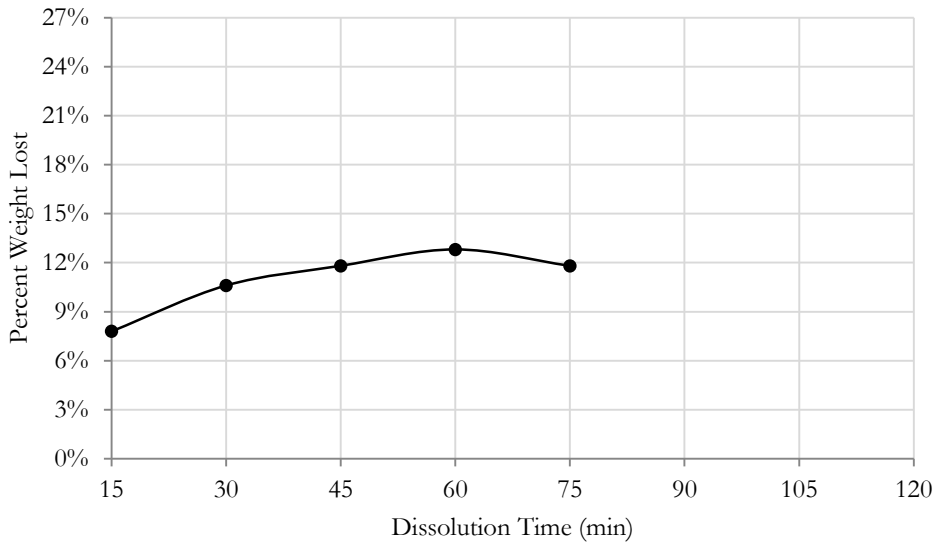

Figure B.7 – Weight Lost vs. Dissolution Time for High Calcium 5

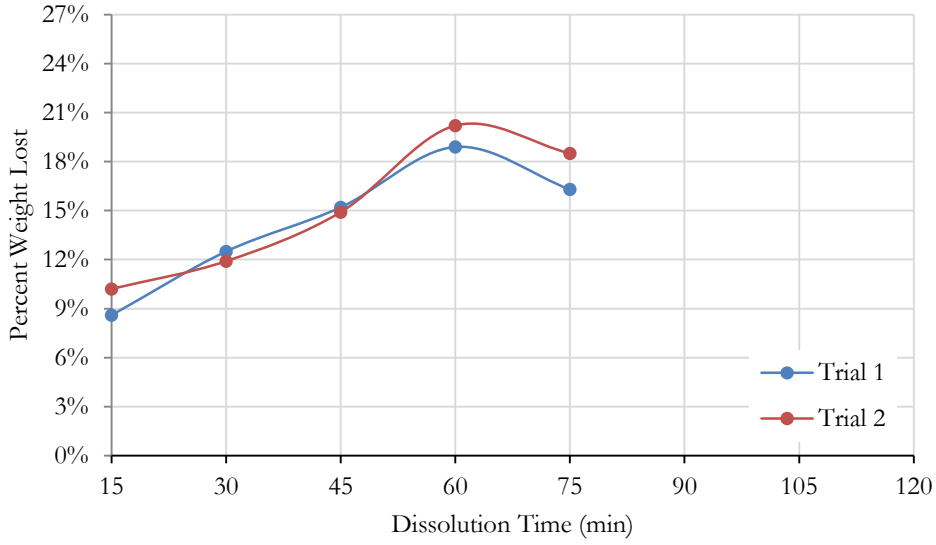

Figure B.8 – Weight Lost vs. Dissolution Time for High Calcium 6

Table B.3 – Set Time Testing Results and Model Predictions

Mix	Critical Variables (% wt. of Mix)				Initial Set (min)	Final Set (min)	Flash Set Prediction	Long Set Prediction
	H_2O	Na_2O	R. SiO_2	CaO				
T1011	14.96	6.33	6.29	21.72	Flash Set		Flash Set	
T1012	14.99	9.08	6.07	20.96	Flash Set		Flash Set	
T1013	15.16	9.26	7.96	20.29	Flash Set		Flash Set	
T1021	18.73	6.07	6.01	20.76	Flash Set		Flash Set	
T1022	18.77	9.14	5.76	19.90	35	75	Flash Set	
T1023	18.75	9.04	9.00	18.96	Flash Set		Flash Set	
T1024	18.73	11.05	7.99	18.67	21	28		
T1031	22.56	5.72	5.73	19.80	Flash Set		Flash Set	
T1032	22.50	5.60	8.98	18.87	Flash Set		Flash Set	
T1033	22.46	8.92	5.49	18.94	47	54		
T1034	22.56	8.99	9.01	17.84	23	34		
T1041	26.21	4.97	5.50	19.00	21	22		Long Set
T1042	26.32	4.99	10.02	17.60	Flash Set			
T1043	26.26	8.01	7.00	17.62	185	205		Long Set
T1046	26.23	11.23	8.47	16.22		Long Set		Long Set
T1051	30.01	5.00	6.00	17.70		Long Set		Long Set
T1052	29.97	5.12	8.98	16.78		Long Set		Long Set
T1053	29.99	8.95	6.02	16.51		Long Set		Long Set
T1054	29.94	9.04	8.99	15.61	56	70		Long Set
T1111	15.00	3.00	6.56	22.63		Long Set	Flash Set	
T1112	15.03	3.01	7.82	22.25	Flash Set		Flash Set	
T1113	14.99	3.00	9.00	21.90	Flash Set		Flash Set	
T1121	15.04	6.99	6.23	21.52	Flash Set		Flash Set	
T1122	15.01	7.02	8.30	20.90	Flash Set		Flash Set	
T1123	15.00	7.01	10.19	20.34	Flash Set		Flash Set	
T1131	14.99	10.99	5.92	20.43	Flash Set		Flash Set	
T1132	14.99	11.01	7.33	20.00	Flash Set		Flash Set	
T1133	14.99	10.99	9.67	19.30	Flash Set		Flash Set	
T1134	14.98	10.99	10.99	18.91	Flash Set		Flash Set	
T1211	22.49	3.01	5.96	20.56	Flash Set		Flash Set	
T1212	22.51	3.02	7.40	20.12	Flash Set		Flash Set	
T1213	22.50	2.99	8.80	19.71		Long Set	Flash Set	
T1221	22.49	7.04	5.63	19.45	Flash Set			
T1222	22.52	6.99	8.71	18.54	10	14		
T1223	22.52	7.01	11.70	17.63	25	32		
T1231	22.50	10.98	5.32	18.36	Flash Set			Long Set
T1232	22.51	10.98	8.13	17.52		Long Set		
T1233	22.51	11.02	10.91	16.67	83	90		
T1311	29.99	3.01	5.36	18.49	Flash Set			Long Set
T1312	30.00	3.01	6.98	18.00		Long Set		Long Set
T1313	30.00	3.12	8.53	17.51		Long Set		Long Set
T1314	30.03	2.98	10.10	17.07		Long Set		Long Set
T1321	29.99	6.99	5.04	17.39	32	100		Long Set
T1322	29.97	6.96	9.20	16.16	165	180		Long Set

Mix	Critical Variables (% wt. of Mix)				Initial Set (min)	Final Set (min)	Flash Set Prediction	Long Set Prediction
	H_2O	Na_2O	R. SiO_2	CaO				
T1323	29.98	6.99	13.30	14.92		Long Set		
T1331	29.96	10.98	4.72	16.30	Flash Set			Long Set
T1332	30.02	11.00	8.64	15.10		Long Set		Long Set
T1333	29.97	11.41	12.44	13.85		Long Set		
T2011	18.73	5.37	11.23	13.69	Flash Set			
T2012	18.77	9.30	10.28	13.05	38	70		
T2013	18.87	9.28	13.29	12.40	24	42		
T2014	18.80	11.82	11.21	12.32	Flash Set			
T2021	22.47	5.36	9.25	13.32	23	30		
T2022	22.46	5.33	14.30	12.26	60	80		
T2023	22.56	9.26	9.32	12.46	Flash Set			
T2024	22.38	9.33	14.34	11.42	73	105		
T2025	22.44	13.29	9.31	11.64	15	26		
T2026	22.52	13.29	13.40	10.75	26	38		
T2031	26.21	5.32	9.30	12.53	25	42		Long Set
T2032	26.26	5.29	14.35	11.45		Long Set		
T2033	26.31	9.31	9.40	11.64	Flash Set			Long Set
T2034	26.26	9.26	13.40	10.81		Long Set		
T2041	29.98	5.35	8.32	11.93	17	36		Long Set
T2042	30.01	5.28	12.39	11.08	87	175		Long Set
T2043	29.97	9.25	8.39	11.09	Flash Set			Long Set
T2044	30.00	11.29	7.40	10.87	98	145		Long Set
T2051	22.51	7.80	12.32	12.15		Long Set		
T2052	21.21	9.99	11.23	12.19	36	50		
T2053	27.00	5.39	9.92	12.22	36	50		Long Set
T2054	20.28	9.73	12.41	12.19		Long Set		
T2055	20.74	6.35	15.44	12.17	Flash Set			
T2056	23.10	8.63	10.72	12.19	Flash Set			
T2111	14.90	3.36	9.82	15.23	90	105	Flash Set	
T2114	15.00	3.35	14.10	14.30	Flash Set		Flash Set	
T2121	14.89	7.35	9.34	14.49	Flash Set		Flash Set	
T2123	15.04	7.32	13.04	13.68	Flash Set		Flash Set	
T2124	14.84	7.28	14.88	13.34	Flash Set		Flash Set	
T2131	14.84	11.37	8.86	13.75	Flash Set		Flash Set	
T2132	14.62	11.25	10.61	13.45	13	34	Flash Set	
T2133	14.98	11.37	12.17	13.02	Flash Set		Flash Set	
T2134	14.84	11.35	13.80	12.71	Flash Set		Flash Set	
T2211	22.45	3.33	8.91	13.83	31	40		
T2212	22.47	3.33	10.44	13.50	95	125		
T2213	22.48	2.79	12.06	13.27		Long Set		
T2214	22.49	3.30	13.58	12.84	Flash Set			
T2221	22.41	7.39	8.43	13.08	15	36		
T2222	22.49	7.31	11.31	12.47	40	46		
T2223	22.52	7.27	14.11	11.88	30	40		
T2224	22.50	7.29	17.17	11.23	Flash Set			

Mix	Critical Variables (% wt. of Mix)				Initial Set (min)	Final Set (min)	Flash Set Prediction	Long Set Prediction
	H_2O	Na_2O	R. SiO_2	CaO				
T2231	22.50	11.33	7.95	12.33	15	22		Long Set
T2232	22.49	11.22	10.15	11.89		Long Set		
T2233	22.52	11.42	12.22	11.40	105	145		
T2234	22.57	11.33	14.58	10.91	Flash Set			
T2311	29.91	3.24	8.03	12.46	16	28		Long Set
T2312	29.99	3.30	9.73	12.07		Long Set		Long Set
T2313	30.06	2.70	11.44	11.82		Long Set		Long Set
T2314	30.08	3.27	13.15	11.33		Long Set		Long Set
T2321	29.97	7.27	7.54	11.69		Long Set		Long Set
T2322	30.10	7.33	8.75	11.40		Long Set		Long Set
T2323	29.95	7.27	9.98	11.18		Long Set		Long Set
T2324	29.99	7.34	11.18	10.90		Long Set		Long Set
T2331	30.00	11.29	7.05	10.94		Long Set		Long Set
T3011	18.74	4.98	12.00	9.29		Long Set		
T3012	18.71	8.93	11.01	8.87	Flash Set			
T3013	18.83	8.93	13.96	8.42	26	46		
T3014	18.79	11.03	11.99	8.41	16	22		
T3021	22.59	5.13	10.97	8.86	Flash Set			
T3022	22.44	5.05	14.98	8.32		Long Set		
T3023	22.38	9.04	10.00	8.47	13	22		
T3024	22.46	8.98	14.99	7.74	185	240		
T3025	22.48	12.99	9.99	7.88	16	42		
T3026	22.72	17.59	12.96	6.76		Long Set		
T3031	26.21	5.02	10.98	8.35	56	230		Long Set
T3032	26.25	4.99	15.00	7.77		Long Set		
T3033	26.30	8.95	10.01	7.91	29	38		Long Set
T3034	26.48	8.98	14.12	7.29		Long Set		
T3041	30.11	5.03	12.00	7.64	24	65		Long Set
T3042	30.05	8.99	10.00	7.37		Long Set		Long Set
T3051	23.12	5.03	13.13	8.49		Long Set		
T3052	29.28	3.59	8.37	8.49		Long Set		Long Set
T3053	26.90	5.56	8.42	8.55		Long Set		Long Set
T3054	24.36	8.55	8.37	8.49		Long Set		Long Set
T3055	21.81	11.05	8.37	8.49	40	90		Long Set
T3056	25.69	6.32	9.32	8.48	Flash Set			Long Set
T3057	23.12	7.28	11.17	8.45		Long Set		
T3058	23.32	8.79	9.43	8.45	50	75		Long Set
T3059	21.84	9.05	10.28	8.50		Long Set		
T3111	15.05	2.81	9.30	10.53		Long Set	Flash Set	
T3114	15.29	2.82	14.67	9.72	Flash Set		Flash Set	
T3121	15.05	7.33	8.72	9.96	Flash Set		Flash Set	
T3124	14.93	7.01	14.29	9.22	Flash Set		Flash Set	
T3131	15.04	10.93	8.41	9.49	14	18		
T3132	14.97	11.12	10.00	9.24	18	54	Flash Set	
T3133	14.91	10.90	11.63	9.04	Flash Set		Flash Set	

Mix	Critical Variables (% wt. of Mix)				Initial Set (min)	Final Set (min)	Flash Set Prediction	Long Set Prediction
	H_2O	Na_2O	R. SiO_2	CaO				
T3134	14.98	10.73	13.25	8.82	Flash Set			
T3211	22.48	2.87	8.38	9.58	14	20		Long Set
T3212	22.53	3.10	10.30	9.26		Long Set		
T3213	22.50	3.01	12.23	9.00		Long Set		
T3214	22.48	2.85	14.23	8.74	20	85		
T3221	22.51	6.91	8.02	9.04	Flash Set			Long Set
T3222	22.59	6.95	10.88	8.61	93	105		
T3223	22.40	7.00	13.74	8.22	46	80		
T3224	22.36	7.04	16.61	7.80	17	42		
T3231	22.49	10.95	7.48	8.54	43	75		Long Set
T3232	22.47	11.03	10.23	8.13		Long Set		
T3233	22.52	11.00	12.94	7.74		Long Set		
T3234	22.52	11.11	15.63	7.34	27	56		
T3311	29.97	2.88	7.62	8.61		Long Set		Long Set
T3312	30.01	3.00	9.67	8.29		Long Set		Long Set
T3313	29.87	2.98	11.63	8.03		Long Set		Long Set
T3314	30.15	2.85	13.63	7.72		Long Set		Long Set
T3321	29.97	7.06	7.07	8.08		Long Set		Long Set
T3324	29.91	6.96	10.28	7.64		Long Set		Long Set
T3331	29.99	10.88	6.64	7.59		Long Set		Long Set
T4111	15.04	2.97	12.00	1.47		Long Set	Flash Set	
T4114	15.07	3.04	13.97	1.43	Flash Set		Flash Set	
T4121	14.97	7.11	8.02	1.47	Flash Set		Flash Set	Long Set
T4124	15.02	7.02	12.98	1.37	Flash Set			
T4131	15.12	11.00	7.09	1.40		Long Set		Long Set
T4134	15.02	11.04	12.10	1.30		Long Set		
T4211	22.45	3.07	7.20	1.41		Long Set		Long Set
T4214	22.46	2.99	14.69	1.26		Long Set		
T4221	22.49	7.51	6.75	1.33		Long Set		Long Set
T4224	22.48	6.95	15.62	1.16		Long Set		
T4231	22.55	10.96	6.40	1.26		Long Set		Long Set
T4234	22.56	11.07	12.48	1.13		Long Set		
T4311	30.04	3.12	6.48	1.27		Long Set		Long Set
T4314	30.05	3.13	13.02	1.13		Long Set		Long Set
T4321	30.11	7.03	6.12	1.19		Long Set		Long Set
T4324	30.10	6.99	9.11	1.13		Long Set		Long Set
T4331	30.04	10.96	5.70	1.12		Long Set		Long Set
T5131	14.94	10.79	7.52	5.49		Long Set		Long Set
T5134	14.97	11.00	12.38	5.07		Long Set		
T6124	15.17	7.07	13.51	6.56		Long Set		
T6131	14.94	11.03	7.60	6.78	85	130		Long Set
T6134	14.51	11.01	12.39	6.34		Long Set	Flash Set	
T6211	22.02	2.99	7.62	6.88		Long Set		Long Set
T6214	22.69	2.93	13.96	6.17		Long Set		
T6221	22.48	7.24	7.17	6.45	75	105		Long Set

Table B.4 – Additional Flash Set Data from Compressive Testing Mixes

Mix	Critical Variables (% wt. of Mix)			Mix Behavior	Flash Set Prediction
	H_2O	Na2O	CaO		
C4901	18.72%	10.84%	1.29%	Mix OK	Mix OK
C6901	22.57%	2.99%	6.63%	Mix OK	Mix OK
C6902	16.72%	9.10%	6.54%	Flash Set	Mix OK
C6904	23.41%	8.25%	6.19%	Mix OK	Mix OK
C6905	18.77%	13.21%	6.16%	Mix OK	Mix OK
C6908	23.68%	4.57%	6.16%	Mix OK	Mix OK
C6909	18.93%	9.37%	6.15%	Flash Set	Mix OK
C6910	18.98%	7.54%	6.15%	Mix OK	Mix OK
C6911	22.36%	6.70%	6.17%	Mix OK	Mix OK
C6912	17.63%	11.45%	6.16%	Mix OK	Mix OK
C6914	23.78%	12.80%	5.62%	Mix OK	Mix OK
C6915	22.28%	10.92%	5.62%	Mix OK	Mix OK

Table B.5 – Compressive Strength Mix Properties

Mix	As Cast Air Content (%)	H_2O Lost During Curing (%)	Final Density (g/cm^3)
C1022	11.86	1.56	2.05
C1024	11.23	2.67	2.02
C1033	12.74	1.39	1.97
C1034	13.47	0.96	1.94
C1041	14.34	1.99	1.88
C1043	12.47	1.60	1.91
C1045	9.95	1.11	1.93
C1046	8.80	1.24	1.94
C1051	15.25	1.80	1.76
C1052	13.61	1.27	1.79
C1053	9.67	2.06	1.91
C1221	13.63	1.88	1.95
C1222	10.79	1.51	2.00
C1231	8.79	1.53	2.01
C1232	11.80	1.29	1.98
C1311	15.45	2.46	1.75
C1314	15.94	2.14	1.76
C1321	14.66	2.58	1.81
C2011	12.80	1.36	2.01
C2012	11.70	1.42	2.03
C2014	8.16	1.26	2.10
C2021	13.32	1.89	1.94
C2023	11.70	1.74	1.97
C2024	9.79	0.97	1.99
C2025	10.54	1.97	1.98
C2026	10.01	0.97	1.98

Mix	As Cast Air Content (%)	H_2O Lost During Curing (%)	Final Density (g/cm^3)
C2031	14.33	1.32	1.87
C2033	14.48	1.21	1.86
C2034	10.49	1.47	1.91
C2041	15.63	1.06	1.80
C2043	12.28	2.07	1.84
C2051	10.76	0.73	1.99
C2053	14.66	1.68	1.84
C2056	11.04	1.19	1.98
C2131	10.66	2.17	2.10
C2134	8.08	0.54	2.16
C2211	14.32	1.44	1.94
C2214	15.05	2.09	1.87
C2221	12.79	1.45	1.97
C2222	11.15	2.25	1.96
C2224	7.89	1.38	2.00
C2231	12.81	1.40	1.96
C2232	10.00	2.02	1.99
C3013	9.07	1.28	2.05
C3021	12.31	1.07	1.95
C3022	12.74	1.37	1.91
C3023	10.86	1.24	1.99
C3024	8.92	1.44	1.99
C3025	10.05	1.47	1.99
C3026	8.58	0.75	2.00
C3031	14.37	1.34	1.85
C3032	12.21	2.30	1.85
C3033	10.65	0.99	1.93
C3034	9.43	1.12	1.92
C3041	14.58	2.23	1.77
C3053	13.16	1.73	1.88
C3054	12.85	1.99	1.91
C3057	11.13	1.31	1.96
C3058	12.57	1.25	1.94
C3059	9.85	1.41	2.01
C3124	9.51	0.81	2.11
C3131	11.95	3.08	2.04
C3134	10.32	0.57	2.10
C3213	14.95	1.75	1.88
C3221	11.32	2.12	1.97
C3222	11.87	1.53	1.95
C3223	10.43	1.25	1.97
C3224	8.08	1.10	2.00
C3231	11.08	1.73	1.99
C3232	11.32	1.87	1.95
C4901	10.30	2.99	1.96

Mix	As Cast Air Content (%)	H_2O Lost During Curing (%)	Final Density (g/cm^3)
C6124	9.37	0.71	2.09
C6131	10.48	3.24	2.04
C6214	15.29	1.28	1.83
C6904	11.69	1.43	1.93
C6905	10.98	3.56	1.96
C6908	13.56	1.22	1.87
C6910	11.29	0.90	1.98
C6911	10.67	1.72	1.95
C6912	8.83	2.83	2.03
C6914	9.03	2.31	1.95
C6915	7.82	2.48	1.98

Table B.6 – Compressive Strength Testing Results and Model Predictions

Mix	Critical Variables (% wt. of Mix)			Coefficient of Variation for 6 Cubes (%)	Experimental Strength (ksi)	Alg. Model Prediction (ksi)	Exp. Model Prediction (ksi)
	H_2O	Na_2O	R. SiO_2				
C1112	14.91	2.83	10.56	-	0.00	2.98	9.80
C1212	22.60	2.85	9.84	-	0.00	2.86	2.88
C2212	22.59	3.28	10.45	-	0.00	3.42	2.37
C6901	22.57	2.99	9.48	-	0.00	3.34	5.17
C6214	22.72	2.93	13.96	8.36	0.34	1.51	0.40
C2214	22.48	3.29	13.58	5.78	0.86	2.18	1.06
C2053	27.20	5.30	9.95	12.56	0.92	4.91	5.65
C3213	22.41	2.95	11.83	5.66	0.97	2.14	0.67
C3026	22.72	17.61	12.64	6.64	1.20	1.93	1.24
C1314	30.04	2.86	12.18	5.95	1.48	1.69	0.02
C1311	30.10	3.00	7.60	3.43	1.81	1.86	0.02
C1051	30.01	4.81	8.17	6.49	1.88	2.61	1.28
C2043	29.98	9.24	8.39	6.01	1.90	2.80	2.20
C1053	30.06	8.81	8.03	10.79	2.04	2.42	2.06
C6914	23.78	12.80	8.43	7.45	2.11	3.33	2.23
C1321	30.00	6.84	7.17	6.48	2.11	1.36	1.46
C2041	29.89	5.32	8.33	11.00	2.29	2.84	1.95
C1045	26.32	11.07	7.62	5.11	2.35	2.31	1.88
C3053	26.87	5.61	8.01	11.84	2.56	2.97	2.49
C4901	18.72	10.84	9.23	6.79	2.66	7.08	7.10
C3231	22.41	10.94	7.08	7.57	3.05	2.17	3.09
C2231	22.60	11.28	7.94	7.81	3.38	3.52	3.33
C2031	26.26	5.25	9.31	8.47	3.41	4.66	4.87
C3054	24.44	8.45	7.95	10.93	3.49	3.38	3.81
C3032	26.18	4.96	14.65	13.68	3.56	4.77	3.62
C1046	26.28	11.12	10.43	8.38	3.60	4.86	3.56
C3022	22.31	5.04	14.58	20.71	3.76	5.46	5.96

Mix	Critical Variables (% wt. of Mix)			Coefficient of Variation for 6 Cubes (%)	Experimental Strength (ksi)	Alg. Model Prediction (ksi)	Exp. Model Prediction (ksi)
	H_2O	Na_2O	R. SiO_2				
C3025	22.45	12.97	9.62	5.91	3.78	4.21	3.25
C6904	23.41	8.25	7.75	6.79	3.82	3.32	4.09
C2232	22.42	11.21	10.15	3.58	3.85	5.71	5.03
C2211	22.43	3.32	8.92	6.51	4.00	4.16	4.04
C2033	26.55	9.16	9.42	9.74	4.15	4.67	4.32
C6908	23.68	4.57	11.45	23.39	4.26	5.36	5.28
C1043	26.22	7.87	9.16	12.45	4.41	4.67	4.92
C1052	29.96	5.24	10.99	7.51	4.41	4.74	5.04
C2221	22.33	7.33	8.45	6.24	4.43	5.13	5.64
C1041	26.32	4.94	7.81	7.69	4.46	2.76	1.78
C2025	22.47	13.21	9.32	4.55	4.58	3.94	2.94
C2023	22.55	9.35	9.30	4.78	4.59	5.93	5.76
C2026	22.55	13.27	13.42	7.49	4.61	4.73	4.57
C3232	23.00	11.08	9.82	10.60	4.69	5.37	4.58
C1231	22.42	10.84	7.58	12.04	4.72	3.08	3.42
C1033	22.64	8.77	7.79	5.62	4.76	3.61	4.36
C1232	22.44	10.79	10.29	11.15	4.79	6.11	5.52
C6915	22.28	10.92	11.75	10.35	4.85	6.87	6.57
C3041	30.09	5.00	11.60	7.76	4.86	4.65	4.00
C1221	22.58	6.89	8.01	8.86	5.06	4.19	4.83
C3033	26.28	9.11	9.62	7.18	5.22	4.97	4.69
C6905	18.77	13.21	7.72	10.48	5.30	4.10	4.65
C3058	23.28	8.82	9.04	10.34	5.41	5.41	5.45
C2021	22.43	5.54	9.23	3.77	6.00	6.17	6.57
C3221	22.55	6.86	7.58	7.80	6.09	3.30	4.26
C3023	22.28	9.01	9.59	6.00	6.69	6.57	6.49
C3031	26.24	5.00	10.57	13.11	6.75	5.27	5.84
C1034	22.62	9.08	11.18	18.47	6.79	7.95	7.99
C2014	18.84	11.79	11.20	5.05	6.93	6.94	7.72
C2222	22.44	7.25	11.30	10.93	6.94	8.60	9.49
C3059	21.87	9.07	9.89	13.96	7.31	7.13	7.00
C2034	26.26	9.24	13.40	13.36	7.52	7.59	7.54
C2056	23.08	8.55	10.71	14.51	7.71	7.56	7.84
C3034	26.51	8.92	13.83	8.58	7.79	7.83	7.84
C1022	18.76	9.06	8.20	10.03	7.87	6.61	7.08
C2012	18.75	9.27	10.28	4.99	7.96	9.76	9.10
C3021	22.73	5.06	10.52	12.84	8.72	6.46	7.44
C3224	22.36	7.03	16.25	3.61	9.11	8.86	9.49
C6131	15.10	11.75	7.49	10.07	9.16	8.51	9.61
C3223	22.32	6.99	13.37	7.57	9.18	9.21	9.91
C6912	17.63	11.45	10.56	5.18	9.19	7.83	8.66
C3057	23.04	7.21	10.76	8.00	9.25	7.84	8.80
C3134	14.82	11.08	12.80	17.44	9.58	10.64	13.16
C3024	22.42	8.99	14.63	11.05	9.63	9.65	9.70

Mix	Critical Variables (% wt. of Mix)			Coefficient of Variation for 6 Cubes (%)	Experimental Strength (ksi)	Alg. Model Prediction (ksi)	Exp. Model Prediction (ksi)
	H_2O	Na_2O	R. SiO_2				
C1024	18.70	10.90	10.28	5.23	9.77	7.83	7.92
C3131	15.08	11.18	7.93	7.34	9.77	9.60	10.00
C3222	22.56	7.01	10.46	10.60	9.81	7.82	8.72
C2224	22.56	7.25	17.20	5.80	10.31	8.88	9.48
C2131	14.91	11.28	8.87	9.59	10.84	10.18	10.76
C6910	18.98	7.54	13.23	20.00	11.16	11.80	11.63
C2051	22.47	7.76	12.34	18.28	11.23	9.23	9.85
C2024	22.37	9.31	14.37	5.74	11.46	9.39	9.45
C1222	22.50	6.84	10.98	4.11	12.02	8.24	9.29
C6911	22.36	6.70	10.51	10.16	12.05	7.92	8.90
C3013	18.77	8.84	13.56	10.22	12.24	11.78	11.51
C2011	18.72	5.36	11.24	7.51	12.51	9.01	10.08
C2134	14.86	11.62	13.74	15.51	13.55	9.15	13.50
C6124	15.01	6.98	13.54	13.89	14.34	14.93	13.86
C3124	15.03	6.99	13.89	5.17	15.02	14.52	14.00

Appendix C

Design Tables

Table C.1 – % wt. Reactive SiO_2 in Mix for Compressive Strength of 2 ksi

		% wt. H_2O in Mix															
		15	16	17	18	19	20	21	22	23	24	25	26	27	28	29	30
% wt. Na_2O in Mix	4							7.31	7.74	8.03	8.25	8.42	8.58	8.73	8.86	9.00	10.51
	5										7.27	7.61	7.86	8.07	8.25	8.41	8.55
	6												7.08	7.41	7.66	7.88	8.06
	7												6.49	6.92	7.26	7.54	7.77
	8												6.26	6.76	7.15	7.47	7.75
	9												6.41	6.94	7.36	7.71	8.02
	10												6.88	7.42	7.87	8.26	8.61
	11												7.63	8.19	8.69	9.14	9.56
	12										7.09	7.94	8.66	9.31	9.91	10.49	11.08
	13									7.22	8.30	9.24	10.10	10.95	11.83	12.82	14.11
	14								7.24	8.65	9.88	11.06	12.31	13.82	16.20		
	15							7.01	8.86	10.49	12.13	14.07	17.19				

Table C.2 – % wt. Reactive SiO_2 in Mix for Compressive Strength of 3 ksi

		% wt. H_2O in Mix															
		15	16	17	18	19	20	21	22	23	24	25	26	27	28	29	30
% wt. Na_2O in Mix	4						7.67	8.05	8.31	8.53	8.71	8.89	9.07	10.33			
	5								7.43	7.79	8.07	8.29	8.48	8.65	8.81	8.95	9.09
	6										7.41	7.73	7.99	8.20	8.39	8.56	8.71
	7											7.36	7.68	7.95	8.18	8.38	8.56
	8											7.27	7.65	7.96	8.23	8.47	8.68
	9											7.48	7.90	8.26	8.57	8.85	9.11
	10										7.43	7.98	8.45	8.86	9.23	9.57	9.90
	11									7.45	8.17	8.78	9.33	9.84	10.32	10.79	11.28
	12								7.46	8.42	9.23	9.97	10.68	11.40	12.18	13.10	14.43
	13							7.36	8.63	9.72	10.75	11.79	12.97	14.56			
	14							8.70	10.17	11.58	13.16	15.32					
	15						8.45	10.41	12.34	14.68							

Table C.3 – % wt. Reactive SiO_2 in Mix for Compressive Strength of 4 ksi

% wt. Na_2O in Mix	% wt. H_2O in Mix																
	15	16	17	18	19	20	21	22	23	24	25	26	27	28	29	30
4				7.09	7.82	8.21	8.49	8.73	8.95	10.54	9.99					
5						7.26	7.76	8.10	8.37	8.59	8.79	8.97	9.14	9.30	9.48	9.67
6								7.48	7.84	8.13	8.37	8.58	8.76	8.92	9.08	9.22
7								7.05	7.51	7.87	8.16	8.41	8.63	8.82	9.00	9.16
8									7.45	7.87	8.21	8.50	8.76	8.99	9.20	9.40
9								7.09	7.67	8.14	8.53	8.88	9.19	9.47	9.74	9.99
10								7.54	8.17	8.70	9.17	9.59	9.98	10.36	10.73	11.11
11							7.38	8.25	8.97	9.60	10.19	10.76	11.33	11.95	12.67	13.65
12						7.09	8.29	9.27	10.14	10.98	11.85	12.84	14.18			
13						8.15	9.49	10.70	11.91	13.30	15.32					
14					7.64	9.49	11.13	12.86	15.10							
15					9.04	11.24	13.56	16.82								

Table C.4 – % wt. Reactive SiO_2 in Mix for Compressive Strength of 5 ksi

% wt. Na_2O in Mix	% wt. H_2O in Mix																
	15	16	17	18	19	20	21	22	23	24	25	26	27	28	29	30
4				7.85	8.30	8.62	8.90	10.60								
5					7.46	7.97	8.32	8.60	8.84	9.05	9.26	9.47	9.70	10.00		
6						7.31	7.80	8.15	8.44	8.68	8.89	9.08	9.25	9.42	9.58	9.73
7							7.46	7.90	8.25	8.54	8.78	9.00	9.20	9.38	9.55	9.71
8							7.40	7.91	8.31	8.65	8.94	9.20	9.44	9.66	9.87	10.07
9							7.60	8.17	8.64	9.04	9.39	9.71	10.02	10.31	10.60	10.89
10						7.26	8.07	8.72	9.27	9.76	10.21	10.66	11.10	11.57	12.09	12.74
11						7.91	8.81	9.58	10.27	10.93	11.62	12.38	13.35	15.20		
12					7.53	8.81	9.87	10.86	11.85	12.99	14.58					
13					8.55	10.03	11.40	12.87	14.82							
14				7.76	9.84	11.70	13.76	16.79								
15				9.04	11.52	14.17										

Table C.5 – % wt. Reactive SiO_2 in Mix for Compressive Strength of 6 ksi

% wt. Na_2O in Mix	% wt. H_2O in Mix																
	15	16	17	18	19	20	21	22	23	24	25	26	27	28	29	30
4			7.74	8.33	8.71	9.04	9.49									
5				7.53	8.10	8.49	8.80	9.06	9.32	9.58	9.90					
6					7.52	8.03	8.40	8.70	8.95	9.17	9.38	9.58	9.77	9.96	10.18	10.42
7					7.14	7.77	8.21	8.56	8.86	9.11	9.34	9.55	9.75	9.94	10.12	10.31
8					7.04	7.75	8.26	8.68	9.02	9.33	9.60	9.86	10.10	10.33	10.57	10.81
9					7.20	7.98	8.57	9.06	9.48	9.86	10.21	10.56	10.90	11.26	11.65	12.11
10					7.61	8.47	9.16	9.75	10.29	10.81	11.34	11.91	12.59	13.62		
11					8.24	9.23	10.07	10.85	11.64	12.52	13.68	16.46				
12				7.69	9.12	10.31	11.44	12.64	14.20	17.35						
13				8.63	10.31	11.87	13.63	16.22								
14			7.39	9.81	11.91	14.25	17.78									
15			8.50	11.31	14.18											

Table C.6 – % wt. Reactive SiO_2 in Mix for Compressive Strength of 7 ksi

% wt. Na_2O in Mix \ % wt. H_2O in Mix	15	16	17	18	19	20	21	22	23	24	25	26	27	28	29	30
4		7.37	8.27	8.75	9.18											
5			7.48	8.18	8.63	8.98	9.29	9.62	11.29							
6				7.66	8.22	8.62	8.94	9.21	9.46	9.70	9.94	10.19	10.50	11.66		
7				7.33	8.00	8.48	8.85	9.16	9.43	9.68	9.91	10.14	10.37	10.61	10.88	11.21
8				7.25	8.02	8.57	9.01	9.37	9.70	10.00	10.29	10.57	10.86	11.17	11.53	12.00
9				7.42	8.27	8.91	9.43	9.89	10.31	10.72	11.13	11.58	12.10	12.85		
10				7.81	8.77	9.52	10.18	10.80	11.41	12.09	12.93	14.50				
11				8.41	9.52	10.47	11.37	12.33	13.54	15.78						
12			7.56	9.24	10.60	11.89	13.34	15.45								
13			8.39	10.33	12.10	14.11	17.17									
14			9.40	11.77	14.29	17.92										
15			8.50	11.31	14.18											

Table C.7 – % wt. Reactive SiO_2 in Mix for Compressive Strength of 8 ksi

% wt. Na_2O in Mix \ % wt. H_2O in Mix	15	16	17	18	19	20	21	22	23	24	25	26	27	28	29	30
4		8.08	8.74													
5		7.22	8.20	8.74	9.16	9.55	10.06									
6			7.71	8.37	8.82	9.18	9.49	9.79	10.09	10.43	10.99					
7			7.42	8.20	8.72	9.12	9.46	9.77	10.05	10.33	10.62	10.95	11.38			
8			7.36	8.24	8.85	9.32	9.73	10.09	10.44	10.78	11.14	11.56	12.14			
9			7.52	8.50	9.21	9.79	10.31	10.79	11.29	11.83	12.53	14.10				
10			7.88	8.99	9.84	10.59	11.31	12.07	13.02	14.76						
11			8.42	9.71	10.80	11.85	13.03	14.75								
12		7.09	9.15	10.72	12.19	13.89	16.51									
13		7.74	10.09	12.08	14.28	17.48										
14		8.52	11.28	13.94	17.43											
15		9.43	12.76	16.45												

Table C.8 – % wt. Reactive SiO_2 in Mix for Compressive Strength of 9 ksi

% wt. Na_2O in Mix \ % wt. H_2O in Mix	15	16	17	18	19	20	21	22	23	24	25	26	27	28	29	30
4	7.42	8.64	10.74													
5		8.11	8.83	9.35	9.90											
6		7.66	8.50	9.03	9.45	9.82	10.20	10.69								
7		7.40	8.35	8.96	9.42	9.80	10.15	10.50	10.88	11.37						
8		7.35	8.41	9.11	9.65	10.11	10.53	10.95	11.42	12.00						
9		7.48	8.67	9.49	10.15	10.75	11.34	11.99	12.86							
10		7.77	9.13	10.12	10.99	11.84	12.84	14.35								
11		8.21	9.78	11.04	12.26	13.70	16.04									
12		8.80	10.66	12.33	14.23	17.09										
13		9.52	11.80	14.13	17.26											
14		10.39	13.25	16.58												
15	7.43	11.43	15.07													

Table C.9 – % wt. Reactive SiO_2 in Mix for Compressive Strength of 10 ksi

% wt. Na_2O in Mix	% wt. H_2O in Mix																
	15	16	17	18	19	20	21	22	23	24	25	26	27	28	29	30
4	8.32	14.02														
5	7.79	8.88	9.57	11.34												
6	7.38	8.59	9.26	9.77	10.26	10.93										
7	7.17	8.49	9.22	9.75	10.21	10.66	11.16	12.02								
8	7.12	8.55	9.39	10.01	10.55	11.08	11.66	12.49								
9	7.20	8.78	9.76	10.54	11.25	12.00	12.97	15.52								
10	7.38	9.16	10.36	11.37	12.41	13.72	16.25									
11	7.66	9.70	11.19	12.59	14.28	16.99										
12	8.02	10.39	12.29	14.33	17.18											
13	8.45	11.24	13.71	16.70												
14	8.95	12.26	15.49													
15	9.52	13.45	17.63													

Table C.10 – % wt. Reactive SiO_2 in Mix for Compressive Strength of 11 ksi

% wt. Na_2O in Mix	% wt. H_2O in Mix															
	15	16	17	18	19	20	21	22	23	24	25	26	27	28	29	30
4	9.22															
5	8.87	9.87	16.35													
6	8.65	9.54	10.22	11.04												
7	8.58	9.53	10.18	10.77	11.44	13.19										
8	8.63	9.70	10.45	11.12	11.83	12.87										
9	8.79	10.04	10.97	11.84	12.85	14.53										
10	9.05	10.54	11.75	12.99	14.65	17.76										
11	9.39	11.21	12.81	14.67	17.43											
12	9.80	12.04	14.20	16.94												
13	10.29	13.04	15.93													
14	10.85	14.22	17.99													
15	11.48	15.57														

Table C.11 – % wt. Reactive SiO_2 in Mix for Compressive Strength of 12 ksi

% wt. Na_2O in Mix	% wt. H_2O in Mix															
	15	16	17	18	19	20	21	22	23	24	25	26	27	28	29	30
4	13.48															
5	10.29	14.44														
6	9.98	10.95	13.22													
7	9.97	10.80	11.64	13.13												
8	10.10	11.03	11.88	12.97	15.36											
9	10.34	11.47	12.54	13.89	16.28											
10	10.66	12.09	13.53	15.42												
11	11.07	12.89	14.85	17.48												
12	11.55	13.87	16.49													
13	12.10	15.01														
14	12.71	16.31														
15	13.40	17.77														

Table C.12 – % wt. Reactive SiO_2 in Mix for Compressive Strength of 13 ksi

% wt. Na_2O in Mix	% wt. H_2O in Mix																
	15	16	17	18	19	20	21	22	23	24	25	26	27	28	29	30
4	16.28															
5	13.23	17.77														
6	11.94	14.24														
7	11.69	12.87	15.02													
8	11.78	12.85	14.33	16.91												
9	12.03	13.28	14.85	17.24												
10	12.39	13.96	15.89													
11	12.83	14.84	17.29													
12	13.35	15.89														
13	13.93	17.11														
14	14.59															
15	15.30															

Table C.13 – Maximum % wt. CaO in Mix to Avoid Flash Set

% wt. Na_2O in Mix	% wt. H_2O in Mix																
	15	16	17	18	19	20	21	22	23	24	25	26	27	28	29	30
4		6.29	9.91	11.82	13.23	14.37	15.34	16.19	16.96	17.66	18.31	18.91	19.48	20.01	20.51	20.99
5		8.54	11.41	13.23	14.62	15.78	16.78	17.66	18.47	19.20	19.88	20.51	21.11	21.67	22.20	22.71
6		9.91	12.57	14.37	15.78	16.96	17.99	18.91	19.75	20.51	21.22	21.88	22.51	23.10	23.66	24.19
7	3.00	10.96	13.53	15.34	16.78	17.99	19.06	20.01	20.87	21.67	22.41	23.10	23.75	24.36	24.94	25.50
8	6.29	11.82	14.37	16.19	17.66	18.91	20.01	20.99	21.88	22.71	23.47	24.19	24.86	25.50	26.11	26.69
9	7.60	12.57	15.11	16.96	18.47	19.75	20.87	21.88	22.81	23.66	24.45	25.19	25.88	26.54	27.17	27.77
10	8.54	13.23	15.78	17.66	19.20	20.51	21.67	22.71	23.66	24.53	25.34	26.11	26.83	27.51	28.16	28.78
11	9.28	13.82	16.39	18.31	19.88	21.22	22.41	23.47	24.45	25.34	26.18	26.97	27.71	28.41	29.07	29.71
12	9.91	14.37	16.96	18.91	20.51	21.88	23.10	24.19	25.19	26.11	26.97	27.77	28.53	29.25	29.94	30.59
13	10.47	14.87	17.49	19.48	21.11	22.51	23.75	24.86	25.88	26.83	27.71	28.53	29.31	30.05	30.75	31.42
14	10.96	15.34	17.99	20.01	21.67	23.10	24.36	25.50	26.54	27.51	28.41	29.25	30.05	30.80	31.52	32.21
15	11.41	15.78	18.47	20.51	22.20	23.66	24.94	26.11	27.17	28.16	29.07	29.94	30.75	31.52	32.25	32.95

Table C.14 – Minimum % wt. CaO in Mix to Avoid Long Set

% wt. R. SiO_2 in Mix	% wt. H_2O in Mix																
	15	16	17	18	19	20	21	22	23	24	25	26	27	28	29	30
7	9.76	9.98	10.34	10.84	11.49	12.28	13.22	14.30	15.52	16.89	18.40	20.06	21.86	23.80	25.89	28.12
8	7.11	7.33	7.69	8.19	8.84	9.63	10.57	11.65	12.87	14.24	15.75	17.41	19.21	21.15	23.24	25.47
9	4.46	4.68	5.04	5.54	6.19	6.98	7.92	9.00	10.22	11.59	13.10	14.76	16.56	18.50	20.59	22.82
10	1.81	2.03	2.39	2.89	3.54	4.33	5.27	6.35	7.57	8.94	10.45	12.11	13.91	15.85	17.94	20.17
11				0.24	0.89	1.68	2.62	3.70	4.92	6.29	7.80	9.46	11.26	13.20	15.29	17.52
12								1.05	2.27	3.64	5.15	6.81	8.61	10.55	12.64	14.87
13										0.99	2.50	4.16	5.96	7.90	9.99	12.22
14												1.51	3.31	5.25	7.34	9.57
15													0.66	2.60	4.69	6.92
16															2.04	4.27
17																1.62

Works Cited

[1] ACI Committee 318, "Building code requirements for structural concrete (ACI 318-05) and commentary (ACI 318R-05)," Farmington Hills, MI, ACI Standard 2005.

[2] M. Ahmaruzzaman, "A review on the utilization of fly ash," *Progress in Energy and Combustion Science*, vol. 36, no. 3, pp. 327-363, June 2010.

[3] American Coal Ash Association, Corrected 2009 coal combustion product (CCP) production & use survey, February 8, 2011.

[4] T. Bakharev, "Geopolymeric materials prepared using class F fly ash and elevated temperature curing," *Cement and Concrete Research*, vol. 35, no. 6, pp. 1224-1232, June 2005.

[5] Jonathan L. Bell and Waltraud M. Kriven, "Formation of an iron-based inorganic polymer (geopolymer)," in *Mechanical Properties and Performance of Engineering Ceramics and Composites IV*, Dileep Singh, Waltraud M. Kriven, and Jonatham Salem, Eds. Hoboken, New Jersey, United States of America: John Wiley & Sons, Inc., 2009, pp. 301-312.

[6] Susan A. Bernal, Erich D. Rodríguez, Ruby Mejia de Gutiérrez, John L. Provis, and Silvio Delvasto, "Activation of metakaolin/slag blends using alkaline solutions based on chemically modified silica fume and rice husk ash," *Waste and Biomass Valorization*, vol. 3, no. 1, pp. 99-108, March 2012.

[7] T. A. Boden, G. Marland, and R. J. Andres, Global, regional, and national fossil-fuel CO2 emissions, 2010.

[8] Nigel W. Chen-Tan, Arie van Riessen, Chi V. Ly, and Daniel C. Southam, "Determining the reactivity of a fly ash for production of geopolymer," *Journal of the American Ceramic Society*, vol. 92, no. 4, pp. 881-887, April 2009.

[9] P. Chindaprasirt, T. Chareerat, S. Hatanaka, and T. Cao, "High-strength geopolymer using fine high-calcium fly ash," *Journal of Materials in Civil Engineering*, vol. 23, no. 3, pp. 264-270, March 2011.

[10] P. Chindaprasirt, T. Chareerat, and V. Sirivivatnanon, "Workability and strength of coarse high calcium fly ash geopolymer," *Cement and Concrete Composites*, vol. 29, no. 3, pp. 224-229, March 2007.

[11] Douglas C. Comrie, John H. Paterson, and Douglas J. Ritcey, "Geopolymer technologies in toxic waste management," in *Géopolymère '88 Proceedings*, vol. 1, Saint-Quentin, France, 1988, pp. 107-123.

[12] M. Criado, A. Fernández-Jiménez, and A. Palomo, "Alkali activation of fly ash. Part III: effect of curing conditions on reaction and its graphical description," *Fuel*, vol. 89, no. 11, pp. 3185-3192, November 2010.

[13] M. Criado, A. Palomo, and A. Fernández-Jiménez, "Alkali activation of fly ashes. Part 1: effect of curing conditions on the carbonation of the reaction products," *Fuel*, vol. 84, no. 16, pp. 2048-2054, November 2005.

[14] Michel Davidovics, Bruno Martin, and Joseph Davidovits, "Past and present experience on the use of carbon-géopolymère compositeTM in formula one and C.A.R.T. racing cars," in *Géopolymère '99 Proceedings*, Saint-Quentin, France, 1999, pp. 141-142.

[15] Joseph Davidovits, *Geopolymer chemistry and applications*. Saint-Quentin, France: Institut Géopolymère, 2008.

[16] Joseph Davidovits, "Geopolymer chemistry and properties," in *Géopolymère '88 Proceedings*, vol. 1, Saint-Quentin, France, 1988, pp. 25-48.

[17] Joseph Davidovits, "Geopolymer chemistry and sustainable development. The poly(sialate) terminology: a very useful and simple model for the promotion and understanding of green-chemistry," in *Geopolymer: Green Chemsitry and Sustainable Development Solutions*, Saint-Quentin, France, 2005, pp. 9-15.

[18] Joseph Davidovits, "Properties of geopolymer cements," in *First International Conference on Alkaline Cements and Concretes*, Kiev Ukraine, 1994, pp. 131-149.

[19] Joseph Davidovits et al., "Geopolymeric cement based on low cost geologic materials. Results from the european research project GEOCISTEM," in *Géopolymère '99 Proceedings*, Saint-Quentin, France, 1999, pp. 83-96.

[20] E. I. Diaz and E. N. Allouche, "Recycling of fly ash into geopolymer concrete: creation of a database," in *Green Technologies Conference*, Grapevine, Texas, 2010.

[21] E. I. Diaz, E. N. Allouche, and S. Eklund, "Factors affecting the suitability of fly ash as source material for geopolymers," *Fuel*, vol. 89, no. 5, pp. 992-996, May 2010.

[22] K. Dombrowski, A. Buchwald, and M. Weil, "The influence of calcium content on the structure and thermal performance of fly ash based geopolymers," *Journal of Materials Science*, vol. 42, no. 9, pp. 3033-3043, May 2007.

[23] P. Duxson et al., "Geopolymer technology: the current state of the art," *Journal of Materials Science*, vol. 42, no. 9, pp. 2917-2933, May 2007.

[24] Peter Duxson and John L. Provis, "Designing precursors for geopolymer cements," *Journal of the American Ceramic Society*, vol. 91, no. 12, pp. 3864-3869, December 2008.

[25] A. Fernández-Jiménez et al., "Quantitative determination of phases in the alkali activation of fly ash. Part I. Potential ash reactivity," *Fuel*, vol. 85, no. 5-6, pp. 625-634, March-April 2006.

[26] A. Fernández-Jiménez and A. Palomo, "Characterisation of fly ashes. Potential reactivity as alkaline cements," *Fuel*, vol. 82, no. 18, pp. 2259-2265, December 2003.

[27] A. Fernández-Jiménez, A. Palomo, and M. Criado, "Microstructure development of alkali-activated fly ash cement: a descriptive model," *Cement and Concrete Research*, vol. 35, no. 5, pp. 1204-1209, May 2005.

[28] A. Fernández-Jiménez, A. Palomo, I. Sobrados, and J. Sanz, "The role played by the reactive alumina content in the alkaline activation of fly ashes," *Microporous and Mesoporous Materials*, vol. 91, pp. 111-119, April 2006.

[29] Chiara F. Ferraris, "Measurement of the rheological properties of high performance concrete: state of the art report," *Journal of Research of the National Institute of Standards and Technology*, vol. 104, no. 5, pp. 461-478, September-October 1999.

[30] Maria Luz Granizo, Santiago Alonso, Maria T. Blanco-Varela, and Angel Palomo, "Alkaline activation of metakaolin: effect of calcium hydroxide in the products of reaction," *Journal of the American Ceramic Society*, vol. 85, no. 1, pp. 225-231, January 2002.

[31] Xiaolu Guo, Huisheng Shi, Liming Chen, and Warren A. Dick, "Alkali-activated complex binders from class C fly ash and Ca-containing admixtures," *Journal of Hazardous Materials*, vol. 173, pp. 480-486, January 2010.

[32] Xiaolu Guo, Huisheng Shi, and Warren A. Dick, "Compressive strength and microstructural characteristics of class C fly ash geopolymer," *Cement & Concrete Composites*, vol. 32, no. 2, pp. 142-147, February 2010.

[33] D. Hardjito and B. V. Rangan, "Development and properties of low-calcium fly ash-based geopolymer concrete," Curtin University of Technology, Perth, Australia, Research Report GC 1 2005.

[34] Erik Jämstorp, Johan Forsgren, Susanne Bredenberg, Håkan Engqvist, and Maria Strømme, "Mechanically strong geopolymers offer new possibilities in treatment of chronic pain," *Journal of Controlled Release*, vol. 146, no. 3, pp. 370-377, September 2010.

[35] Erik Jämstorp et al., "Polymer excipients enable sustained drug release in low pH from mechanically strong inorganic geopolymers," *Pharma Sciences*, vol. 2, pp. 23-28, 2012.

[36] Andrew P. Jones, Jeffrey W. Hoffmann, Dennis N. Smith, Thomas J. Feeley III, and James T. Murphy, "DOE/NETL's phase II mercury control technology field testing program: preliminary economic analysis of activated carbon injection," *Environmental Science & Technology*, vol. 41, no. 4, pp. 1359-1364, January 2007.

[37] Steven H. Kosmatka, Beatrix Kerkhoff, and William C. Panarese, *Design and Control of Concrete Mixtures*, Fourteenth Edition ed. Skokie, Illinois, United States of America: Portland Cement Association, 2002.

[38] G. Kovalchuk, A. Fernández-Jiménez, and A. Palomo, "Alkali-activated fly ash: effect of thermal curing conditions on mechanical and microstructural development - part II," *Fuel*, vol. 86, no. 3, pp. 315-322, February 2007.

[39] W. M. Kriven, M. Gordon, B. L. Ervin, and H. Reis, "Corrosion protection assessment of concrete reinforcing bars with a geopolymer coating," *Developments in Porous, Biological and Geopolymer Ceramics: Ceramic Engineering and Science Proceedings*, vol. 28, no. 9, pp. 373-381, December 2009.

[40] Sanjay Kumar, Rakesh Kumar, T. C. Alex, A. Bandopadhyay, and S. P. Mehrotra, "Effect of mechanically activated fly ash on the properties of geopolymer cement," in *Geopolymer: Green Chemistry and Sustainable Development Solutions*, Saint-Quentin, France, 2005, pp. 113-116.

[41] Sanjay Kumar, Rakesh Kumar, and S. P. Mehrotra, "Influence of granulated blast furnace slag on the reaction, structure and properties of fly ash based geopolymer," *Journal of Materials Science*, vol. 45, no. 3, pp. 607-615, February 2010.

[42] W. K. W. Lee and J. S. J. van Deventer, "Structural reorganisation of class F fly ash in alkaline silicate solutions," *Colloids and Surfaces A: Physicochemical and Engineering Aspects*, vol. 211, no. 1, pp. 49-66, November 2002.

[43] W. K. W. Lee and J. S. J. van Deventer, "The effect of ionic contaminants on the early-age properties of alkali-activated fly ash-based cements," *Cement and Concrete Research*, vol. 32, no. 4, pp. 577-584, April 2002.

[44] W. K. W. Lee and J. S. J. van Deventer, "The effects of inorganic salt contamination on the strength and durability of geopolymers," *Colloids and Surfaces A: Physicochemical and Engineering Aspects*, vol. 211, no. 2-3, pp. 115-126, December 2002.

[45] Ekkehard Liefke, "Industrial applications of foamed inorganic polymers," in *Géopolymère '99 Proceedings*, Saint-Quentin, France, 1999, pp. 189-199.

[46] Ke-Liang Li, Guo-Hong Huang, Jian Chen, Dong Wang, and Xiu-Sheng Tang, "Early mechanical property and durability of geopolymer," in *Geopolymer: Green Chemistry and Sustainable Development Solutions*, Saint-Quentin, France, 2005, pp. 117-120.

[47] Chao Li, Yu Li, Henghu Sun, and Longtu Li, "The composition of fly ash glass phase and its dissolution properties applying to geopolymeric materials," *Journal of the American Ceramic Society*, vol. 94, no. 6, pp. 1773-1778, June 2011.

[48] Zongjin Li and Sifeng Liu, "Influence of slag as additive on compressive strength of fly ash-based geopolymer," *Journal of Materials in Civil Engineering*, vol. 19, no. 6, pp. 470-474, June 2007.

[49] Maricela Lizcano, Andres Gonzalez, Sandip Basu, Karen Lozano, and Miladin Radovic, "Effects of water content and chemical composition on structural properties of alkaline activated metakaolin-based geopolymers," *Journal of the American Ceramic Society*, vol. 95, no. 7, pp. 2169-2177, July 2012.

[50] Richard E. Lyon et al., "Fire-resistant aluminosilicate composites," *Fire and Materials*, vol. 21, no. 2, pp. 67-73, March 1997.

[51] Donald Macphee and Ines Garcia-Lodeiro, "Activation of aluminosilicates - some chemical

considerations," in *Proceedings of the Second International Slag Valorisation Symposium: The Transition to Sustainable Materials Management*, Leuven, Belgium, 2011, pp. 51-61.

[52] "Materials Cost Index," *Engineering News-Record*, p. 27, March 2012.

[53] Benjamin C. McLellan, Ross P. Williams, Janine Lay, Arie van Riessen, and Glen D. Corder, "Costs and carbon emissions for geopolymer pastes in comparison to ordinary portland cement," *Journal of Cleaner Production*, vol. 19, no. 9-10, pp. 1080-1090, June-July 2011.

[54] P. K. Mehta, "Studies on blended Portland cements containing Santorin earth," *Cement and Concrete Research*, vol. 11, no. 4, pp. 507-518, July 1981.

[55] J. M. Miranda, A. Fernández-Jiménez, J. A. González, and A. Palomo, "Corrosion resistance in activated fly ash mortars," *Cement and Concrete Research*, vol. 35, no. 6, pp. 1210-1217, June 2005.

[56] J. Morris and S. Hodges, "Corrosion of metals in fly ash-based geopolymers," in *Geopolymer: Green Chemistry and Sustainable Development Solutions*, Saint-Quentin, France, 2005, pp. 51-55.

[57] Ali Nazari, Gholamreza Khalaj, and Shadi Riahi, "ANFIS-based prediction of the compressive strength of geopolymers with seeded fly ash and rice husk-bark ash," *Neural Computing and Applications*, vol. 22, no. 3-4, pp. 689-701, March 2013.

[58] Ángel Palomo, Santiago Alonso, Ana Fernandez-Jiménez, Isabel Sobrados, and Jesús Sanz, "Alkaline activation of fly ashes: NMR study of the reaction products," *Journal of the American Ceramic Society*, vol. 87, no. 6, pp. 1141-1145, June 2004.

[59] Dimitrios Panias, Ioanna P. Giannopoulou, and Theodora Perraki, "Effect of synthesis parameters on the mechanical properties of fly ash-based geopolymers," *Colloids and Surfaces A: Physicochemical and Engineering Aspects*, vol. 301, pp. 246-254, July 2007.

[60] Alain Porte and Marie Jazet, "Aircraft conduit," WO/2008/015361, February 7, 2008.

[61] Portland Cement Association Economic Research Department, U.S. cement industry fact sheet, 2002.

[62] Portland Cement Association Market Research, Survey of mineral admixtures and blended cements in ready mixed concrete, October 2000.

[63] PQ Corporation, Soluble silicates price schedule - potassium silicates, November 15, 2011.

[64] PQ Corporation, Soluble silicates price schedule - sodium silicates, November 15, 2011.

[65] John L. Provis, Grant C. Lukey, and Jannie S. J. van Deventer, "Do geopolymers actually contain nanocrystalline zeolites? A reexamination of existing results," *Chemistry of Materials*, vol. 17, no. 12, pp. 3075-3085, June 2005.

[66] J. L. Provis and J. S. J. van Deventer, "Geopolymerisation kinetics. 2. Reaction kinetic

modelling," *Chemical Engineering Science*, vol. 62, no. 9, pp. 2318-2329, May 2007.

[67] Radhakrishna , A. Shashishankar, B. C. Udayashankar, and M. V. Renuka Devi, "Compressive strength assessment of geopolymer composites by a phenomenological model," *Journal of Reinforced Plastics and Composites*, vol. 29, no. 6, pp. 840-854, March 2010.

[68] Michael Schmidt and Hod Lipson, "Distilling free-form natural laws from experimental data," *Science*, vol. 324, no. 5923, pp. 81-85, April 2009.

[69] R. Sersale and G. Frigione, "Portland-zeolite-cement for minimizing alkali-aggregate expansion," *Cement and Concrete Research*, vol. 17, no. 3, pp. 404-410, May 1987.

[70] Sindhunata , J. S. J. van Deventer, G. C. Lukey, and H. Xu, "Effect of curing temperature and silicate concentration on fly-ash-based geopolymerization," *Industrial & Engineering Chemistry Research*, vol. 45, no. 10, pp. 3559-3568, May 2006.

[71] František Škvára, Jan Šlosar, Jan Bohunek, and Alena Marková, "Alkali-activated fly ash geopolymeric materials," in *Proceedings of the 11th International Congress on the Chemistry of Cement (ICCC)*, Durban, South Africa, 2003.

[72] Shan Somayaji, *Civil Engineering Materials*, Second Edition ed. Upper Saddle River, New Jersey, United States of America: Prentice Hall, 2001.

[73] M. D. J. Sumajouw and B. V. Rangan, "Low-calcium fly ash-based geopolymer concrete: reinforced beams and columns," Curtin University of Technology, Perth, Australia, Research Report GC 3 2006.

[74] J. C. Swanepoel and C. A. Strydom, "Utilisation of fly ash in a geopolymeric material," *Applied Geochemistry*, vol. 17, no. 8, pp. 1143-1148, August 2002.

[75] Judith Taylor and Ruth Liao, "Chlor-alkali market stable," *ICIS Chemical Business*, p. 22, January 2011.

[76] J. Temuujin, R. P. Williams, and A. van Riessen, "Effect of mechanical activation of fly ash on the properties of geopolymer cured at ambient temperature," *Journal of Materials Processing Technology*, vol. 209, no. 12-13, pp. 5276-5280, July 2009.

[77] Ravindra N. Thakur and Somnath Ghosh, "Effect of mix composition on compressive strength and microstructure of fly ash based geopolymer composites," *ARPN Journal of Engineering and Applied Sciences*, vol. 4, no. 4, pp. 68-74, June 2009.

[78] The Dow Chemical Company, "Caustic Soda Solution Handbook," 2010.

[79] United States Environmental Protection Agency, Inventory of U.S. greenhouse gas emissions and sinks: 1990-2010, April 15, 2012.

[80] United States Geological Survey, Cement statistics, December 13, 2011.

[81] J. G. S. van Jaarsveld, J. S. J. van Deventer, and G. C. Lukey, "The characterisation of source materials in fly ash-based geopolymers," *Materials Letters*, vol. 57, no. 7, pp. 1272-1280, January 2003.

[82] J. G. S. van Jaarsveld, J. S. J. van Deventer, and G. C. Lukey, "The effect of composition and temperature on the properties of fly ash- and kaolinite-based geopolymers," *Chemical Engineering Journal*, vol. 89, pp. 63-73, October 2002.

[83] S. E. Wallah and B. V. Rangan, "Low-calcium fly ash-based geopolymer concrete: long-term properties," Curtin University of Technology, Perth, Australia, Research Report GC 2 2006.

[84] T. H. Wee, A. K. Suryavanshi, S. F. Wong, and A. K. M. A. Rahman, "Sulfate resistance of concrete containing mineral admixtures," *ACI Materials Journal*, vol. 97, no. 5, pp. 536-549, September 2000.

[85] Luqian Weng, Kwesi Sagoe-Crentsil, Trevor Brown, and Shenhua Song, "Effects of aluminates on the formation of geopolymers," *Materials Science and Engineeering: B*, vol. 117, no. 2, pp. 163-168, March 2005.

[86] Claire E. White, John L. Provis, Thomas Proffen, and Jannie S. J. van Deventer, "Molecular mechanisms responsible for the structural changes occurring during geopolymerization: multiscale simulation," *AIChE Journal*, vol. 58, no. 7, pp. 2241-2253, July 2012.

[87] Frank Winnefeld, Andreas Leemann, Martin Lucuk, Pavel Svoboda, and Markus Neuroth, "Assessment of phase formation in alkali activated low and high calcium fly ashes in building materials," *Construction and Building Materials*, vol. 24, no. 6, pp. 1086-1093, June 2010.

[88] C. K. Yip, G. C. Lukey, and J. S. J. van Deventer, "The coexistence of geopoylymeric gel and calcium silicate hydrate at the early stage of alkaline activation," *Cement and Concrete Research*, vol. 35, no. 9, pp. 1688-1697, September 2005.